AN EFFICIENT STRATEGY FOR THE INVERSION OF BIDIRECTIONAL REFLECTANCE MODELS WITH SATELLITE REMOTE SENSING DATA

by

JEFFREY LAWRENCE PRIVETTE

B.A., The College of Wooster, 1987

B.S.E., University of Michigan, 1988

M.S., University of Colorado, 1991

A thesis submitted to the

Faculty of the Graduate School of the

University of Colorado in partial fulfillment

of the requirements for the degree of

Doctor of Philosophy

Department of Aerospace Engineering Sciences

1994

This thesis for the Doctor of Philosophy degree by

Jeffrey Lawrence Privette

has been approved for the

Department of

Aerospace Engineering Sciences

by

Dr. William J. Emery, Advisor

Dr. Brian Curtiss

Dr. Robert R. Leben

Dr. Ranga B. Myneni

Dr. David S. Schimel

Dr. Carol A. Wessman

Privette, Jeffrey Lawrence (Ph.D., Aerospace Engineering Sciences)

An Efficient Strategy for the Inversion of Bidirectional Reflectance Models with Satellite Remote Sensing Data

Thesis directed by Professor William J. Emery

The angular distribution of radiation scattered by the earth surface contains information on the structural and optical properties of the surface. Potentially, this information may be retrieved through the inversion of surface bidirectional reflectance distribution function (BRDF) models. This thesis details the limitations and efficient application of BRDF model inversions using data from ground- and satellite-based sensors.

A turbid medium BRDF model, based on the discrete ordinates solution to the transport equation, was used to quantify the sensitivity of top-of-canopy reflectance to vegetation and soil parameters. Results were used to define parameter sets for inversions. Using synthetic reflectance values, the invertibility of the model was investigated for different optimization algorithms, surfaces and sampling conditions. Accurate solutions were obtained in all cases except for an overhead sun, an optically-thick canopy and sampling geometries exclusively in the orthogonal plane. Surface state parameters (e.g., spectral albedo, absorbed radiation) were retrieved more reliably than model parameters.

Inversions were also conducted with field data from a ground-based radiometer. First, a soil BRDF model was inverted for different soil and sampling conditions. A condition-invariant solution was determined and used as the lower boundary condition in canopy model inversions. Canopy parameters were retrieved accurately when reflectance was sampled under preferred conditions (spectral and angular). Estimates of shortwave albedo and surface absorbed radiation were also accurate; estimates of canopy absorbed radiation exceeded measured values.

Finally, a scheme was developed to improve the speed and accuracy of inversions. The scheme weights empirical data with the partial derivative of angular reflectance with respect to a model parameter. Inversions with data from the satellite-based Advanced Very High Resolution Radiometer

(AVHRR) were conducted with this scheme. The inversions accurately retrieved leaf area index and leaf optical properties.

This research relied extensively on data from the First International Satellite Land Surface Climatology Project (ISLSCP) Field Experiment (FIFE). This experiment was conducted on grasslands near Manhattan, Kansas. Results can provide a foundation for inversions of BRDF models on a larger scale.

Formal references for much of this work are, or will be, available as indicated below.

Privette, J. L., Myneni, R. B., Tucker, C. J. and Emery, W. J. (1994), Invertibility of a 1-D discrete ordinates canopy reflectance model, *Remote Sens. Environ.*, 48:89-105.

Privette, J. L., Myneni, R. B., Emery, W. J. and Pinty, B. (1995), Inversion of a soil reflectance model for use in vegetation BRDF models, *J. Geophys. Res.* (in print, expected late 1995, FIFE Special Issue II).

Privette, J. L., Myneni, R. B., Emery, W. J. and Hall, F. G. (1996), Optimal sampling conditions for estimating grassland parameters via reflectance model inversions, *IEEE Trans. Geosci. Remote Sens.* (in print, expected January, 1996).

Privette, J. L., Emery, W. J., and Schimel, D. S. (1996), Inversion of a vegetation reflectance model with NOAA AVHRR data, *Remote Sens. Environ.* (submitted, October, 1995).

Dedication

For 12 years, I have loitered in the halls of higher education.

During this time, many talented professors have patiently shared the burden of my formal education. I truly believe some of these individuals to be among the brightest there are. Still, the greatest lessons I have learned in life have been least associated with formal instruction. Infinitely more important than the results to be found in these pages, or most others, are the lessons of Myrtle Tyson Privette and George G. McClelland. It is in reverence and humble adoration that I dedicate this thesis to my grandmother and grandfather.

Regarding their wisdom as eternal, I feel both honored and obligated to share it here. However, because their footsteps no longer grace this earth, my grandparents cannot be consulted for reference. As my own words would undoubtedly do injustice, I defer to the thoughts of a more seasoned poet who, I must assume, shared my grandparents' vision:

> To laugh often and much; to win the respect of intelligent persons and the affection of children; to earn the appreciation of honest critics and endure the betrayal of false friends; to appreciate beauty; to find the best in others; to leave the world a bit better, whether by a healthy child, a garden patch or a redeemed social condition; to know even one life has breathed easier because you have lived. This is to have succeeded.
>
> — Ralph Waldo Emerson

If these seem the sentiments of angels and saints, then Emerson successfully captured in pen that which I witnessed in actions. For it is precisely these, an angel and a saint, that I believe I knew and loved as Grandmother and Granddad.

Acknowledgments

First and foremost, this dissertation would not exist without the love and support I have received from my family. From offering advice when I was a tentative freshman to listening patiently when I rambled on as a doctoral student, their encouragement has been endless. When my confidence wavered, theirs was unfailing. It is my hope that some of the wisdom they have imparted to me is manifest in the pages which follow.

My friends deserve far greater acknowledgment than can be provided here, however I thank them (particularly the Billvillians) for the great hikes, ski trips, bike rides, hockey games, stimulating discussions (some even non-political!) and—most importantly—sincere friendships. Besides ensuring we were familiar faces at the restaurants and coffee houses throughout Boulder, they were always quick to place a beer in my hands when work threatened to become an obsession. An extra "thank you" goes to Dan, Waleed, Ray and Barb, Chuck, Gary, Cindy and Richard, and a long distance thanks goes to Tash (Go Blue!), Ranga, Paul P., Jaby and Rich. In different ways, each of them has contributed to my education and happiness.

Credit is also due to my doctoral committee members: Bill Emery (Advisor), Brian Curtiss, Bob Leben, Ranga Myneni, Dave Schimel and Carol Wessman. Even after a lifetime of work, I will remain but a student of their knowledge and expertise. Extra thanks goes to two members. Besides being my advisor, Bill academically and financially supported my various endeavors—whether in the Pacific Ocean, in Europe, or just down the hall. Although our disagreements were at times infamous, I truly believe they stimulated better research. Despite his own busy research, Ranga kindly agreed to work with an aimless student intern at Goddard in June, 1992. Since that time, he has simultaneously managed to be a fair critic, patient mentor, and good friend. Stated simply, my understanding of and fascination with science took a leap upon meeting him.

I gratefully acknowledge the financial sponsorship of the U.S. Department of Energy through the Graduate Fellowships for Global Change, administered by the Oak Ridge Institute for Science and Education. Financial support has also been provided by the Department of Aerospace Engineering Sciences at U. of Colorado and a NASA EOS/IDS program under the leadership of Bob Dickinson. Some of this work was completed during internships at various laboratories. I thank Bob Dickinson (NCAR), Jim Tucker (NASA/GSFC) and Bernard Pinty (U. Blaise Pascal, France) and their staffs for the wonderful opportunities and experiences.

A large number of scientists, most associated with the FIFE campaign, have helped provide the data or algorithms used in my work. These persons include Ranga Myneni, Forrest Hall, Piers Sellers, Don Strebel, Dan Kimes, Jon Ranson, Robert Fraser, Eric Vermote, Didier Tanré, Brian Markham, Fred Huemmrich, Scott Goetz, Yuangui Li and James McManus at NASA/GSFC; Betty Walter-Shea, Mark Mesarch, Blaine Blad and Cindy Hays at U. of Nebraska; Bob Dickinson, Wim Van Leeuwen and Alfredo Huete at U. of Arizona; Andres Kuusk at Estonian Acad. of Sci.; Stephane Jacquemoud at U. of Paris; Wilfred Brutsaert of Cornell U.; S. M. Glenn of Oklahoma Biological Survey; D. J. Gibson of Southern Illinois U.; A. Retta, G. Harbers, L. Ballou and the staff of the Evapotranspiration Laboratory at Kansas State U.; the staff of NOAA/NESDIS; Dave Schimel and Timothy Kittel of NCAR; Gudrun Schlüessel of U. of Hamburg; and Ray Kokaly, Keith Oleson and Richard Slonaker of U. of Colorado. In many cases, overworked and underpaid graduate students (or undergrads) helped collect data that now bears only their advisors' names. My doctoral work could not have been completed without the efforts of these individuals.

Finally, it would be criminal to write a dissertation on BRDF model inversions without acknowledging the substantial contributions of Narendra Goel, now at Wayne State University (MI). Dr. Goel and his colleagues pioneered this area of research beginning in 1983. Their seminal papers have educated and provided a foundation for many students and professionals, especially me.

CONTENTS

TABLES

FIGURES

CHAPTER I

INTRODUCTION

In the present climate of environmental uncertainty, significant emphasis has been placed on process models (e.g., biogeochemistry, ecosystem, and climate) to predict the impact of both natural and anthropogenic forcing. This attention has prompted increasingly detailed treatments of various model subsystems and the relationships between them. Parallel to these developments has been the demand for more accurate and comprehensive earth system data. These data are required for both model initialization and result validation [Sellers, 1993].

Soil and vegetation properties strongly affect the transfer of energy, mass, momentum and trace gases between the earth's surface and atmosphere. Thus, process models rely on accurate surface data for meaningful results. For example, global fields of rainfall, temperature and motion in General Circulation Models (GCMs) are affected by surface albedo [Shukla and Mintz, 1982]. Studies suggest this albedo must be accurate to within ±0.05 [Henderson-Sellers and Wilson, 1983]. Such accuracy requires some knowledge of the vegetation cover [Dickinson, 1983].

Other important climatological variables, such as momentum exchange rates, are directly related to plant morphological properties such as leaf area index (LAI), leaf angle distribution (LAD), and vegetation roughness [Sellers et al., 1986]. Similarly, photosynthetically active radiation absorbed (APAR) by vegetation is correlated with photosynthetic rates and plant growth in the absence of limiting stresses [Monteith, 1972]. In part, photosynthetic rates determine the amount of carbon fixed by leaves and hence affect the carbon cycle and net primary production.

Since surface conditions vary in both space and time, measurements over large regions (e.g., mesoscale and global) must be made at a relatively high frequency (e.g., biweekly). This is a formidable task. Due to economic and accessibility constraints, satellite remote sensing is currently

the only practical means for obtaining such measurements. Nevertheless, the determination of relevant variables from remote sensing data remains an inexact science.

Because satellites effectively travel through a vacuum, only electromagnetic (EM) or gravitational events may be detected [Verstraete et al., 1994]. Earth surface remote sensing depends only on the former. Three EM spectral regions—optical, thermal and microwave—have been used to obtain surface information. In land applications, thermal remote sensing has primarily been used to assess surface temperature and hydrological properties such as potential evapotranspiration and canopy conductance [Taconet et al., 1986]. Although microwave frequencies are not climatologically important, they appear useful for assessing vegetation structure and water content, biomass and soil moisture. Since some microwave frequencies are relatively unaffected by atmospheric conditions, their use may prove particularly valuable in cloudy areas. Nevertheless, optical remote sensing (0.4-3.0 μm) appears to hold the most promise. There are at least two significant reasons for this. First, unique interactions between organic molecules and shortwave radiation provide useful spectral signatures. Second, since optical radiation is reflected rather than emitted, changes in the source (sun) and sensor positions result in angular signatures. Optical methods have been used to estimate LAI, biomass, fraction of APAR (fAPAR), stomatal conductance, and potential evapotranspiration, among other variables. The potential for unraveling additional information from optical radiation warranted the present investigation.

Either correlative or physically-based techniques may be used to determine surface information from optical data. Correlative techniques rely on empirical or intuitive relationships between surface conditions and measured radiation. They are computationally efficient but may be site or sampling condition dependent. Physically-based techniques rely on radiative transfer models which relate fundamental surface parameters (e.g., LAI, leaf optical properties) to scene reflectance. While computationally more expensive, physical models permit the simulation of all radiatively active media (e.g., background, canopy and atmosphere). Below, applications of both techniques are briefly discussed.

Most correlative techniques utilize spectral reflectance information. For example, simple transforms of red and near-infrared (NIR) reflectance—particularly the Normalized Difference Vegetation Index (NDVI) [Tucker et al., 1985]—have been used to assess LAI, biomass, fAPAR, and vegetation health. The second derivative of reflectance spectra can be used to assess LAI and fAPAR [Hall et al., 1990]. Recently, spectroscopic techniques have been used to determine biochemistry and canopy physiology [Wessman, 1994]. Absorption peak parameters such as width, depth, skewness and symmetry allow assessment of leaf water, cellulose, lignin, chlorophyll and other pigments. By comparing field spectra to laboratory leaf spectra, species identification has been possible. Moreover, the fractional contributions of scene end members (macroscopic reflectance classes such as soil, vegetation, and shade) may be estimated.

Temporal and spatial correlative techniques may be grouped together as scene models—multiple spatial samples are required for application. Temporal transforms rely on the profile of spectral reflectance with time. They have been used to determine species information, stage of growth and vegetation health [Badhwar et al., 1982]. Spatial information may also be used, although growth patterns—including row structure in agricultural areas—are poor discriminators of species [Gerstl and Simmer, 1986]. Hybrid correlative methods have also been developed. For example, spectral and temporal techniques were combined to create the tasseled-cap transformation of Kauth and Thomas [1976]. This method traces the growth of vegetation in multispectral space.

Physically-based optical techniques have primarily utilized the angular distribution of scattered radiation. Angular distributions can be interpreted via surface Bidirectional Reflectance Distribution Function (BRDF) models, which predict directional reflectance for a given solar position and set of parameters. Through inversion, BRDF models have been used to estimate morphological (e.g., LAI, LAD) and optical (leaf reflectance and transmittance, soil single scattering albedo) properties [Goel, 1988]. Upon parameter determination, some BRDF models can also simulate the change in surface state parameters (e.g., albedo, fAPAR) over diurnal cycles.

Recently, some efforts have been directed toward combining BRDF and leaf spectral reflectance models [Jacquemoud, 1993]. By utilizing multidirectional and multispectral information, these hybrid

models may allow the simultaneous retrieval of canopy morphology and some leaf constituents. To date, however, high spectral resolution radiometers which point off-nadir have been regulated to aircraft. Finally, some studies suggest that optical polarization data may contain useful information [Vanderbilt et al., 1991]. Again, however, instruments which measure the polarization of optical radiation have yet to be placed in orbit.

In the development of surface data sets for process models, physically-based techniques may be superior to correlative techniques. First, since they are based on radiative transport theory, physical models can be modular such that specific interactions (e.g., photon interactions with topography, atmosphere, soil, plant organs, litter, snow, etc.) may be selectively included. Hence, these models can be adapted for any climate or geographic area. Second, physical models can be comprehensively validated with ground truth data. Similarly, model parameters may be fixed with measured or intuitively reasonable values such that reflectance behavior of particular canopies can be inferred. Third, physical models allow the retrieval of biologically or climatologically important properties and states. Finally, physical models require fewer parameters to describe scattering characteristics over multiple frequencies since physical laws and some parameters (e.g., LAI) are spectrally invariant [Strahler, 1994]. Nevertheless, there have been few applications of physically-based models to satellite data for the retrieval of surface parameters.

The present research was undertaken to determine the limitations of and an efficient method for BRDF model inversions. *A priori*, this study was limited to grassland applications. Grasslands cover approximately 16% of earth's land surface (Figure 1.1) and account for nearly 10% of the its net productivity [Coombs et al., 1985]. In addition, some results suggest grasslands are one of the most climatologically sensitive earth covers [David Schimel and Ranga Myneni, personal communication]. Thus, grasslands may be early indicators of a changing climate. Probably the most comprehensive effort to analyze and measure a grassland system occurred during the First International Satellite Land Surface Climatology Project (ISLSCP) Field Experiment (FIFE) [Sellers et al., 1988]. This campaign—conducted non-continuously from 1987 through 1993—included the coordinated measurement of surface and atmospheric properties by ground, aircraft and satellite-based sensors. FIFE

data were used extensively in the present study. This allowed unprecedented validation of BRDF inversion methods and results.

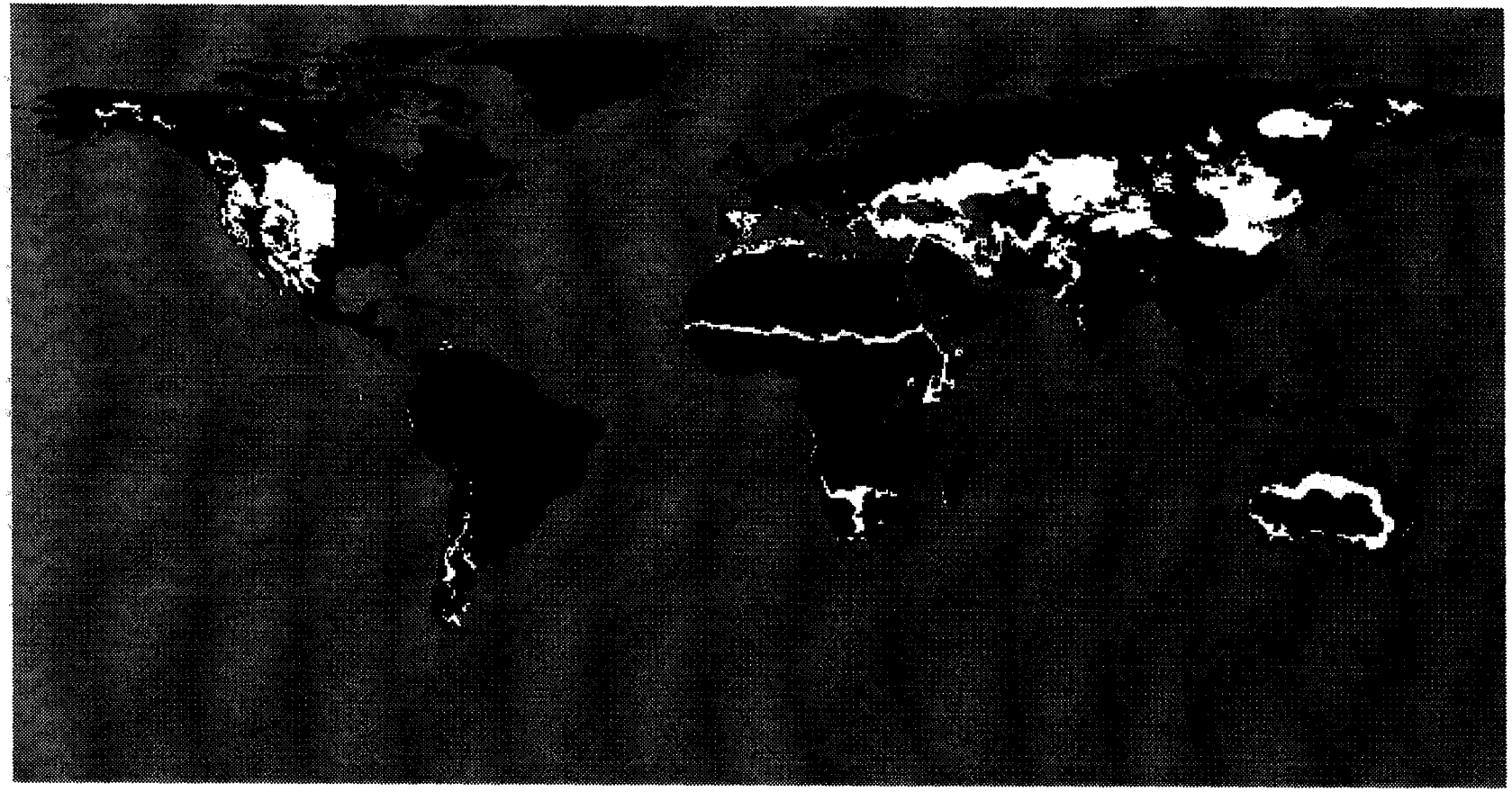

Figure 1.1. Approximate locations of natural grasslands (yellow) and tundra (red) on earth.

Our goal was to develop a method for the accurate and efficient inversion of a BRDF model with satellite remote sensing data. However, the canopy BRDF model utilized in this study had previously not been inverted. Therefore, an incremental approach was pursued as follows. First, the invertibility of the model was demonstrated for a series of standard problems using error-free synthetic data. Next, a soil BRDF model, employed as the lower boundary condition in the canopy model, was inverted using field data from a ground-based radiometer. Values for five spectrally invariant parameters were determined; these soil parameters were fixed in the canopy model. One spectrally dependent parameter, soil single scattering albedo, remained variable. The coupled soil and canopy BRDF model was then inverted with field data from a ground-based radiometer. Results suggested that inversions with satellite data were possible. Anticipating increased noise in satellite data, a scheme was developed to improve the speed and accuracy of inversions. In this scheme, empirical data are differentially weighed, depending on sun-target-sensor geometries, to determine the solution. Finally, the weighting scheme was applied to model inversions with data from the Advanced Very High Resolution Radiometer (AVHRR).

The specific outline of this thesis is as follows. In Chapter II, formal and practical definitions of the inversion problem are developed. In Chapter III, criteria used to determine an appropriate BRDF model are discussed and details of the chosen model are presented. In Chapter IV, the sensitivity of top-of-canopy (TOC) reflectance to model parameters is determined for a range of optical depths (LAI). In addition, different optimization algorithms for model inversions are assessed. In Chapter V, analyses of different spectral bands, view angles, and solar angles for model inversions are detailed. In addition, the impact of reflectance data errors and satellite sampling geometries is evaluated. In Chapter VI, the FIFE campaign and its relevant data sets are discussed. In Chapter VII, the lower boundary condition for the FIFE canopy model is determined. This chapter includes an analysis of reflectance sampling requirements for a semi-physically-based soil model. In Chapter VIII, a coupled soil and vegetation model is inverted with ground radiometer data from FIFE. The accuracy of retrieved parameters is investigated with respect to spectral band and solar angle. In addition, fAPAR and albedo estimates are formulated and compared with empirical data. In Chapter IX, previous results are combined into an

operational inversion strategy for AVHRR data. This requires a reduction in the number of adjustable model parameters. In addition, the estimation of site-wide parameters is described. Finally, a method for differentially weighting individual reflectance samples is introduced. Using AVHRR data, critical input parameters (e.g., LAI, leaf reflectance) for earth process models are retrieved. In Chapter X, conclusions and recommendations for future work are outlined.

CHAPTER II

INVERSE CANOPY MODELING

A. Formalization of Remote Sensing System

As discussed by Goel [1988], the optical remote sensing environment may be modeled as a series of subsystems, including:

a) the solar source, defined by a set of parameters $\{a_i\}$ including spectral intensity, $I(\lambda)$, and location, (θ_s, ϕ_s), where θ_s represents the solar zenith angle (SZA) and ϕ_s represents the solar azimuth angle,

b) the atmosphere, defined by a set $\{b_i\}$ of properties including spatially dependent concentrations and spectrally dependent optical properties,

c) the vegetation canopy, defined by a set $\{c_i\}$ including optical and structural properties of vegetation components (leaves, stalks, stems, etc.), planting geometry and distribution, and environmental properties (temperature, humidity, wind speed, precipitation),

d) the background or soil, defined by a set $\{d_i\}$ of properties such as optical properties, roughness, texture, and moisture profile, and

e) the radiation sensor, defined by a set $\{e_i\}$ of properties which may include spectral sensitivity, aperture, calibration, and view geometry (θ_v, ϕ_v), where θ_v represents the view zenith angle (VZA) and ϕ_v represents the view azimuth angle.

Most parameters in these subsystems have a spectral dependence and many have a spatial and temporal dependence. The set $\{R_i\}$ of radiation properties detected by a sensor is therefore dependent on the spectral, spatial, angular, dielectrical and temporal properties of $\{a_i\}$, $\{b_i\}$, $\{c_i\}$, $\{d_i\}$ and $\{e_i\}$, i.e.,

$$\{R_i\} = f(a_i, b_i, c_i, d_i, e_i). \qquad (2.1)$$

The determination of parameter values (e.g., $\{c_i\}$) from radiation properties may be conceptualized as,

$$\{c_i\} = g(R_i, a_i, b_i, d_i, e_i). \quad (2.2)$$

This is referred to as the *inverse problem*, where $\{c_i\}$ are the retrieved parameters.

B. Conceptual Description of the Inversion Problem

For the purposes of this work, it is assumed that the solar, atmospheric and sensor parameters are known and their effects can be modeled, and that $\{R_i\}$ is limited to spectral radiance (or directional reflectance), R_i. Therefore, Equation (2.1) is reduced to

$$R_i = f(c_i, d_i; a_i, b_i, e_i), \quad (2.3)$$

where $\{a_i\}$, $\{b_i\}$, and $\{e_i\}$ are effectively fixed.

The state variables $\{c_i, d_i\}$ of the surface transport equation describe the distribution, orientation and optical behavior of the scatterers. If f is non-time dependent, the state variables must remain invariant during the collection of R_i. Clearly, if $\{c_i, d_i\}$ contains p members, then at least $n = p$ independent equations in form of Equation (2.3) are required to uniquely determine the state variables. However, if the subsystems $\{a_i\}$, $\{b_i\}$, and $\{e_i\}$ do not change, then only one independent equation exists. In this case, the system is unsolvable [Verstraete et al., 1994].

To determine $\{c_i, d_i\}$, additional independent equations must evolve from variations in solar, atmospheric and/or sensor parameters. Assuming horizontal homogeneity of the surface, the solar zenith and azimuth angles (θ_s, ϕ_s), view zenith and azimuth angles (θ_v, ϕ_v) and sensor spectral wavelength (λ) are the most controllable or readily determined parameters. By changing one or more of these parameters for each sample, a system of independent equations can be formed [adapted from Verstraete et al., 1994],

$$\begin{aligned} R_1 &= f(c_i, d_i; a_{i,1}, b_{i,1}, e_{i,1}) \\ R_2 &= f(c_i, d_i; a_{i,2}, b_{i,2}, e_{i,2}) \\ &\vdots \\ R_n &= f(c_i, d_i; a_{i,n}, b_{i,n}, e_{i,n}). \end{aligned} \quad (2.4)$$

If $n < p$, this system is underdetermined and more samples are necessary. If $n = p$, there is normally no unique solution due to model and measurement inaccuracies. If $n > p$, there is no single solution because the system is overdetermined. In this case, however, a statistically "best" solution can be determined.

C. Practical Description of the Inversion Problem

For most physically-based models, convolutions in f preclude a simple form of g as conceived in Equation (2.2). Hence, iterative techniques must be employed to solve the system (Equation 2.4). In practice, four main components are required, including: 1) measured angular reflectance (R_j) with the associated measurement parameters ($a_{i,j}$, $b_{i,j}$, $e_{i,j}$), 2) a BRDF model (f), 3) an optimization algorithm, and 4) a figure-of-merit function (or simply, "merit function").

During model inversion, the optimization algorithm iteratively adjusts the vegetation and soil parameters $\{c_i, d_i\}$ until the modeled reflectance most closely resembles the measured reflectance (Figure 2.1). The merit function provides a numerical measure of this "resemblance." In most cases, a least-squares function [Goel and Strebel, 1983], ε^2, is utilized,

$$\varepsilon^2 = \sum_{j=1}^{n} w_j \, [R_j - R_j^*]^2 \qquad (2.5)$$

where R_j is the spectral reflectance for a given scan and solar angle geometry, R_j^* is the geometrically-analogous model estimate, and w_j is a weighting function value. In some studies, the difference term in Equation (2.5) is divided by the measured reflectance [Nilson and Kuusk, 1989]. Assuming the reflectance data are relatively noise-free and the BRDF model is reasonably accurate, the parameter values minimizing ε^2 represent those of the surface from which the reflectance data were measured.

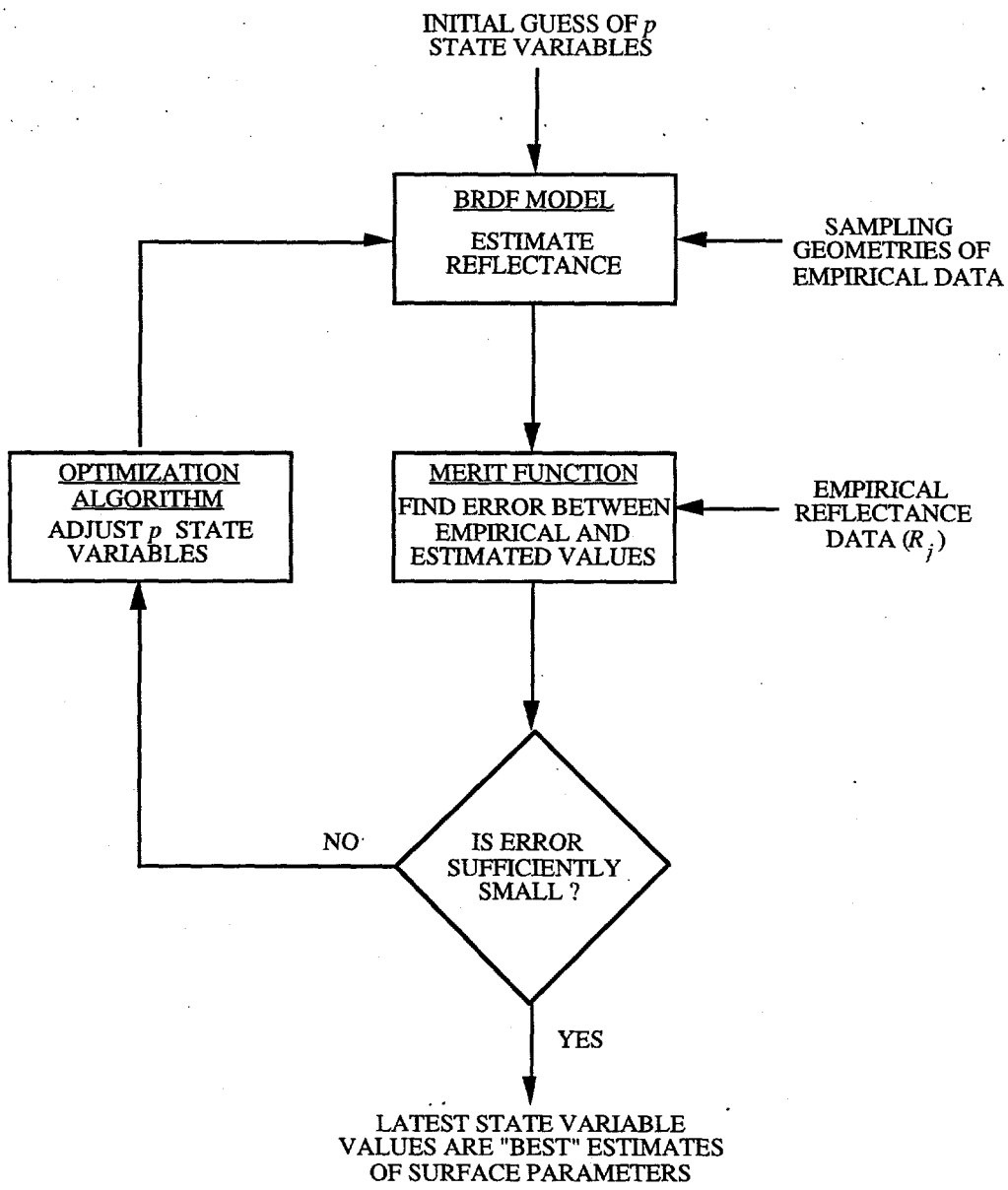

Figure 2.1. Flow diagram of the BRDF inversion problem.

Only reflectance data from visible and NIR spectral bands are sufficiently uncorrelated such that independent equations can evolve due to wavelength differences. To form additional equations for the system (Equation 2.4), variations in sun-target-sensor geometry are required [Sellers et al., 1993]. In this study, variations in sampling geometry were used exclusively in creating data sets (R_j , j = 1, 2, ..., n) for inversion.

CHAPTER III

THE BIDIRECTIONAL REFLECTANCE MODEL

A. Definition

Reflectance from natural media is anisotopic (i.e., a function of direction). A BRDF model mathematically describes this anisotropy. Specifically, it predicts the magnitude of radiation scattered into an infinitesimal cone at a given direction by a medium illuminated by an infinitesimal cone of radiation at a second given direction. Hence, the BRDF model determines "bidirectional" reflectance.

At least three scattering processes—coherence, surface and volume—may contribute to bidirectional reflectance [Strahler, 1994]. Coherence occurs when the mean free path of multiple scattering is similar in size to the wavelength. Although Hapke et al. [1993] suggest that photon-stomatal interactions may cause coherent effects (strong backscattering peaks), present vegetation BRDF models do not simulate this. Both surface and volume scattering are modeled, however. Surface scattering includes both shadowing effects and scatterer specular reflectance. Shadowing depends on the geometric size of the scatterers relative to their spatial orientation. The hot spot phenomenon—a reflectance peak in the retro-solar direction—is caused by the absence of shadowing at low phase angles. Specular reflectance is primarily important for leaves due to their waxy outer layer. Volume scattering generally refers to multiple scattering and is scale dependent. While some models simulate volume scattering within a single leaf, others generalize the volume scattering over optically semi-infinite soil or vegetation.

At the macroscopic scale, the convolution of surface and volume scattering effects is largely governed by the optical properties and geometrical orientation of the scatterers. In most cases, reflectance and transmittance of plant organs (e.g., leaves, stems, and bark) and soil particulates (e.g.,

mineral and organic matter) compose the relevant optical properties. Structural aspects include the soil particulate shape, size and distribution (and the complementary interstices characteristics), the plant organ composition, shape, size, orientation and distribution within the plant, and the shape, size, orientation and distribution of plants within a spatial resolution element of the sampling instrument. Litter or thatch, defined as the dead organic material on the soil surface, also affects surface reflectance. Both optical and structural properties may vary spatially and temporally due to growth stages (e.g., budding, blossoming, senescence), climatic conditions (e.g., wind, soil moisture, precipitation events, temperature) and anomalous events (e.g., anthropogenic disturbances, disease, animal and insect infestation).

B. Review of BRDF Model Development and Classes

Since the earliest canopy model was formulated in 1954 [Monsi and Saeki], a large number of surface BRDFs have been developed [Myneni and Ross, 1991]. The models may be grouped according to five classes: empirical, geometrical, turbid medium, hybrid, and computer simulation models.

Empirical models are based on simple mathematical functions which can assume the form of realistic reflectance distributions. Although "layers" of functions may be added to specifically accommodate scattering phenomena (e.g., the hot spot), the mathematics is not physically-based. Empirical models by Walthall et al. [1985], Roujean et al. [1992] and Rahman et al. [1994] have been inverted for the estimation of surface albedo and/or for the correction of surface anisotropy.

Geometrical models simulate heterogeneous scenes with geometrical objects (e.g., cones, spheroids, ellipsoids, cubes) protruding from a surface [e.g., Otterman, 1984; Li and Strahler 1985; 1992; Jasinski, 1990]. Optical behavior of the objects is constant or simplified. Reflectance anisotropy is determined primarily by the fractions and spatial orientation of shaded and sunlit surfaces (both canopy and ground) for a particular sun-target-sensor geometry. Geometrical models have been inverted to retrieve canopy structure [Li and Strahler, 1985; Wu and Strahler, 1994; Hall et al., 1994] and optical information [Otterman et al., 1987].

Turbid medium models simulate a canopy with a cloud of infinitesimal platelets having the optical properties of plant organs (most commonly leaves) [Shifrin, 1953]. Although the platelets are randomly distributed within plane-parallel layers, their angular distribution can be prescribed according to the LAD of true canopies [Ross and Nilson, 1966]. The models generally include single and multiple scattering; the former is determined quasi-analytically, while the latter must be approximated. Drawbacks of the turbid medium approach include the absence of scattering behavior caused by the finite size of actual scatterers (e.g., shading) and the non-random orientation of scatterers (e.g., leaf clumping). Recent advances [Marshak, 1989; Verstraete et al., 1990; Myneni and Ganapol, 1991; Kuusk, 1994] have compensated for these shortcomings. Turbid medium models are particularly appealing due to their mathematical simplicity and hence computational efficiency. Many have been inverted, most notably by Goel and his colleagues [Goel, 1988, and references therein], Camillo [1987], Pinty, Verstraete and their colleagues [1989; 1990; Dickinson et al., 1990; Iaquinta and Pinty, 1994], Kuusk and his colleagues [1991b; 1994; Nilson and Kuusk, 1989], Liang and Strahler [1994a-b], and Privette and his colleagues [1994a; 1994c; Schluessel et al., 1994].

Hybrid models combine the spatial heterogeneity of geometrical models with the realistic transport treatment of turbid medium models. This permits the simulation of gap probabilities and path length distributions along with single and multiple scattering [e.g., Norman and Welles, 1983; Li et al., 1994]. Nevertheless, this complexity results in relatively high computational expense. Thus, operational inversions of these models appear impractical.

Computer simulation models represent the latest approach to the heterogeneous BRDF problem. These models rigorously trace photon interactions with an arrangement of discrete scatterers. Although computationally expensive, these models accurately simulate within-canopy spatial heterogeneity (e.g., organ size distributions, leaf clumping, gaps) and scene-scale heterogeneity (e.g., topography). Other models must either neglect or approximate these conditions with quasi-empirical formulations. While several models have been developed [Ross and Marshak, 1988; Goel et al., 1991; Borel et al., 1991; Lewis and Muller, 1992], their computational expense reduces the likelihood that they will be adopted for inversion applications [Antyufeev and Marshak, 1990].

C. Specification of a Lower Boundary Condition

Although the earliest canopy models assumed a semi-infinite optical depth [Ross, 1981], their generalization to finite optical depths required the specification of a lower boundary condition. The simplest solution was a Lambertian reflector. The importance of specifying the Lambertian reflectance correctly is clear given the characteristic differences in soil and vegetation spectra—particularly over the red and NIR wavelengths [Tucker and Miller, 1977].

Nevertheless, the anisotropy in soil reflectance is also well known [Irons et al., 1992]. Similar to vegetation bidirectional reflectance, it has been modeled using empirical parameterizations [Walthall et al., 1985], Monte Carlo techniques [Cooper and Smith, 1985], and formulations based on the radiative transfer equation for semi-infinite media [Hapke, 1981; Pinty et al., 1989; Jacquemoud et al., 1992]. Others have attempted to model soil bidirectional reflectance using erect geometric shapes that cast shadows [e.g., Norman et al., 1985; Cierniewski, 1987]. Studies dedicated to the inversion of soil models include Pinty et al. [1989], Deering et al. [1990], Jacquemoud et al. [1992], Irons et al. [1992] and Privette et al. [1994b].

Presently, few vegetation BRDF models include anisotropic soil reflectance. Notable exceptions include the ray tracing model of Kimes et al. [1985b], the Monte Carlo model of Cooper and Smith [1985], and the turbid medium models of Norman et al. [1985], Myneni et al. [1992], Schluessel et al. [1994], and Liang and Strahler [1994b]. Naturally, models without anisotropic soil reflectance are less accurate under low LAI conditions.

D. Model Choice and Description

The selection of a physical-based BRDF model for the present study was guided by three primary criteria. First, the limitations to the BRDF inversion problem were sought. This required that the model be highly accurate—possibly at the expense of computational efficiency. Moreover, it

required a model based on measurable parameters such that validation was possible. Second, since grasslands are effectively horizontally homogeneous at the resolution of environmental radiometers, a one dimensional (1-D) formulation was sufficient. A 1-D model only allows surface variability in the vertical direction. Finally, because grassland canopies are generally not optically semiinfinite, the ability to specify a lower boundary condition was necessary.

Based on these criteria, two turbid medium models by Myneni were utilized [Myneni et al., 1988; Myneni et al., 1992]. CANTEQ is a 1-D BRDF model based on the discrete ordinates solution to the radiative transfer equation [Shultis and Myneni, 1988; Stewart, 1990]. In benchmark comparisons, the discrete ordinates method was found to be four digit accurate. The model has been validated against reflectance data from soybean [Myneni et al., 1988], maize [Myneni et al., 1988], prairie grassland [Asrar et al., 1989] and several other agricultural crops [Stewart, 1990].

CANTEQ depends primarily on measurable physical properties. Specifically, canopy depth is specified with the LAI parameter. The statistical orientation of platelets in the turbid medium is specified according to the LAD of the simulated canopy. Although CANTEQ originally simulated five idealized LADs (planophile, erectophile, plagiophile, extremophile, and uniform), a later extension utilizes the continuous Beta distribution [Goel and Strebel, 1984]. The Beta distribution depends on four parameters ($\mu(\theta)$, $\nu(\theta)$, $\mu(\varphi)$, $\nu(\varphi)$) which may be determined analytically from leaf angle data. Leaf reflectance anisotropy is modeled by combining diffuse and specular phase functions. Diffuse scattering is bi-Lambertian [Ross, 1981]; its magnitude depends on the leaf reflectance (ρ) and transmittance (τ). Specular leaf reflectance depends on the refractive index (η) [Vanderbilt and Grant, 1985; Nilson and Kuusk, 1989]. A canopy hot spot approximation is also included by adjusting the canopy extinction coefficient for the once-scattered radiation [Marshak, 1989; Stewart, 1990]. The magnitude of the hot spot is specified with the HSP parameter.

A Lambertian soil represents the lower boundary condition. Thus, model validity is reduced in low LAI conditions. The upper boundary condition includes direct solar irradiance plus isotropic diffuse irradiance. The relative magnitudes are specified by the ratio (γ) of direct-to-total irradiance. Fractions of absorbed and reflected radiation are determined based on energy balance arguments. In addition,

canopy photosynthetic efficiency (CPE) values can be calculated via a semi-empirical leaf physiology model [Collatz et al., 1991] coupled to the BRDF model. CPE is the ratio of carbon fixed by the canopy (μ mol CO_2) per incident PAR energy (μ mol photons). The physiology model was developed for C_3 species and gives net photosynthesis as a function of environmental and leaf parameters and stomatal conductance.

The discrete ordinates method is used to solve the radiative transport equation. In this method, photons are restricted to travel in a finite number of directions. These directions are chosen to be the ordinates of a quadrature scheme such that the angular integrals are evaluated accurately. The spatial derivative is approximated by a finite difference scheme, resulting in a system of algebraic equations which can be solved by iteration on the scattering integral. Methods to accelerate this iteration are also included in CANTEQ. All calculations in this study utilized six ordinates per octant for a total of 48 directions in the unit sphere.

DISORD is a 3-D successor to CANTEQ. It too accounts for all surface and volume scattering mechanisms and includes a hot spot formulation. In addition to allowing horizontal heterogeneity, DISORD differs from CANTEQ in its boundary conditions. In DISORD, both may be anisotropic. Anisotropic soil reflectance is simulated using the turbid medium model of Jacquemoud et al. [1992]. This model is a function of six parameters, five of which may be considered spectrally independent. The upper boundary condition is specified with an atmospheric model. This model presently includes Rayleigh and aerosol scattering but neglects gaseous absorption. Note that isotropic diffuse irradiance was assumed throughout this study. Since DISORD was developed after the present research had begun, both CANTEQ and DISORD were utilized. Here, DISORD was used in 1-D mode.

Throughout this study, R denotes a hemispherical directional reflectance factor (HDRF) (Nicodemus, 1970). An HDRF is the ratio of radiance scattered by a surface in a given direction to the radiance scattered by a lossless Lambertian reflector, i.e.,

$$R(\theta_v, \phi_v) = \mathrm{HDRF}(\theta_v, \phi_v) = \pi L(\theta_v, \phi_v) / E , \qquad (3.1)$$

where $L(\theta_v, \phi_v)$ [W m^{-2} sr^{-1}] denotes the surface scattered radiance and E [W m^{-2}] denotes the irradiance. Although most BRDF models estimate radiance for a unit solid angle, physical sensors must integrate radiance over finite solid angles. Hence, in comparisons with empirical data, it is assumed that

$$R(\theta_v, \phi_v) = \int_{\varphi_v - \Delta\varphi}^{\varphi_v + \Delta\varphi} \int_{\theta_v - \Delta\theta}^{\theta_v + \Delta\theta} R(\theta, \phi) \cos\theta \sin\theta \, d\theta \, d\varphi. \qquad (3.2)$$

Single "effective" wavelengths are also assumed. For readability, individual $R(\theta_v, \phi_v)$ and the distribution of $R(\theta_v, \phi_v)$ are both referred to as "reflectance."

CHAPTER IV

PRELIMINARY ISSUES ON MODEL INVERTIBILITY

Although *a priori* information may be mathematically formulated to assist in solving the inverse problem, the solution is otherwise based strictly on the minimization of the merit function—the physical sensibility of the solution is not assessed. If a correct solution is not obtained, the model may not be invertible (i.e., the relationship between reflectance and model parameters is not one-to-one) for the given problem configuration [Goel, 1988]. Two conditions are required for model invertibility: the solution must be unique, and the solution must be stable. The uniqueness of a solution is determined by the presence and severity of local minima in the model parameter space. These minima represent incorrect parameter sets for which model estimates resemble the measured data. Solution stability requires that the global minimizer not change significantly for reasonable errors in the data.

The stability and uniqueness of a solution may be compromised by data overdetermination. Overdetermination occurs when too many model parameters are used to determine the reflectance behavior. In a forward execution of the model, this is unimportant. In an inverse problem, it is very important. Parameters which do not sufficiently affect the top-of-canopy (TOC) radiance cannot be retrieved from reflectance data. Their values at the global minimum are therefore inconsequential. This results in a poorly defined minimum. Moreover, since these "excess" parameters are not well determined by the data, low noise levels in the data may significantly alter their retrieved values. Clearly, these concerns imply that only the most influential model parameters should be adjusted during an inversion. The determination of an appropriate parameter set can be accomplished through a sensitivity study. Besides reducing the probability of non-sensible solutions, a smaller parameter set also reduces the time necessary to minimize the merit function.

A. General Sensitivity Study

The sensitivity of CANTEQ was tested over a wide range of canopy conditions. The method implemented required forward computation of a large number of synthetic reflectance sets. Bias was eliminated by using a random number generator to produce parameter values within reasonable and physically plausible limits. Reflectance was recorded at 15° intervals in VZA (0-75°) and 45° intervals in azimuth (0-180°) (26 total directions). For a given synthetic canopy, each parameter was in turn perturbed by 10% of its theoretical range and a new reflectance distribution was computed. The sum of squares of differences between the original reflectance and the perturbed reflectance was recorded. This statistic was used to indicate the model's sensitivity to that parameter.

This exercise was conducted for 400 synthetic canopies at two different SZAs (5 and 30°). Canopies were binned by LAI in intervals of 0.25 for $0 < LAI < 2$, and 0.5 for $2 < LAI < 5$. For each bin, principal component analysis was performed on the sum of squares of differences. Since the first principal component axis, by definition, was in the direction of maximum variance, the numerical weighting of each parameter's contribution to that axis provided a measure of the model's relative sensitivity to the parameters.

The results of this analysis are shown for red and NIR wavelengths in Figures 4.1a-b. While the graphs are qualitatively similar, close inspection reveals important differences. As might be expected, soil reflectance is most important in thin canopies (low LAI). At red, LAI is nearly as influential as soil reflectance in determining TOC reflectance. At NIR, however, it is significantly less influential. The highly absorbing leaves at red wavelengths decrease the effects of soil on TOC radiance, whereas at NIR the highly scattering leaves have considerably less impact on the soil contribution. In both cases, leaf optical properties have relatively minor influence in thin canopies. With increasing LAI, sensitivity to leaf optical properties increases and sensitivity to soil reflectance and LAI decreases. The sensitivity curves cross at about $LAI = 1.0$ for both wavelengths. This suggests that for canopies of $LAI < 1.0$, soil reflectance and LAI are most influential in determining TOC reflectance, whereas for $LAI > 1.0$, leaf optical properties (reflectance and transmittance) are most

influential. Beyond an LAI of about 2.0, TOC reflectance is essentially insensitive to perturbations in LAI or soil reflectance. This insensitivity has been observed in empirical data for all spectral bands at sufficiently high LAI [Chance and LeMaster, 1977]. These sensitivities are consistent with those found by Goel et al. [1984] using SAIL [Verhoef, 1984] and a more theoretical sensitivity analysis.

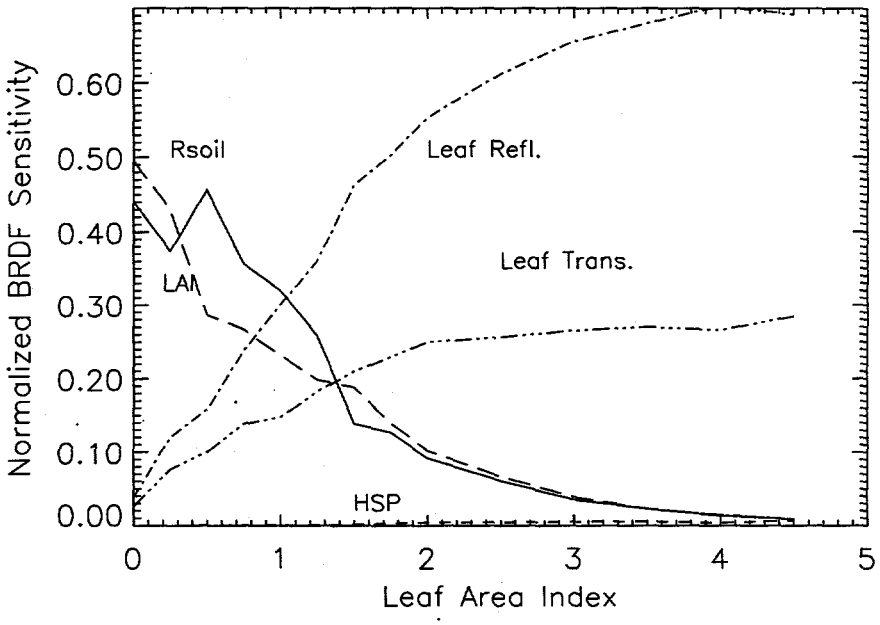

Figure 4.1a. Normalized reflectance sensitivity to five model parameters for increasing LAI at red wavelengths.

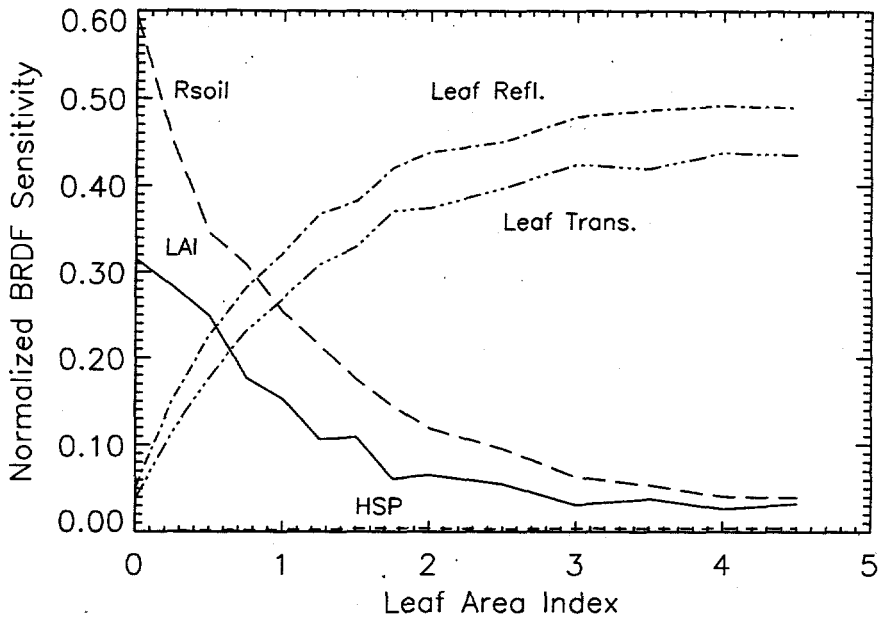

Figure 4.1b. Same as Figure 4.1a, but for NIR wavelengths.

The NIR and red results differ significantly for optically thick canopies. In the red case, TOC reflectance is considerably more sensitive to leaf reflectance than to transmittance. Since the leaf albedo at red is low, it is highly probable that irradiance will be absorbed in one of the upper leaf layers. Even if a photon penetrates to the lower layers or to the soil, there is a high probability that it will be absorbed on its upwelling travel. Therefore, the influence of perturbations in leaf transmittance is minimized by high leaf absorption. For the same reason, the multiply scattered component of red TOC radiance is insignificant compared to the once-scattered component. Since only multiply scattered radiation emanates from shaded areas, red TOC reflectance drops off markedly beyond the hot spot area. Shaded areas are not visible to the sensor at low phase angles (i.e., near the hot spot). In the NIR, TOC reflectance is nearly equally sensitive to perturbations in leaf reflectance and transmittance. Multiple scattering is significant at NIR wavelengths. Thus, if a photon penetrates the canopy and is reflected at a lower leaf level or the soil, there remains a relatively high probability that it will exit the canopy top. Since both the leaf reflectance and transmittance determine this probability, both

parameters significantly influence TOC reflectance. The asymptotic tendency of the curves suggests that sensitivities remain approximately the same for canopies of LAI > 3.0. It appears that TOC reflectance is rather insensitive to perturbations in the hot spot parameter for most canopies.

B. Selection of an Optimization Algorithm

Upon establishing model sensitivity, the inversion problem can be addressed. The task of adjusting model parameters until the merit function is minimized is regulated to a multidimensional optimization algorithm. Broadly, algorithms may be classified according to their reliance on function derivatives. Generally, merit functions which are non-differentiable, or for which finite-difference derivatives are computationally expensive, are minimized most efficiently with non-derivative based optimization algorithms. While such algorithms operate only on merit function values, most attempt to infer derivative information via other techniques. Merit functions with analytical or computationally inexpensive derivatives may be inverted with more efficient algorithms which require derivative information.

Accurate, physically-based BRDF models such as CANTEQ are non-differentiable and relatively computationally expensive. This implies a non-derivative based optimization algorithm is most efficient. However, recent studies suggest that no single algorithm is superior for all inversion scenarios [Jacquemoud et al., 1994]. Although somewhat burdensome, determining the most efficient algorithm may require a series of experiments with different routines. Thus, three commonly used minimization routines were tested here: a downhill simplex method [Nelder and Mead, 1965; subroutine AMOEBA from Press et al., 1986], a conjugate direction set method [subroutine POWELL from Press et al., 1986], and a quasi-Newton method [subroutine E04JAF from Numerical Algorithms Group, 1990].

Although complete algorithm description is beyond the scope of this thesis, differences between the three deserve some attention. The simplex method requires initial specification of the p + 1 simplex vertices in the p-parameter space. Beginning with the vertex producing the largest merit

function value (poorest fit), the algorithm attempts to find a lower merit function position by reflecting the vertex through the face of the simplex. If the new merit function value is lower than those of all other vertices, a larger reflection is attempted. If the original reflection does not represent an improvement over the second worst vertex, the simplex contracts by moving the worst vertex closer to the others. This is repetitively continued. When all $p + 1$ vertices produce fits to within a user-defined tolerance, the program terminates. While simplex theory may be less sophisticated than others, it is considered robust and useful for discontinuous functions or functions subject to numerical inaccuracies [Numerical Algorithms Group, 1990].

Beginning from a single initial position, the conjugate direction set method conducts single line minimizations, accurate to within a user-defined tolerance, in each of the current p conjugate directions to arrive at the minimum for a given iteration. It then compares the current minimum to the previous iteration's minimum. If the two estimates are within a second user-defined tolerance of each other, the program terminates. If the difference is greater than the allowed tolerance, the conjugate directions are redefined based on the vector between the two minima, and another iteration is executed.

The NAG quasi-Newton algorithm is similar to the direction set method in that it accumulates function information based on successive line minimizations. The two differ in the way they gather and store this gradient information. Unlike the direction set method, the quasi-Newton algorithm approximates the second partial derivative (Hessian) matrix at each iteration based on information for the latest search direction. This algorithm is efficient but intended for continuous functions with continuous first and second partial derivatives [Numerical Algorithms Group, 1990]. In contrast to the direction set and simplex algorithms, NAG E04JAF does not allow a user-defined termination criteria.

In the following experiment, the optimization algorithms were judged on two criteria. First, the algorithm needed to correctly determine the global minimizer given error-free reflectance data. This required that the routine avoid local "traps" (minima) and proceed even when the slope of the merit function was small. The former condition is difficult to achieve since there presently are no error-free numerical techniques for distinguishing a global minimizer from a local (non-global) minimizer.

Second, if multiple algorithms find the global minimizer, the algorithm which does so with the fewest model evaluations (least computational expense) is preferable.

In this study, the ability to specify termination criteria proved to be important. Figure 4.2 illustrates typical performances (change in $\log[\varepsilon^2]$ with number of function evaluations) of the three routines. The NAG routine consistently gave the poorest performance. In several inversions using synthetic reflectance data, the NAG routine terminated when the solution was incorrect. This may be the result of having to use predefined rather than user-specified termination criteria. Furthermore, in cases where the NAG solution was correct, several thousand function evaluations were often required. The direction set method, in allowing user-specified tolerances, permitted tuning such that the routine could find the correct solution. However, this tuning often resulted in an excessive number of function evaluations. The simplex algorithm consistently produced the best results. In cases where the quasi-Newton method produced incorrect solutions and where the direction set method produced the correct solution but required several thousand function evaluations, the simplex method efficiently found the correct solution in 500 to 600 function evaluations. The superiority of the simplex algorithm suggests the merit function may not have continuous first and second partial derivatives. Based on these findings, the simplex algorithm was used exclusively for all subsequent inversions of CANTEQ and DISORD.

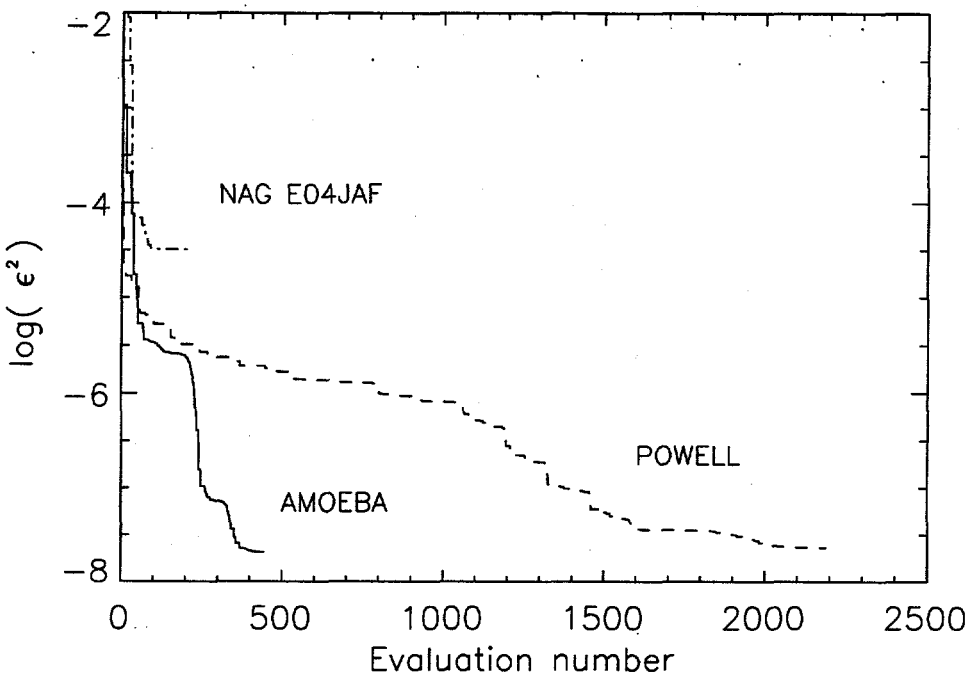

Figure 4.2. Typical convergence efficiencies, as shown by the log of the merit function, for optimally-tuned minimization routines AMOEBA, POWELL, and NAG E04JAF. The correct solution was (LAI = 3.0, HSP = 4.0, ρ = 0.0607, τ = 0.0429, Soil Refl. = 0.2). The inversion solutions were AMOEBA (3.0, 4.1, 0.0608, 0.0426, 0.19), POWELL (3.0, 4.0, 0.0607, 0.0430, 0.20), and E04JAF (0.1, 2.0, 0.0001, 0.0001, 0.03). The initial parameter estimates for POWELL and E04JAF were the same.

C. Conclusions

Using a novel application of principal component analysis, the sensitivity of a TOC reflectance was determined for canopies of arbitrary optical depth. In general, the TOC reflectance was primarily sensitive to soil reflectance and LAI for LAI < 1. For canopies of LAI > 1.5, reflectance was primarily sensitive to leaf optical properties. At red wavelengths, this sensitivity was significantly greater for leaf reflectance than for leaf transmittance. The sensitivities were nearly equal at NIR wavelengths. Sensitivity to HSP was low for all canopies

Three common optimization routines were also assessed. None of the routines required function derivatives. A simplex routine consistently minimized the merit function in the fewest number (500-600) of model evaluations. As CANTEQ (or DISORD) requires approximately 2 s to

execute on a Sun Sparcstation 10, a complete inversion may be completed in less than 20 min. Moreover, this routine appears less vulnerable to local minima traps than the others.

CHAPTER V

THE INVERTIBILITY OF A DISCRETE ORDINATES REFLECTANCE MODEL

A. Domain of Applicability

In practice, the invertibility of a BRDF model is not guaranteed [Goel, 1988]. For example, multiple parameter sets may produce the minimum value of the merit function. Moreover, the merit function may exhibit insufficient variation such that the optimization routine will fail. Therefore, before CANTEQ is inverted with empirical reflectance data, it is useful to determine its invertibility using synthetic, error-free data.

In this study, synthetic reflectance data were created through forward model calculations. Directional reflectances at 15° VZA (0-75°) and 45° view azimuth angle (0-180°) intervals were calculated. Since the reflectance of 1-D models is symmetric about the principal plane, data in the third and fourth octants provide no new information. In addition to reflectance, absorbed radiation, spectral albedo and canopy photosynthetic efficiency (CPE; at red wavelengths only) were evaluated [Myneni et al., 1992]. A standard atmosphere was assumed such that 80% of the incident irradiance was direct radiative flux.

A base case canopy was defined by assigning parameters values representative of those generally encountered in practice. An SZA of 30° and a uniform LAD were assumed. Variations to the base case were created by assigning widely varying but reasonable parameter values, one at a time. Conditions in the base and variation cases at red and NIR wavelengths are given in Tables 5.1 and 5.2, respectively. Note that leaf optical properties were varied only for the red wavelength. Since LAD was not variable in these inversions, one planophile (erectophile) case denotes that although the reflectance

distribution was calculated with a planophile (erectophile) LAD, the inversion was attempted assuming a uniform LAD.

Table 5.1. Parameter values for the base case and its variations at red wavelengths. Base case values were used where data are absent. Leaf optical data from birch and maple trees provided by Forrest Hall [personal communication].

Case	Description	SZA (°)	LAD	LAI	HSP	ρ	τ	Soil Refl.
1	Base Case	30	Uniform	3.0	4.0	0.0607	0.0429	0.200
3	Dark Soil							0.075
5	Low LAI			1.0				
7	High LAI			8.0				
9	Doubled Opt. Prop.					0.1214	0.0858	
10	Halved Opt. Prop.					0.0304	0.0215	
11	High Sun	5						
13	Low Sun	60						
15	Planophile LAD		Planophile					
17	Planophile LAD		Planophile (uniform for inversion)					
19	Erectophile LAD		Erectophile					
21	Erectophile LAD		Erectophile (uniform for inversion)					

Table 5.2. Same as Table 5.1, but for NIR wavelengths.

Case	Description	SZA (°)	LAD	LAI	HSP	ρ	τ	Soil Refl.
2	Base Case	30	Uniform	3.0	4.0	0.4357	0.5089	0.350
4	Dark Soil							0.150
6	Low LAI			1.0				
8	High LAI			8.0				
12	High Sun	5						
14	Low Sun	60						
16	Planophile LAD		Planophile					
18	Planophile LAD		Planophile (uniform for inversion)					
20	Erectophile LAD		Erectophile					
22	Erectophile LAD		Erectophile (uniform for inversion)					

Note that perfect results were unlikely since the synthetic reflectance values were truncated at the fourth decimal place. The truncation was employed for two reasons: a) the computational results are unstable past four decimal places over different machines, and b) current field reflectance measurements are not accurate past four decimal places. Therefore, minor discrepancies are to be expected in the retrieved parameters.

Inversion results for red are shown in Figures 5.1a-d. In general, most parameter values are retrieved to within about 5% of their correct values. Significantly larger errors occurred in five cases. In Case 7, denoting a dense canopy (LAI = 8.0), the inversion overestimates LAI by 23% and underestimates soil reflectance by 23%. This is not surprising since this canopy is optically semi-infinite; the TOC reflectance is relatively insensitive to LAI in such cases (Figure 4.1a). In Case 10,

denoting dark leaves (leaf optical properties halved), the inversion underestimates leaf transmittance by 100% and overestimates the hot spot parameter by 9%. The large leaf transmittance error is understandable considering the highly absorbing leaves and hence the minor contribution of radiance scattered from lower canopy levels. In Case 11, denoting near normal solar incidence, only LAI and leaf reflectance are retrieved with reasonable accuracy (5% and 8%, respectively). Generally, azimuthal symmetry increases as SZA decreases. Thus, the information content of the reflectance distribution also decreases [Goel and Strebel, 1983; Shultis and Myneni, 1988]. In Cases 17 (planophile) and 21 (erectophile), an incorrect LAD caused significant errors. Indeed, only leaf reflectance and LAI (Case 17 only) are retrieved to within 10% of their correct values. Therefore, in the present inversion configuration, prior knowledge of the actual LAD may be necessary.

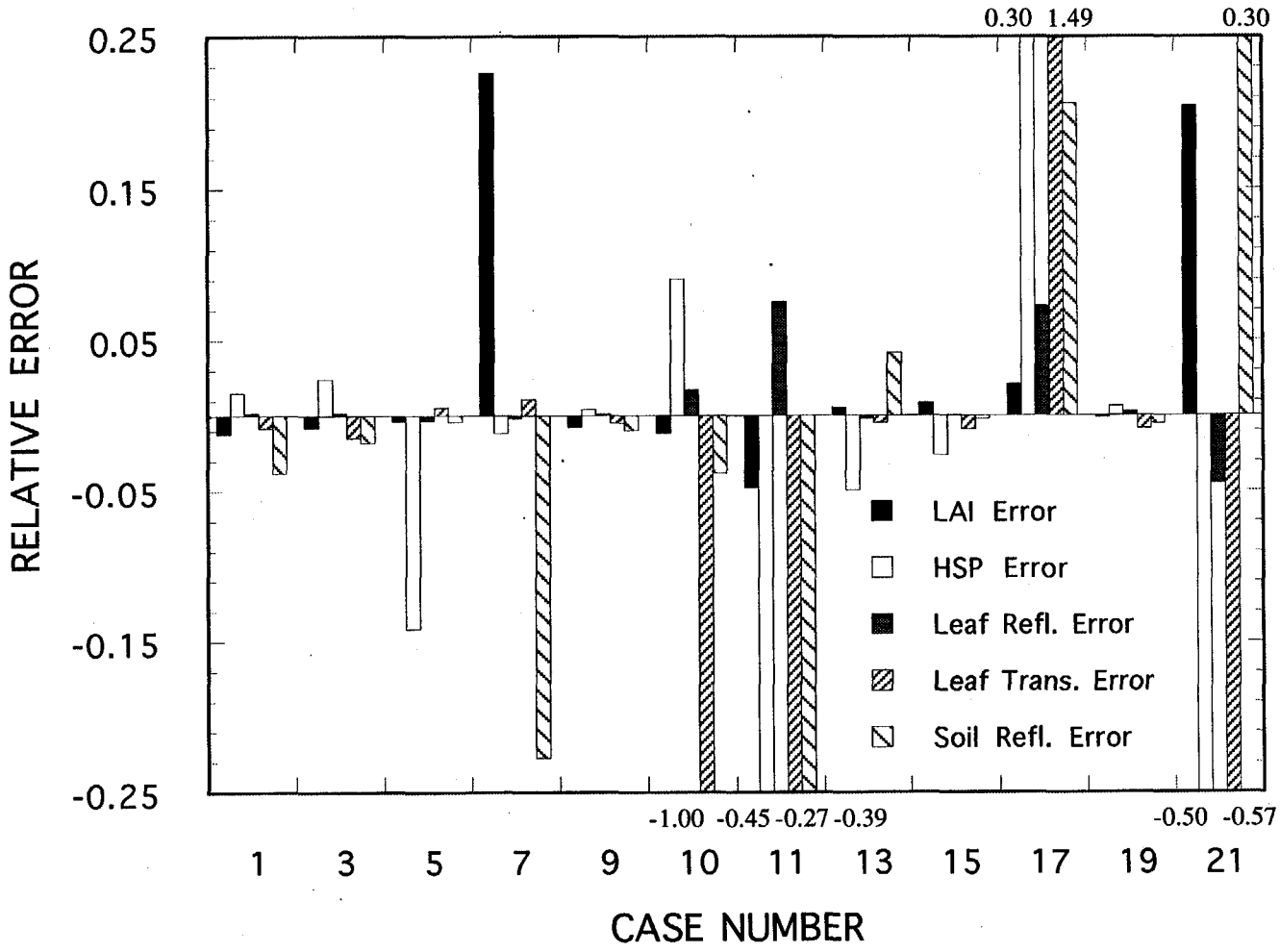

Figure 5.1a. Relative errors in retrieved parameters for perturbation cases at red wavelengths.

"Retrieved" and correct spectral albedo, fAPAR and CPE are shown in Figures 5.1b-d. The retrieved surface state values were determined by forward execution of the model using retrieved parameter values. While spectral albedo estimates are highly accurate (below 0.5% relative error), small errors are evident in fAPAR (up to 10%) and CPE estimates (up to 11%). Of particular importance are Cases 7, 10, 11, 17 and 21. Despite significant errors in retrieved parameters, the surface state variables are well estimated in these cases.

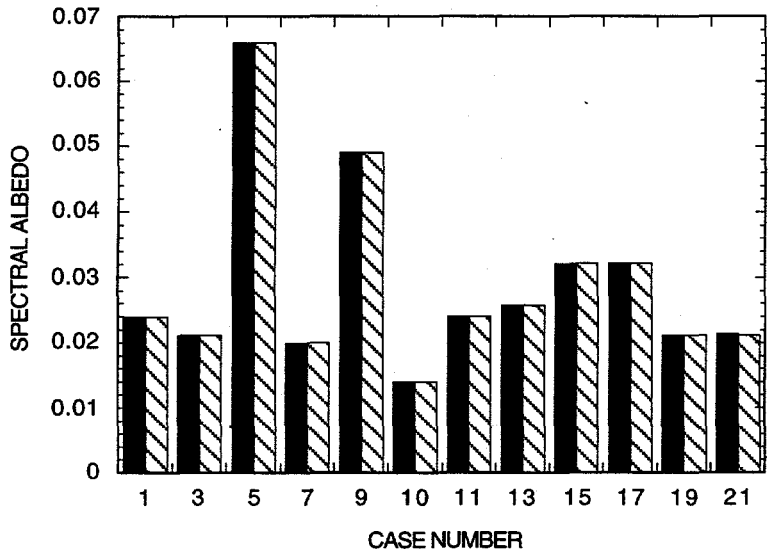

Figure 5.1b. Comparison of retrieved and actual spectral albedo for red wavelength cases. Black bars represent retrieved values, hatched bars represent actual values. Case descriptions are given in Table 5.1.

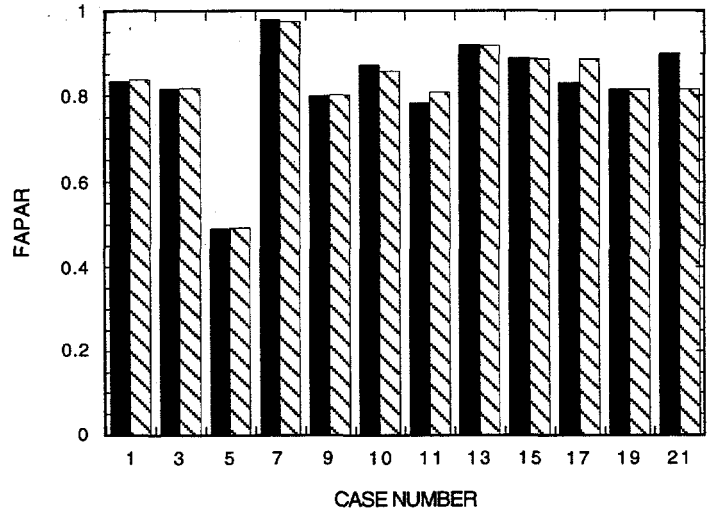

Figure 5.1c. Same as Figure 5.1b, but for fAPAR.

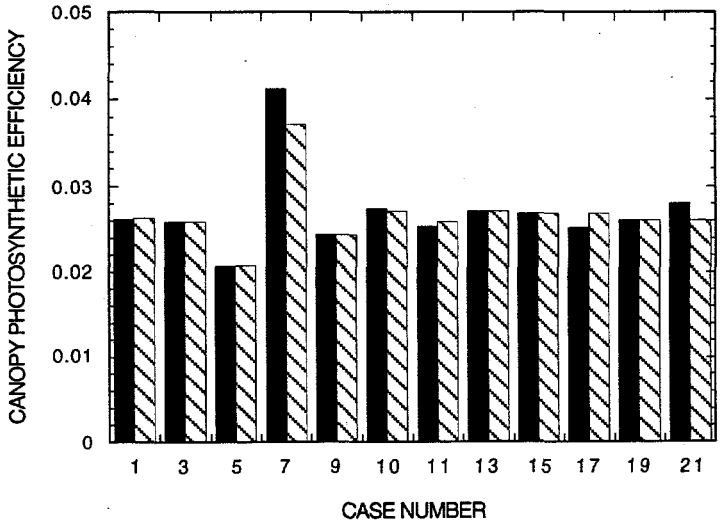

Figure 5.1d. Same as Figure 5.1b, but for canopy photosynthetic efficiency (CPE).

Relative errors in retrieved parameters at NIR wavelengths are shown in Figure 5.2a. Soil reflectance (16 to 67% relative error) is systematically overestimated in all cases since scattering by

leaves dominates TOC reflectance. This is a result of the relative difference in leaf and soil albedo. The difficulty in accurately retrieving NIR soil reflectance is well documented [Goel and Thompson, 1984a; 1984c]. The remaining parameters are generally retrieved to within 5% of their correct values. As might be expected, cases which are problematic in the red are similarly problematic in the NIR. Specifically, a near normal solar incidence and the use of an incorrect LAD produce the largest errors. While a near normal solar incidence yields an LAI overestimation of 23% in the red, an underestimation of 27% occurs in the NIR.

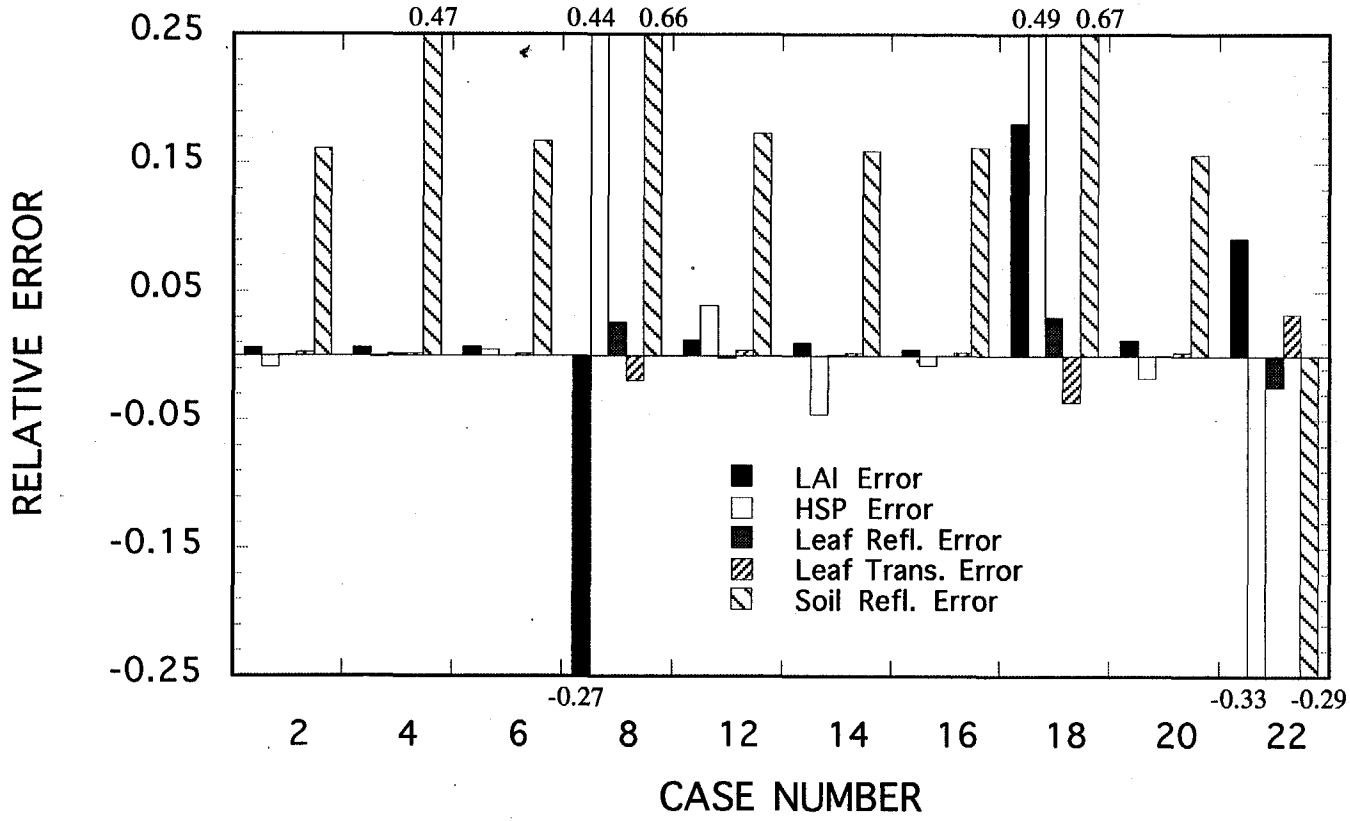

Figure 5.2a. Relative errors in retrieved parameters for perturbation cases at NIR wavelengths.

Differences in the NIR spectral albedo and fraction of absorbed radiation (fANIR) are shown in Figures 5.2b-c. The retrieved spectral albedo values are highly accurate (below 1% relative error) in all cases while fANIR estimates are generally reasonable. The worst case, in which a uniform LAD is incorrectly assumed (planophile is correct), produces a 38% relative error.

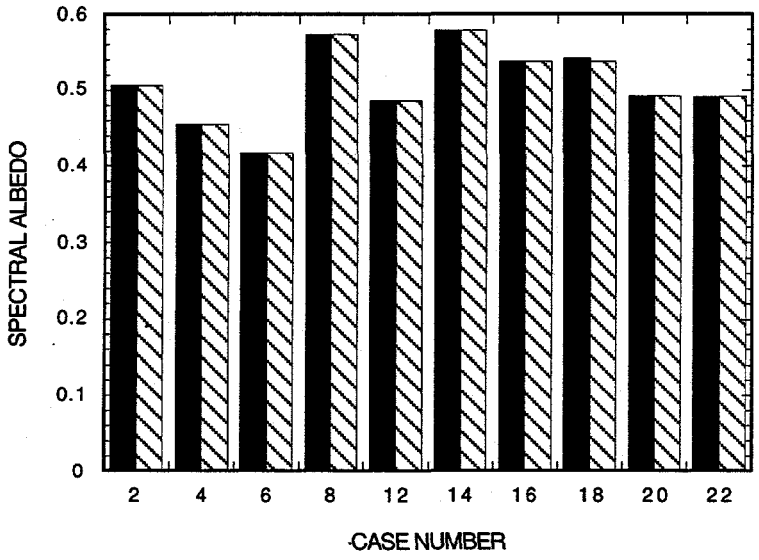

Figure 5.2b. Comparison of retrieved and actual NIR spectral albedo for NIR wavelength cases. Black bars represent retrieved values, cross-hatched bars represent actual values. Case descriptions are given in Table 5.2.

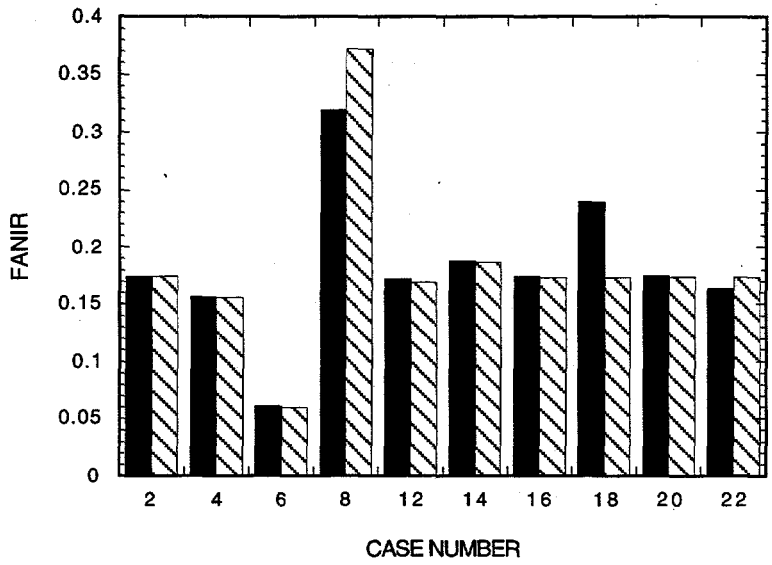

Figure 5.2c. Same as Figure 5.2b, but for fANIR.

B. Solution Dependence on Sampling Geometry

Presently, reflectance data at equal angular increments of 15° zenith and 45° azimuth are not available from satellite borne instruments. Therefore, model invertibility with sampling geometries of existing and planned satellite systems was assessed. Three geometries were investigated here: the planned Multi-angle Imaging SpectroRadiometer (MISR) [Diner et al., 1989] sampling geometry in the principal azimuthal plane (i.e., nine VZAs in the plane defined by the sun, target, and target zenith), the MISR geometry in the orthogonal plane (vertical plane perpendicular to the principal plane), and the afternoon sampling geometries of the NOAA-11 AVHRR. The latter were realized for a nine day period and an earth target at 40° N latitude. The view angles were in and around the principal plane. For this study, only the red and NIR base cases were considered.

While the AVHRR sensor is advantageous due to its large view angles, daily sampling, and current operational mode, the necessity of using samples collected over multiple days is not ideal.

Indeed, the temporal invariance of a true canopy is neither certain nor expected. Moreover, the minimum Ground Instantaneous Field Of View (GIFOV) of 1.2 km^2 may result in subpixel heterogeneity for which a 1-D model cannot account. While a unique SZA should apply to each sample, a single value (30°) was used here. The use of multiple SZAs has been shown to improve results [Goel et al., 1984], however canopies exhibiting heliotropism may violate the assumption of temporal invariance [Kimes and Kirshner, 1983].

Figure 5.3a (red wavelengths) shows relative errors in the retrieved parameters for the sampling geometries. Although errors are low (< 5%) for both geometries, they are lower for the MISR geometry in the principal plane compared to the full hemisphere geometry. This probably occurs because TOC reflectance is most characteristic in the principal plane [Kuusk, 1991a]. Thus, additional samples off the principal plane may have a negative effect by decreasing the per-sample information content. It is not surprising then that errors are largest (up to 50% relative) for the MISR geometry perpendicular to the principal plane. Finally, the AVHRR geometry produces reasonably small errors (less than 8% relative).

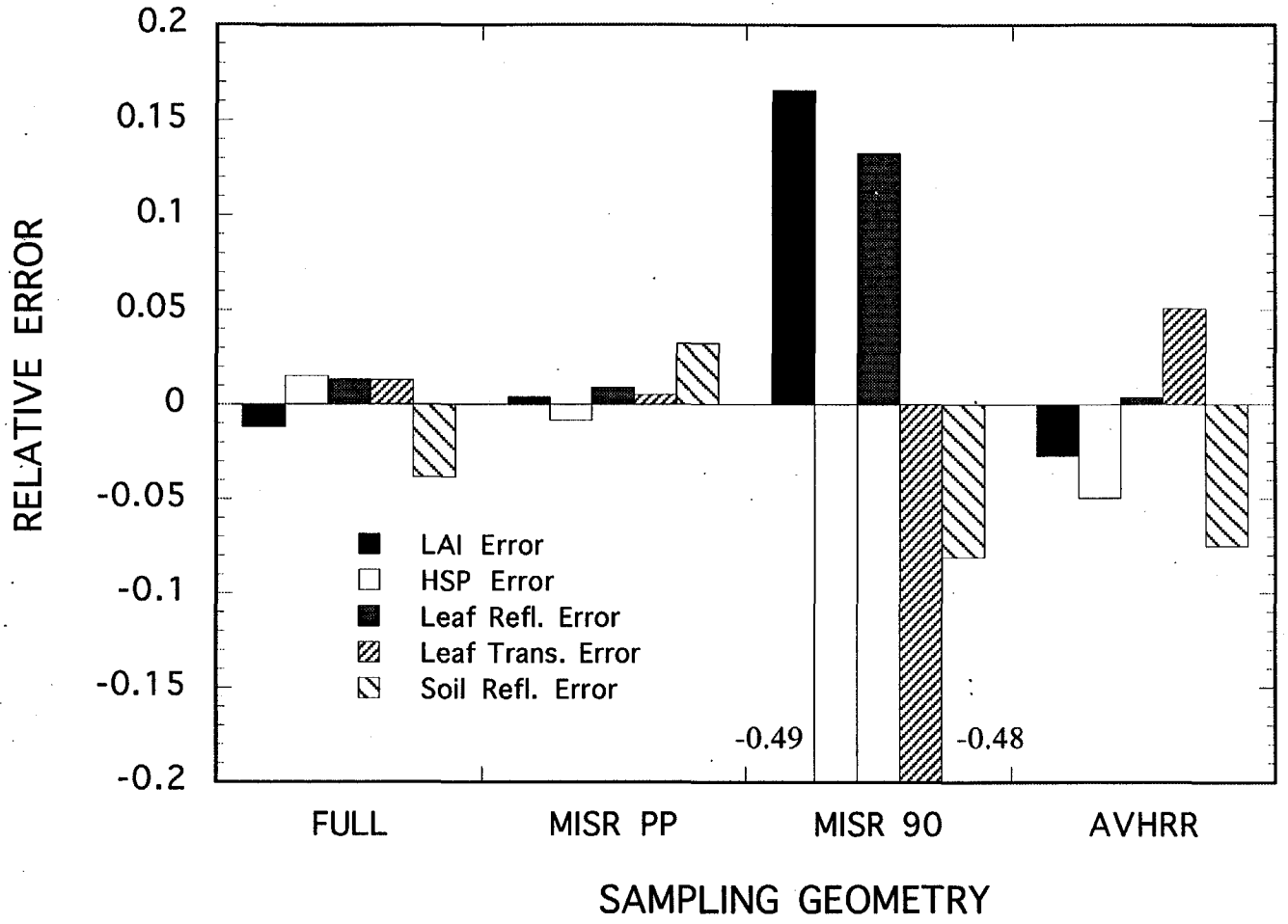

Figure 5.3a. Relative errors in base case inversions at red wavelengths using sampling geometries representing equal angular increments of 15° zenith and 45° azimuth (FULL), MISR view zenith angles in the principal plane (MISR PP), MISR view zenith angles perpendicular to the principal plane (MISR 90), and 9 days of NOAA-11 AVHRR afternoon passes (AVHRR).

Differences between correct and retrieved spectral albedo, fAPAR and CPE values are shown in Figures 5.3b-d. Surface states parameters appear to be more stable than the canopy parameters as evidenced by their relatively small errors (less than 5%). Excluding the MISR geometry perpendicular to the principal plane, all relative errors are below 1%.

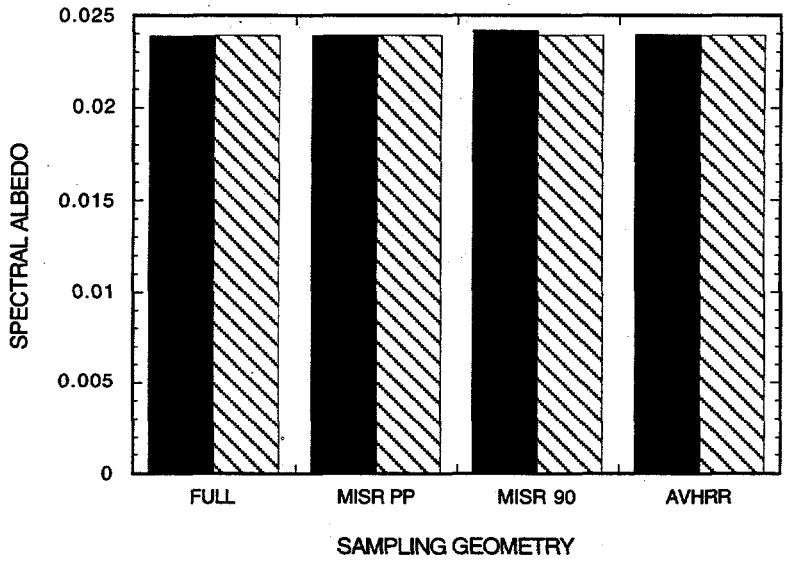

Figure 5.3b. Retrieved and actual spectral albedo at red wavelengths for different sampling geometries. Descriptions of sampling geometries are as in Figure 5.3a. Black bars represent retrieved values, hatched bars represent actual values.

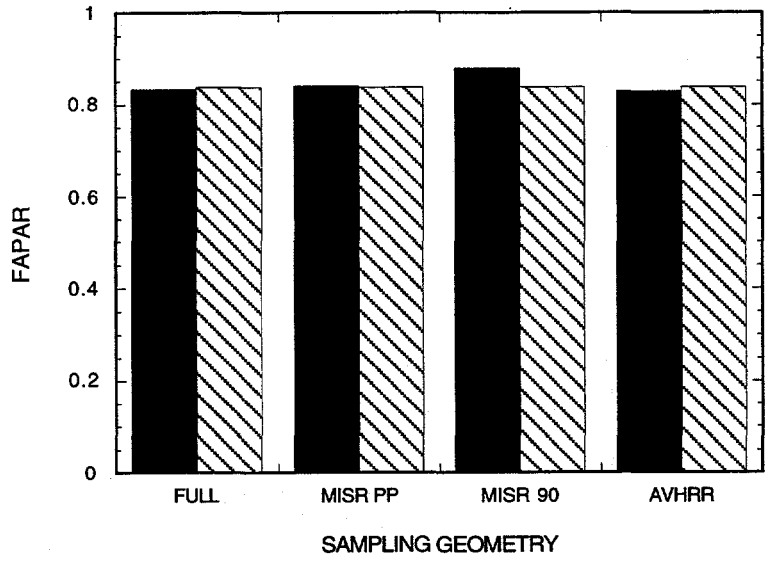

Figure 5.3c. Same as in Figure 5.3b, but for fAPAR.

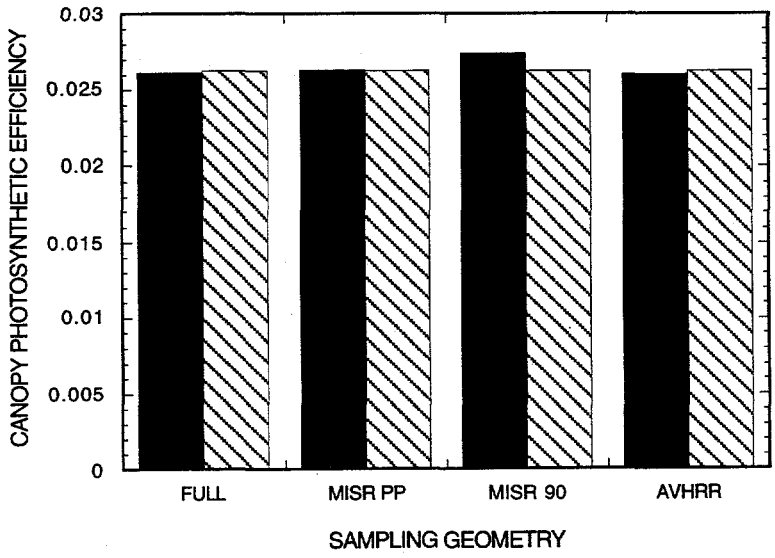

Figure 5.3d. Same as Figure 5.3b, but for canopy photosynthetic efficiency (CPE).

Relative deviations in canopy parameters at NIR are shown in Figure 5.4a. As in Section A, soil reflectance is overestimated (up to 17%). Again, sampling perpendicular to the principal plane results in the largest errors. However, excluding soil reflectance, all errors are below 10% for all geometries. Excluding the MISR geometry perpendicular to the principal plane, errors are below 2%. As shown in Figures 5.4b and 5.4c, NIR spectral albedo and absorbed radiation are retrieved with high accuracy (less than 1% relative error) for all sampling geometries.

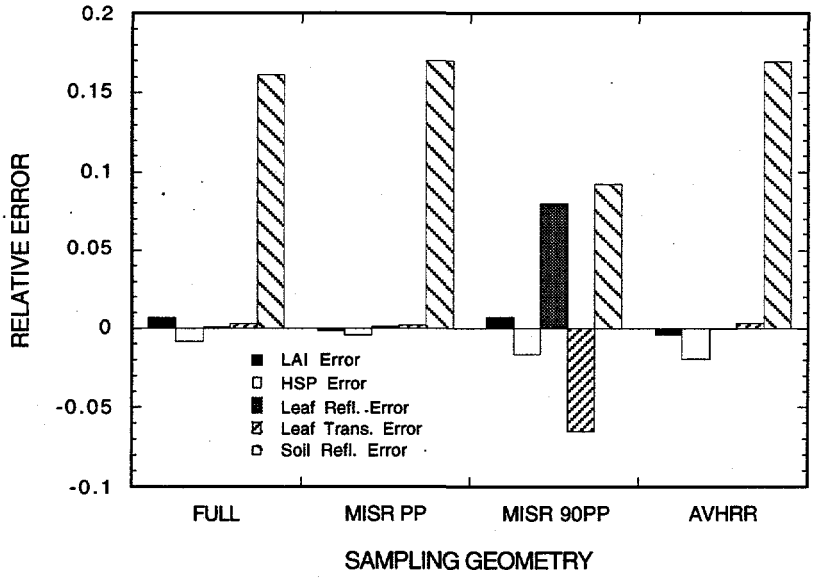

Figure 5.4a. Relative errors in retrieved parameters at NIR wavelengths using different sampling geometries. "FULL" denotes equal angular increments of 15° zenith and 45° azimuth, "MISR PP" denotes MISR view zenith angles in the principal plane, "MISR 90PP" denotes MISR view zenith angles in the orthogonal plane, and "AVHRR" denotes nine days of NOAA-11 AVHRR afternoon passes.

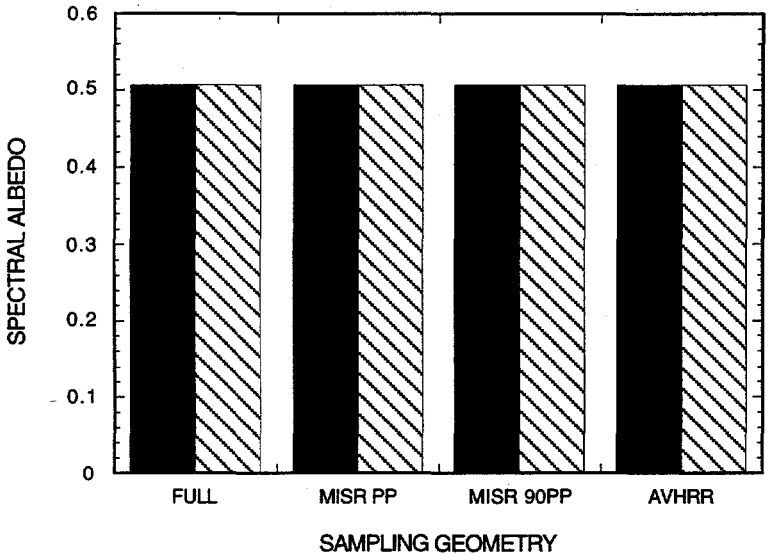

Figure 5.4b. Retrieved and actual spectral albedo at NIR wavelengths for different sampling geometries. Descriptions of sampling geometries are as in Figure 5.4a. Black bars represent retrieved values, hatched bars represent actual values.

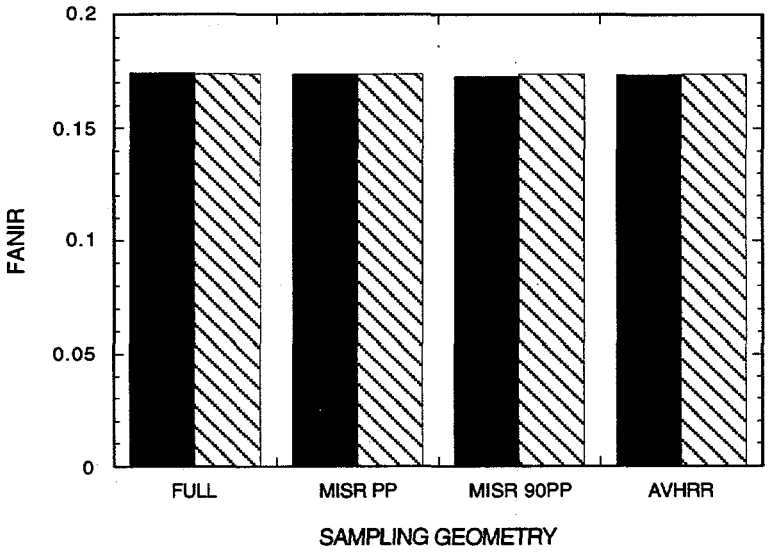

Figure 5.4c. Same as Figure 5.4b, but for fANIR.

C. Effects of Noise in Reflectance Data

In an inversion problem, model parameters may be excessively sensitive to the reflectance values [Goel, 1988]. In this case, small errors in measured reflectance may result in large errors in retrieved parameters. To assess this possibility with CANTEQ, random gaussian noise was added to synthetic reflectance data for the base cases. Relative noise levels of 2- to 10% variance, at 2% increments, were tested. The mean value of the noise was zero. The model was inverted for 30 realizations of noise at each level and at each wavelength.

Mean errors in the retrieved parameters at red wavelengths are shown in Figures 5.5a-g. All parameters except leaf transmittance are overestimated. The hot spot parameter and soil reflectance are the most adversely affected by the noise. As the model was found to be least sensitive to these parameters in the sensitivity study, this result is expected. Relative errors in leaf optical properties and LAI remain below 7% for all noise levels. These are, respectively, the parameters to which the model was most sensitive in the sensitivity study. Leaf reflectance, with a maximum error of less than 2%, is retrieved most accurately. In general, errors increase with increasing noise.

The one standard deviation confidence intervals express the sensitivity of the retrieved values to different realizations of noise at a given level. Only the leaf transmittance confidence intervals increase steadily (greater uncertainty) with increasing noise. Trends for other parameters are not obvious. Leaf reflectance (<9%) and the hot spot parameter (<85%) produce the smallest and largest confidence intervals, respectively. Although the model was found to be least sensitive to the hot spot parameter in the sensitivity study, the results suggest that the hot spot parameter and leaf reflectance errors may be correlated. This is plausible since strong backscattering may be due to either high leaf reflectance (an optical property) or a large hot spot parameter (a structural property), or both. Therefore, these parameters may not be independent for inversion purposes.

The mean retrieved fAPAR values are slightly overestimated. All mean errors are less than 3% (less than 1% if the 2% noise level is ignored). The relative invariance of the surface state parameters, despite large errors in some canopy parameters, is consistent with the sensitivity and

sampling geometry results. Spectral albedo is consistently underestimated, however all mean errors are less than 0.5%. The confidence intervals bound errors between ±2.5%.

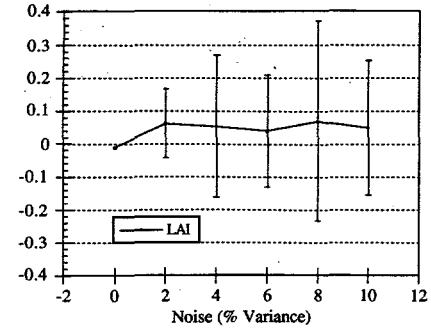

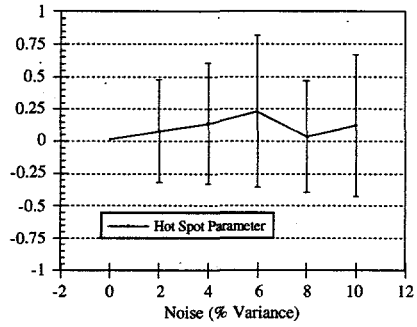

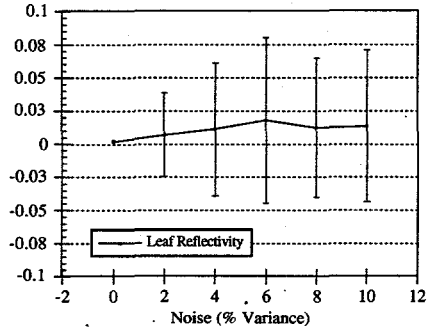

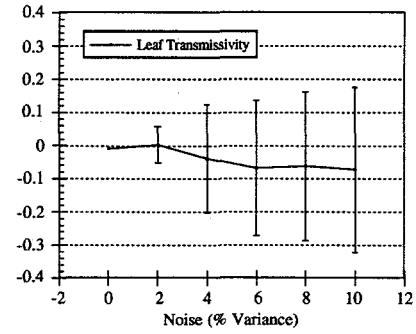

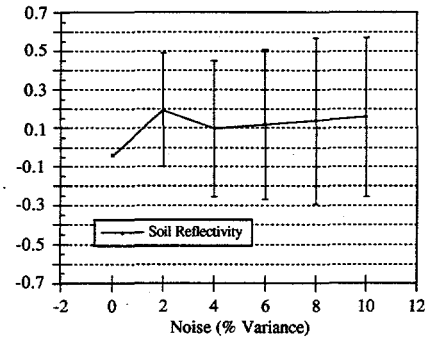

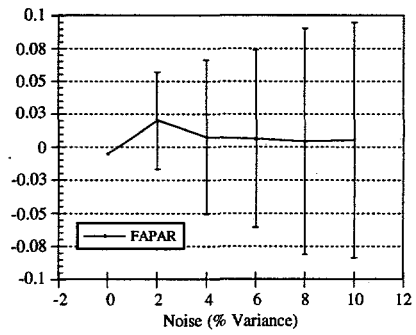

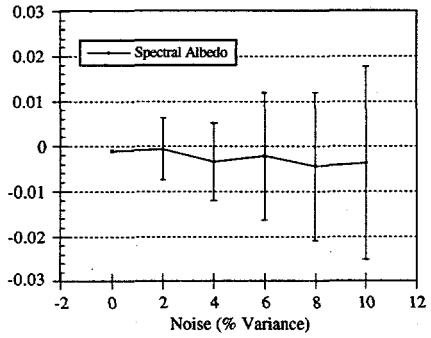

Figure 5.5a-g. Mean relative errors and standard deviations of retrieved model and surface state parameters at red wavelengths. Note the ordinate scales differ.

As with inversions at red wavelengths, most parameter estimates at NIR exceed the true parameter values (Figures 5.6a-g). Only leaf transmittance and soil reflectance are underestimated. Mean relative errors in LAI and leaf optical properties are less than 10%. Mean relative errors in soil reflectance and the hot spot parameter are up to 18% and 43%, respectively. As with results at red wavelengths, the NIR results are somewhat predictable based on the sensitivity study. For instance, the leaf transmittance and reflectance errors are comparable in the NIR, but the reflectance errors are substantially lower than the transmittance errors in the red. This was suggested by the model's significantly greater sensitivity to leaf reflectance at red but not at NIR. The increase in errors with increasing noise is more obvious in the NIR results. Moreover, the widening of the confidence intervals with increasing noise occurs for all parameters. Only the confidence intervals for the leaf optical properties are reasonable (<26%). Limits for all other parameters exceed 50%. The largest intervals occur for LAI and the hot spot parameter. This follows from the sensitivity study which suggested the model was least sensitive to these parameters for base case conditions.

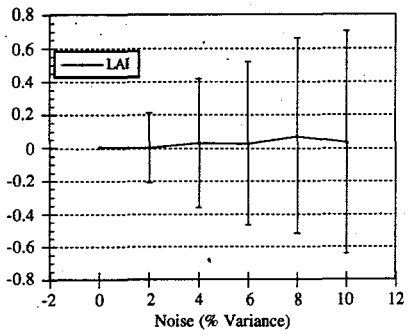

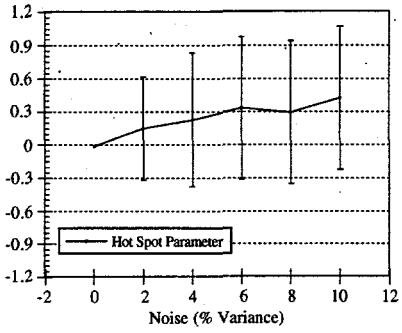

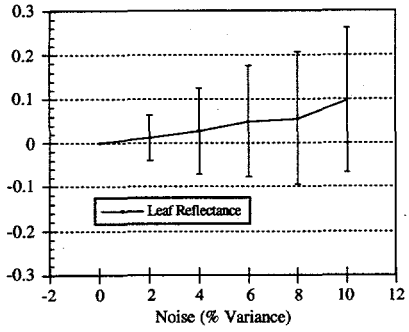

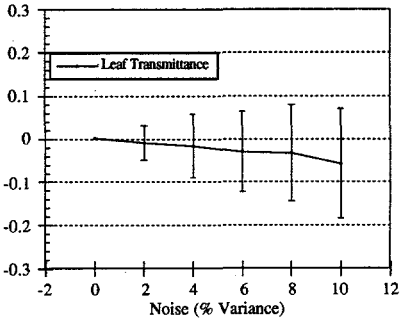

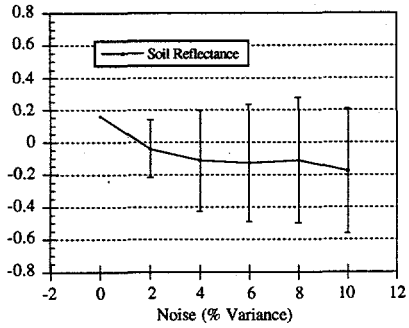

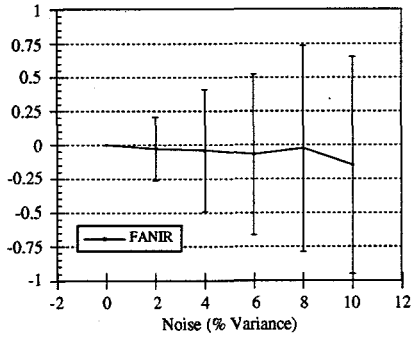

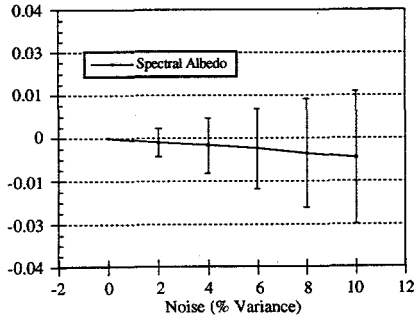

Figure 5.6a-g. Same as Figure 5.5, but for NIR wavelengths.

Similar to those at red wavelengths, errors in surface state parameters at NIR are small. Both fANIR and spectral albedo are underestimated. Mean fANIR errors are below 15% for all noise levels, and below 8% through 8% noise. The confidence intervals for this parameter are significant—up to 100% relative error for 10% noise. The mean errors in spectral albedo are less than 1% for all noise levels. The confidence intervals remain below 3% error. There is no clear correlation of errors in surface state parameters with parameter errors.

In general, these results suggest that LAI is most accurately retrieved from red reflectance data. Indeed, although the mean errors are comparable between the two wavelengths, the standard deviations are significantly greater in the NIR. Goel and Strebel [1983] corroborate this result for thin canopies. Note that since noise levels were relative, their absolute magnitudes were larger in the NIR. Thus, poorer results in NIR were expected. In addition, NIR wavelengths may be preferable for inversions with data from optically thicker canopies. Note that a relatively bright soil was used in this study, yet Goel et al. [1984] found that a darker soil is preferable for the retrieval of LAI in the NIR. Although the results for the hot spot parameter are less clear, the red wavelength inversions appear more reliable. The preferential use of red reflectance data for the retrieval of structural properties (e.g., the hot spot parameter and LAI) is corroborated by Kuusk [1991a].

These results suggest that, for up to 10% gaussian noise in the reflectance data, most parameters may be retrieved to within a reasonable error (7% at red, 10% at NIR). The relative stability of the leaf optical properties agrees with results found by Goel et al. [1984]. Accuracy of the hot spot parameter and soil reflectance appears to be most vulnerable to noise at both wavelengths. The largest mean errors for these parameters are below 23% in the red and 43% in the NIR. The surface state variables appear to be more stable than the canopy parameters and apparently can be retrieved with high accuracy (<3% for all parameters except fANIR). However, because red reflectance from vegetation is significantly lower than NIR reflectance, the signal-to-noise ratio may be lower at red wavelengths for empirical data.

D. Conclusions

The invertibility of the discrete ordinates model was shown for typical conditions using synthetic, noise-free data. In general, solutions were reasonably accurate except for cases of high LAI, low SZA and incorrect LAD specification. Soil reflectance was systematically overestimated at NIR wavelengths. Even for cases with incorrect solutions, estimates of spectral albedo, absorbed radiation and canopy photosynthetic efficiency were accurate. Inversions using data collected under satellite sampling schemes were reasonably accurate in most cases. The only exception was the case of orthogonal plane samples. Principal plane samples resulted in the most accurate solutions. Again, soil reflectance was overestimated at NIR wavelengths.

Effects of gaussian noise in empirical data were also tested. Parameters to which TOC reflectance was least sensitive were retrieved least accurately. Parameters to which reflectance was most sensitive were retrieved with less than 10% relative error for noise of 10% relative variance. Surface state parameters remained accurate for all noise levels.

CHAPTER VI

DESCRIPTION OF FIELD DATA

Results in Chapter V demonstrate that CANTEQ is invertible under most conditions with noise free data. Moreover, most parameters can be retrieved with reasonable accuracy when moderately noisy data exist. In building toward the goal of inversions with satellite data, inversions were attempted with data from The First ISLSCP Field Experiment (FIFE). DISORD, for which CANTEQ is a limiting case, was used through the remainder of this study.

A. FIFE Description

FIFE was a five year, international study of a grassland climate and ecosystem [Sellers et al., 1988]. The experiment was conducted on a 15 km x 15 km site near Manhattan, Kansas (39° 0' latitude, 96° 3' longitude) (Figure 6.1). The Konza Prairie Long Term Ecological Research (KPLTER) area (3487 hectares), for which previous and continuing records are available, constituted the northwest corner of the FIFE site. The Konza area consisted mainly of native tallgrass prairie vegetation. It is owned by The Nature Conservency and managed by Kansas State University with support from the National Science Foundation. The remainder of the FIFE site was privately held and consisted mostly of grazed and burned grassland. To a reasonable degree, the terrain was flat (±50 m elevation), had natural homogeneous vegetative cover, and had strong climatic forcing.

Figure 6.1. Thematic land cover map of FIFE area.

FIFE included the coordinated measurement of soil, canopy and atmospheric parameters via ground, aircraft and space-borne detectors. Four Intensive Field Campaigns (IFCs)—periods in which ongoing data collection was augmented with more comprehensive measurements—were conducted in 1987. In an effort to measure canopy "dry down" conditions, an additional IFC was conducted in August, 1989. Only data from 1989 were used in this study with ground-based radiometer data (Chapters VII and VIII). Site 916 (4439-ECV), located near the center of the FIFE area, was chosen for this investigation (see Figure 6.1). This choice was based on the relatively moist conditions, availability of extensive ancillary data, and comprehensive radiometric measurements. Site 916 underwent a prescribed burning in the spring of 1989 to eliminate dead vegetation from previous years. This resulted in a comparatively dense canopy over the summer months. The predominate vegetation included three C_4 grasses: little bluestem (*Andropogon scoparius* Michx), big bluestem (*Andropogon gerardii* Vitmin), and indian grass (*Sorghastrum mutan* L. Nash). The site was not grazed or cultivated. The soil was of the Dwight Series.

B. Reflectance Data Description

Initial inversions utilized reflectance data from a Modular Multiband Radiometer (MMR; Barnes Engineering Co., Stamford, CT). These data were collected by a team from the University of Nebraska [Walter-Shea et al., 1992]. MMR data were chosen based on the availability of independent leaf, soil and TOC reflectance measurements. The MMR had seven bands in the shortwave spectrum (0.45-0.52, 0.52-0.60, 0.63-0.69, 0.76-0.90, 1.15-1.30, 1.55-1.75, and 2.08-2.35 μm). It had a 15° instantaneous field of view (IFOV) and was mounted approximately 3.5 m off the ground. This resulted in a GIFOV of about 0.75 m^2 at nadir.

A circle of six 3 m x 3 m plots was defined at site 916. Five of the plots were left intact and sampled for TOC reflectance. The sixth was razed with a string trimmer to expose bare soil. Root systems and stem stubble were left intact. The MMR sampled each of the plots at seven VZAs in the principal plane (Figure 6.2). Zenith angle uncertainty was ±2° and azimuthal angle uncertainty was

±10°. Typically, three samples were collected at each angle. In this study, all samples at a given VZA and SZA were averaged.

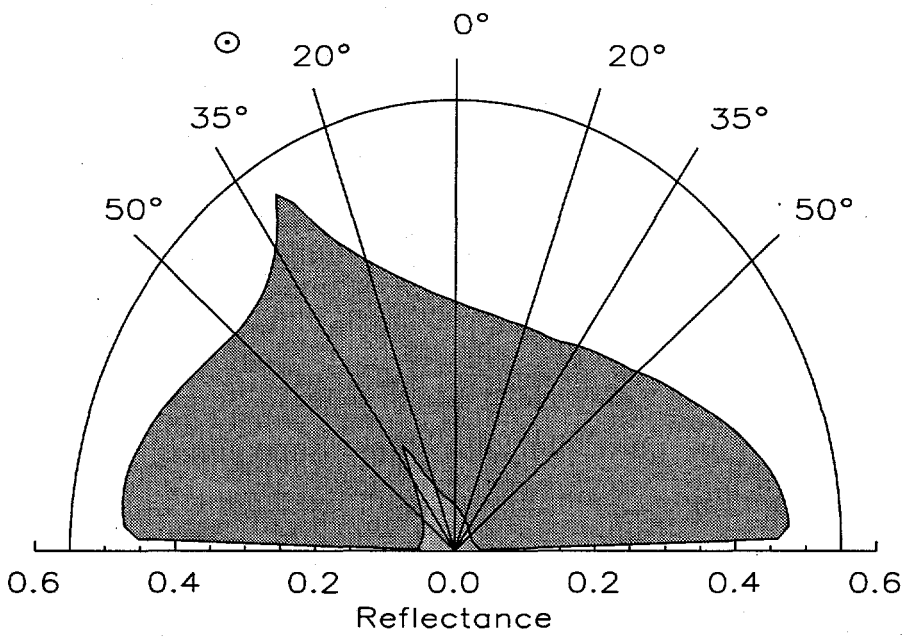

Figure 6.2. Sampling geometry of the FIFE ground MMR instrument. The plane of the paper represents the principal plane, and the radial lines represent view zenith angles. The dark (light) shaded region depicts the band 4 NIR (band 3 red) reflectance as determined through forward modeling. The solar zenith angle was 30°.

The MMR boom and housing shadowed the target area at some sun-target-sensor geometries. Thus, all data were checked, via trigonometric analysis, for shadow contamination. Contaminated samples were eliminated from further consideration.

C. Determination of Model Parameters from *In Situ* Data

For a site-specific sensitivity analysis and model validation, it was necessary to determine model parameter values from *in situ* data. As only LAI was measured for the actual mixed canopy (vs. per species), the determination of other parameters required an averaging scheme. This task was complicated by the absence of data for some species. The process used is described below.

FIFE investigators recorded species abundance at 15 plots using the modified Daubenmire method [Abrams and Hulbert, 1987]. Species with less than 5% live green cover in a plot were not recorded. In the present study, mean species abundances were determined and normalized. The resulting fractions were considered the site abundances. Species with abundance < 2% were disregarded. The remaining eight species and their site abundances are given in Table 6.1.

Table 6.1. Normalized species abundances used to determine canopy parameters at site 916. Species with less than 2% abundance were disregarded. Rows without data indicate species for which measured property data were not available.

Species	Site Means	Leaf Optical Properties	Leaf Angles
Little bluestem	0.240	0.331	
Big bluestem	0.222	0.306	0.493
Indian grass	0.157	0.216	0.349
Purple love grass	0.152		
Blue gramma	0.051		
Switchgrass	0.047	0.065	0.105
Lead plant	0.035	0.048	
Inland ironweed	0.024	0.033	0.054

Of the eight species, leaf optical data were available for six species and LAD data were available for four. Abundance fractions were therefore summed and renormalized for both parameters (Table 6.1). Mean canopy values were determined through an abundance-weighted averaging of species data. When multiple sample sets existed, data obtained closest in time to 4-8 August 1989 (or during the same period of plant life) were used. Leaf optical properties were determined by combining both abaxial and adaxial data for green leaves. Yellow leaf data were not used since these data were not available for every species and since dead leaf LAI << green leaf LAI. The zenith LAD was determined by weighting the fraction of a species' leaves occupying each zenith angle bin by that species' fractional abundance. The resulting distribution was then used to determine the Beta coefficients ($\mu(\theta)$, $\nu(\theta)$). The HSP parameter was specified with a reasonable value based on previous studies [Stewart, 1990].

Mean parameter values are reported in Table 6.2. The LAI value is the green leaf average from five destructive samples. LAD results suggest the canopy was predominately erectophile with a mean tilt angle of 65.1°. This result agrees well with values determined via inverse optical methods [Welles

and Norman, 1991]. Although azimuthal LAD data were collected, a uniform distribution was assumed here.

Table 6.2. Means and standard deviations of spectrally-variant parameters at site 916 in early August, 1989. Spectrally-invariant parameter values were {LAI, $\mu(\theta)$, $\nu(\theta)$} = {1.94 ± 0.61, 0.860 ± 0.063, 2.244 ± 0.368}. The standard deviation of LAI was determined from site 916 data; remaining values were determined from all available data.

	ρ		τ	
Band	μ	σ	μ	σ
1	0.101	0.026	0.041	0.021
2	0.174	0.036	0.144	0.041
3	0.097	0.050	0.053	0.054
4	0.452	0.032	0.490	0.038
5	0.424	0.059	0.510	0.051
6	0.320	0.046	0.436	0.048
7	0.252	0.082	0.318	0.067

D. Determination of Irradiance Parameter

Because diffuse irradiance was assumed to be isotropic throughout this study, the ratio (γ) of direct-to-total irradiance was sufficient to specify the irradiance distribution. However, γ could not be directly evaluated for MMR bands from FIFE data sets. Therefore, the 5S radiative transfer model [Tanré et al., 1990] was used. The 5S model was configured with atmospheric data from FIFE. Specifically, the column water vapor, ozone abundance and aerosol optical depth were determined from sun photometer and radiosonde data. Values were updated for each MMR data set. The thermodynamic profile was determined from the US62 standard atmosphere, and a continental aerosol distribution was assumed. The MMR band sensitivities were assumed constant over the full band, half power (FBHP) wavelengths. Results indicate that γ increases with wavelength while its variance decreases (Figure 6.3). This suggests that spectrally-independent parameters may be more accurately retrieved at longer wavelengths.

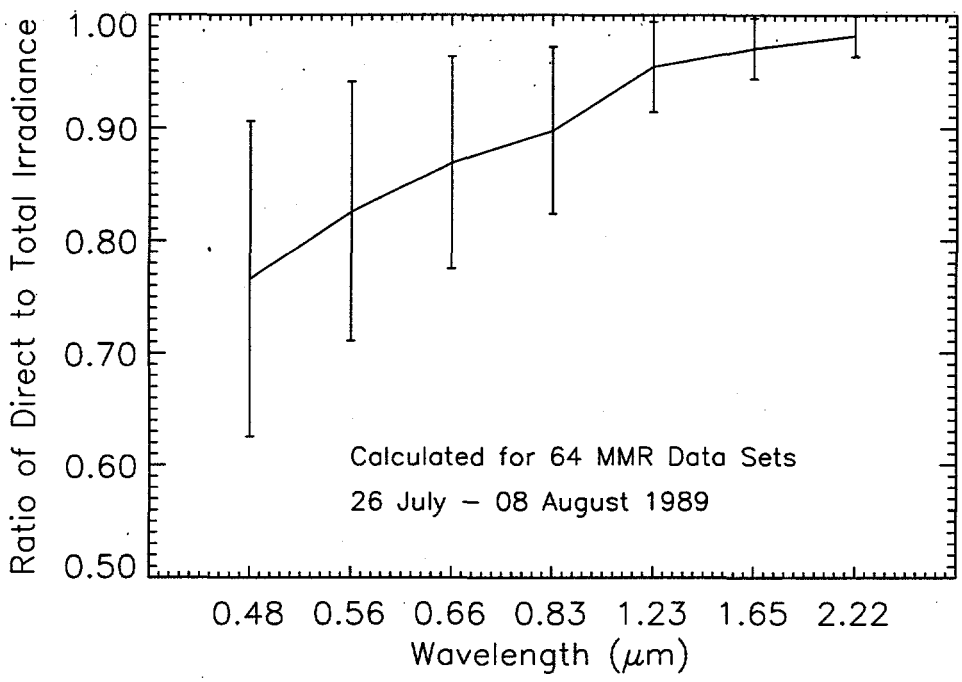

Figure 6.3. Means and standard deviations of γ with wavelength for 64 measurement periods during IFC-5. Note values are given for the center wavelengths of MMR bands. The abscissa scale is not linear.

E. Conclusions

Data from a ground-based MMR instrument were used for model inversions. The MMR had seven bands over the visible and NIR wavelengths. Since MMR data were collected for leaf optical properties, soil reflectance and TOC reflectance, validation of retrieved solutions will be possible. MMR data from site 916, gathered during IFC-5, will be used exclusively for subsequent inversions. This site was burned during the spring of the year but was not grazed. Compared to other sites, this site maintained a thicker canopy through the summer in part due to fortuitous precipitation events.

Site 916 parameters were determined by weighting *in situ* data for individual species by the species fractional abundances. Estimates of leaf tilt angle were consistent with values determined via inverse optical methods. The fraction (γ) of direct-to-total irradiance could not be determined from MMR measurements. Thus, values were estimated using a radiative transfer model and measured

atmospheric properties (ozone, precipitable water and aerosol optical depth). Mean values of γ increased and variance decreased with increasing wavelength. These results suggest that spectrally invariant surface parameters may be estimated more accurately from inversions with data from longer wavelengths.

CHAPTER VII

A LOWER BOUNDARY CONDITION FOR THE FIFE CANOPY MODEL

As shown in Chapter V, the TOC reflectance for thin canopies may be strongly impacted by soil reflectance. To determine whether a Lambertian (1 parameter) or anisotropic (6 parameter) lower boundary condition is most appropriate for conditions at site 916, a separate study of soil reflectance was conducted.

A. Background

The effects of soil reflectance anisotropy on TOC reflectance were initially investigated by Kimes and his colleagues [Kimes et al., 1980; Kimes, 1983; Kimes et al., 1985]. Kimes [1983] noted that sparse canopies (< 30% ground cover) exhibit greater reflectance variability with changing SZAs than do complete canopies. The reflectance of a sparse canopy is characterized by a strong backscatter peak in the retro-solar direction for low SZA. This was attributed to the high gap probability at small SZAs and the strong backscatter of the comparatively bright soil at red wavelengths. The TOC reflectance decreases substantially with increasing VZA since the gap probability decreases. Kimes [1983] further noted that a sparse canopy behaves similarly to a complete canopy at high SZAs since the gap probability for the solar irradiance decreases. This reduces the impact of soil reflectance over all view angles. Soil effects are less noticeable in the NIR since soil reflectance is significantly lower than vegetation reflectance at these wavelengths.

The initial attempts to model a sparse canopy with anisotropic soil reflectance were by Kimes et al. [1985b]. This effort involved using a simple analytical model [Walthall et al., 1982] as the lower boundary of a ray-tracing canopy model [Kimes and Kirchner, 1982]. Through the systematic

analysis of scattering components, Kimes et al. [1985] were able to attribute net reflectance characteristics to underlying mechanisms. Similar relationships were reported by Cooper and Smith [1985], who used a Monte Carlo model, and by Norman et al. [1985], who coupled the Cupid vegetation model to a simple, shadow-based soil model.

Despite these pioneering efforts, few studies on thin canopy reflectance have been reported. For example, the dependence of TOC reflectance on soil reflectance anisotropy for different wavelengths, canopies, and soils has not been systematically addressed. The variance of TOC reflectance with soil moisture has also been neglected. In fact, errors in canopy reflectance caused by the assumption of a Lambertian soil have yet to be quantified. It seems reasonable that, under some conditions, a Lambertian soil assumption may be suitable.

B. Soil Model Description

As noted in Chapter III, soil reflectance in DISORD may be treated as Lambertian or anisotropic. The anisotropic model [Jacquemoud et al., 1992] is a 6-parameter extension of the Hapke model for planetary regoliths [Hapke, 1981]. The model uses two-term Legendre polynomials to approximate the backscatter (b, c) and forward scatter (b', c') regimes of the phase function. A roughness parameter (h) allows increased reflectance in the retro-solar direction to simulate a hot spot. The lone physical parameter is the soil single scattering albedo (ω_s). This parameter varies with wavelength and soil moisture.

C. Errors With A Lambertian Soil Assumption

The effects of soil reflectance anisotropy on TOC reflectance were gauged at different LAI levels by comparing synthetic TOC reflectance determined over Lambertian and anisotropic soil models. The anisotropic soil model was specified with parameter values obtained for a rough clayey soil [Jacquemoud et al., 1992]. Single scattering albedo values for slightly moist conditions were used.

The SZA was set to 30°. To determine the appropriate Lambertian reflectance for comparison, the anisotropic reflectance was sampled in 26 directions—evenly spaced—over the upper hemisphere. The Lambertian reflectance determined by a least squares fit of the anisotropic reflectance was used. All canopy and irradiance parameters, excluding the varying LAI, were set to values encountered at site 916 (Table 6.2). Although turbid medium models are not well suited for thin canopy conditions, low LAI values were included so that general trends would be obvious.

Errors in red TOC reflectance caused by Lambertian soil reflectance are shown in Figure 7.1. Most notable is the large reflectance deficit in the retro-solar direction. Strong backscattering (hot spot) in true soil reflectance leads to this effect [Kimes, 1983]. Naturally, this effect is most pronounced at low LAI values and decreases as the canopy path length increases with LAI. Equally predictable is the overestimation of forward scattering since actual soil reflectance decreases markedly in the forward directions [Kimes, 1983]. These effects do not occur for some smooth soils [Jacquemoud et al., 1992]. Finally, the decrease in errors with increasing VZA (forward or backward) illustrates the effects of increasing path length on upwelling radiance.

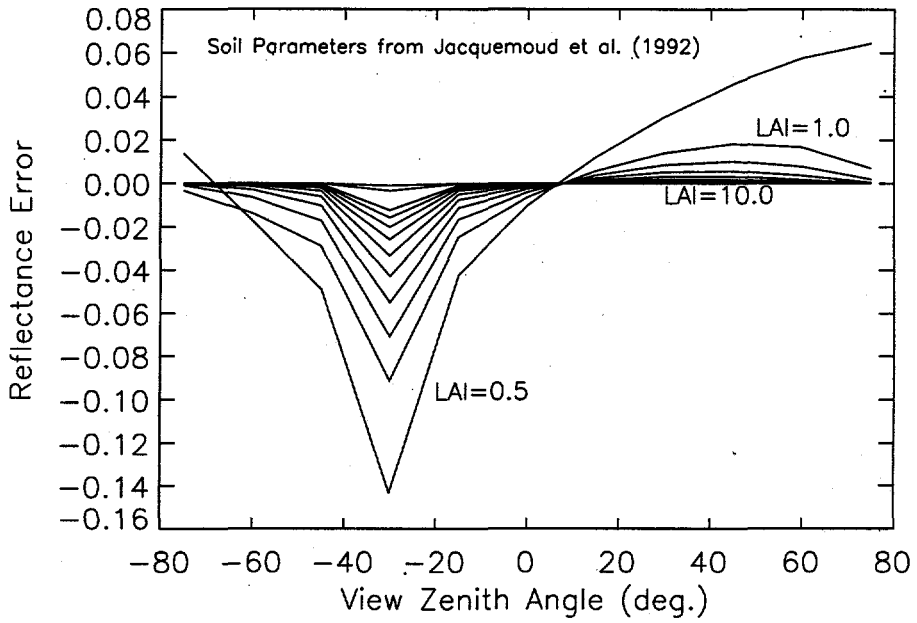

Figure 7.1. Error in top-of-canopy reflectance at red wavelengths due to a Lambertian (vs. anisotropic) soil model. LAI increments are 0.5 for 0.5 < LAI < 5.0, and 2.5 for 5.0 < LAI < 10.0. The SZA was -30°.

Errors for NIR reflectance are similar (Figure 7.2). Although absolute errors in NIR are slightly larger than in red, they are significantly smaller relative to the canopy reflectance. This can be explained by the differences in soil and vegetation spectra. While vegetation acts primarily as an absorber over the relatively bright soil at red wavelengths, vegetation is typically brighter in the NIR. In addition, high multiple scattering in the canopy moderates the impact of soil reflectance anisotropy at NIR wavelengths.

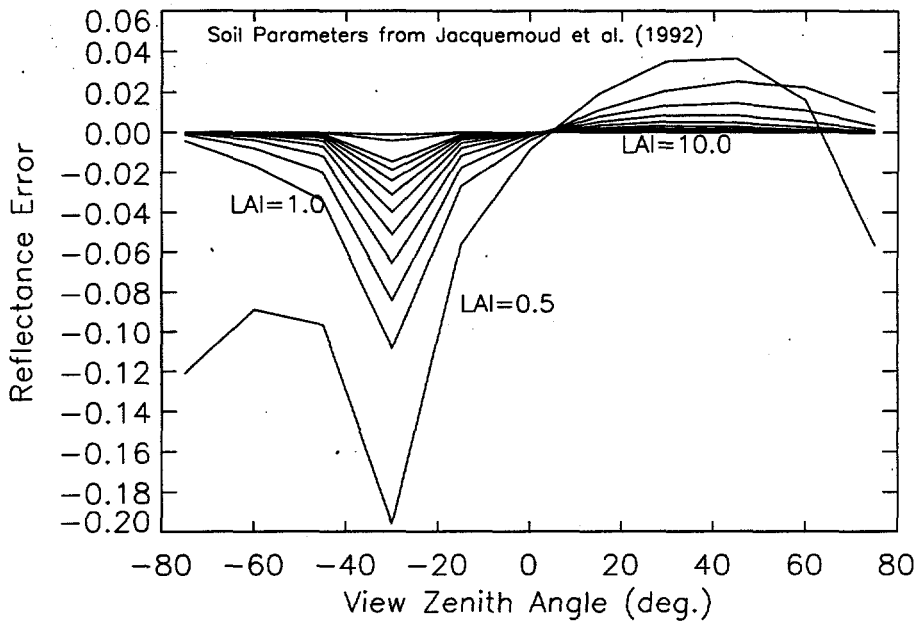

Figure 7.2. Same as Figure 7.1, but at NIR wavelengths.

Therefore, substantial errors in TOC reflectance may occur with Lambertian soil reflectors in low LAI conditions. Relative errors are largest at red wavelengths (up to 58% for the cases investigated). The view angles at which the maximum errors occur depend on the specified Lambertian reflectance and SZA, but appear to be independent of LAI. In the cases shown, errors are greatest in the retro-solar direction. Errors decrease with VZA. As LAI increases, errors decrease and become negligible over all view angles for an LAI near 10.0. This value is significantly greater than the previously reported value of about 3.0 [Cooper and Smith, 1985; Goel, 1988].

D. Sensitivity of TOC Reflectance to Soil Parameters

Since LAI measurements indicated the mean green LAI at site 916 was about 1.94 (accounting for about 80% of the above-ground biomass), an anisotropic soil model was necessary to accurately model the site 916 conditions.

At least six canopy parameters may be successfully retrieved in a DISORD inversion assuming a Lambertian soil (see Chapter V). However, the potential addition of six parameters for soil anisotropic reflectance meant DISORD would contain 11 adjustable parameters. To avoid overdetermination of the data, the parameter set was reduced. As shown in Chapter V, parameters producing the greatest change in TOC reflectance for small perturbations (analogous to the largest partial derivatives) are the same parameters that can be most accurately retrieved via model inversion. In contrast, parameters producing minimal changes may be fixed without significant loss of accuracy.

A sensitivity study of the simulated FIFE canopy was conducted to determine which, if any, of the soil model parameters may be fixed. The site 916 canopy was simulated using measured parameter values (see Table 6.2). Model estimates compared favorably to measured data, despite the limitations of the turbid medium approximation at low LAI. A "baseline" TOC reflectance distribution was therefore computed using the clayey soil model [Jacquemoud et al., 1992] as a lower boundary. The reflectance was sampled at seven VZA in the principal plane (coincident with directions used in MMR sampling). Next, each soil and canopy parameter was perturbed in turn by 10% of its imposed range, both positively and negatively. Parameter ranges were based either on theoretical or empirical information but generally defined reasonable limits. For each perturbation, the sensitivity (S) of the model to the perturbation was recorded, where

$$S = \frac{\mathrm{RMS}}{\overline{R_j^b}}\,100, \tag{7.1}$$

and,

$$\mathrm{RMS} = \sqrt{\frac{1}{7}\sum_{j=1}^{7}(R_j - R_j^b)^2}, \tag{7.2}$$

where R_j^b is the baseline reflectance in direction j, R_j is the geometrically-analogous reflectance of the perturbed distribution, and $\overline{R_j^b}$ is the mean baseline reflectance. This exercise was repeated for three SZAs (30, 45 and 60°) and two wavelengths (red and NIR).

Sensitivity values for the soil parameters are shown in Tables 7.1 and 7.2. Results suggest that ω_s produces approximately twice the effect of any other soil parameter. This trend occurs for all SZA and both wavelengths. The greater impact of soil reflectance at red wavelengths, compared to NIR, is consistent with Figures 7.1 and 7.2. The soil roughness and phase function parameters {h, b, c, b', c'} produce significantly smaller changes. Sensitivity values for these parameters were nearly always lower than those produced by canopy parameters.

Table 7.1. Sensitivity (S) of TOC reflectance in band 3 (red) to perturbations in soil model parameters. Values are shown for three SZAs.

	30°	45°	60°
ω_s	13.652	10.234	5.356
h	0.468	0.375	0.206
b	7.911	5.825	3.262
c	6.825	5.187	3.125
b'	6.246	3.426	1.977
c'	4.127	3.287	1.236

Table 7.2. Same as Table 7.1, but for band 4 (NIR).

	30°	45°	60°
ω_s	5.612	4.453	3.014
h	0.341	0.283	0.208
b	2.852	2.095	1.342
c	1.313	0.874	0.460
b'	2.475	1.663	1.054
c'	0.795	0.531	0.018

E. Invariance of Soil Roughness and Phase Function Parameters

Based on the results above, the soil roughness and phase function parameters {h, b, c, b', c'} were held constant for the DISORD inversions. Determination of appropriate values was complicated by the wide range of conditions (spectral bands, solar angles and moisture levels) over which the values

must apply. The determination of unique values for each condition was considered impractical and operationally unrealistic.

If the roughness parameter truly describes the roughness of the soil, this parameter should be independent of wavelength, solar direction and moisture content. The same may not apply to the phase function parameters. However, upon extensive inversion studies with laboratory reflectance data, Jacquemoud et al. [1992] concluded that the set $\{h, b, c, b', c'\}$ is invariant for a given soil. This was attributed to the dependence of these parameters on the refractive indices (real part) and the low spectral dependence of these indices. This claim does not require that any single parameter be invariant over these conditions, only that the set remain approximately constant.

Note that these conclusions were not derived theoretically, but were based on experimental evidence. Moreover, the parameter independence with soil moisture was invalid for smooth soils—particularly those with high clay content—since these soils exhibit a large specular effect near saturation, but a decreased specular effect and increased backscatter with drying.

F. MMR Soil Reflectance Data

As described in Chapter VI, one of the six MMR plots at site 916 was cleared of vegetation and sampled for soil reflectance. Soil data from five days (26-28 July; 4 and 8 August, 1989) were used in the present study. Characteristics of the data are given in Table 7.3. Although burn residue covered the soil in the late spring and early summer [Forrest Hall, personal communication], the soil surface probably reached a steady reflectance state by August [John Norman, personal communication].

Table 7.3. Characteristics of soil reflectance data. FIFE data are from site 916, plowed field data are from Kimes et al. [1985], and remaining data are from Van Leeuwen and Huete [1993].

Data Set	VZA (°)	View Azimuth Planes (°)	Spectral Bands	SZA (°)	Instrument IFOV (°)
FIFE soil	-50, -35, -20, 0, 20, 35, 50	0	7	20-60	15
plowed field	-75 to 75, every 15	0-135, every 45	2	26, 30, 45	12
crust	-48, -37, -25, -12, 0, 11, 24, 35, 46 (approx.)	0, 90	46	37, 38	15
dry sand 1	same	same	same	28, 27	same
dry sand 2	same	same	same	28, 25	same
gravel	same	same	same	24, 23	same
wet sand	same	same	same	24, 26	same

Moisture data, obtained from gravimetric measurements in the top 5 cm of substrate, show two drying events over this period (see Figure 7.3). The average moisture decreased from 36% on 26 July to 26% on 28 July, and from 36% on 4 August to 25% on 8 August. To approximate beneath-canopy moisture conditions, the bare soil plot was covered with plastic mulch between measurement days. The mulch allowed the penetration of moisture but hindered the regrowth of vegetation. This mulch was removed in the morning before measurements began. However it was not, as a rule, replaced after each measurement. Thus, the exposed soil was subject to accelerated drying on measurement days [Blaine Blad, personal communication].

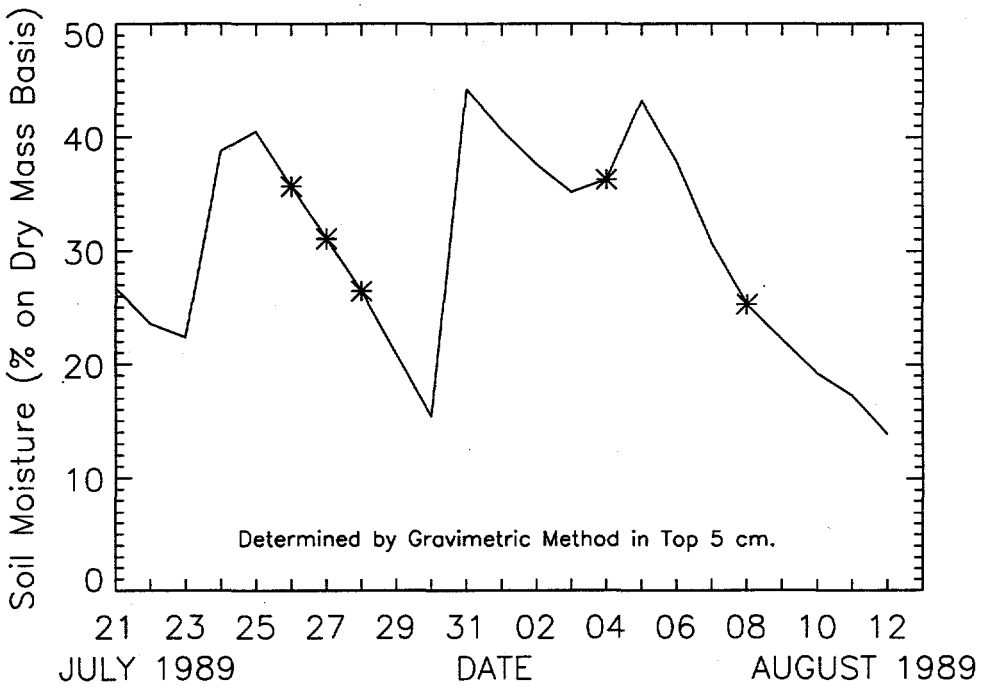

Figure 7.3. Variation of soil moisture at FIFE site 916 during IFC-5. Asterisks (*) indicate moisture levels for dates used in this study.

G. Accounting for Diffuse Irradiance in Soil Model

As the reflectance data (R_j) of Jacquemoud et al. [1992] were collected under laboratory conditions, there was no need to account for diffuse irradiance in the calculation of R_j^* (Equation 2.5). When compared to field data, however, R_j^* must account for diffuse irradiance. If this correction is not included, retrieved parameter sets would embody information on both the soil and the illumination conditions and hence not be atmospherically invariant.

Although natural diffuse irradiance is anisotropic, an isotropic formulation was developed for this study. The scheme utilized an equally-weighted quadrature procedure to determine the additional reflectance for each R_j^*. Due to its isotropic nature, this parameterization depended only on the fraction of direct-to-total irradiance, γ.

The effect of diffuse irradiance on principal plane reflectance is shown in Figure 7.4 for a clayey soil. The magnitude of the hot spot decreases due to the reduction in direct irradiance. Furthermore, scattering in the forward domain increases due to backscattering of diffuse irradiance. The general effect of increased diffuse irradiance is to make surface reflectance more Lambertian. Indeed, if the direct component is reduced to zero such that all irradiance is diffuse (as might exist on a cloudy day), the angular reflectance over the principal plane is nearly constant. These results are consistent with those of Irons et al. [1992], who used a geometrical optics soil model.

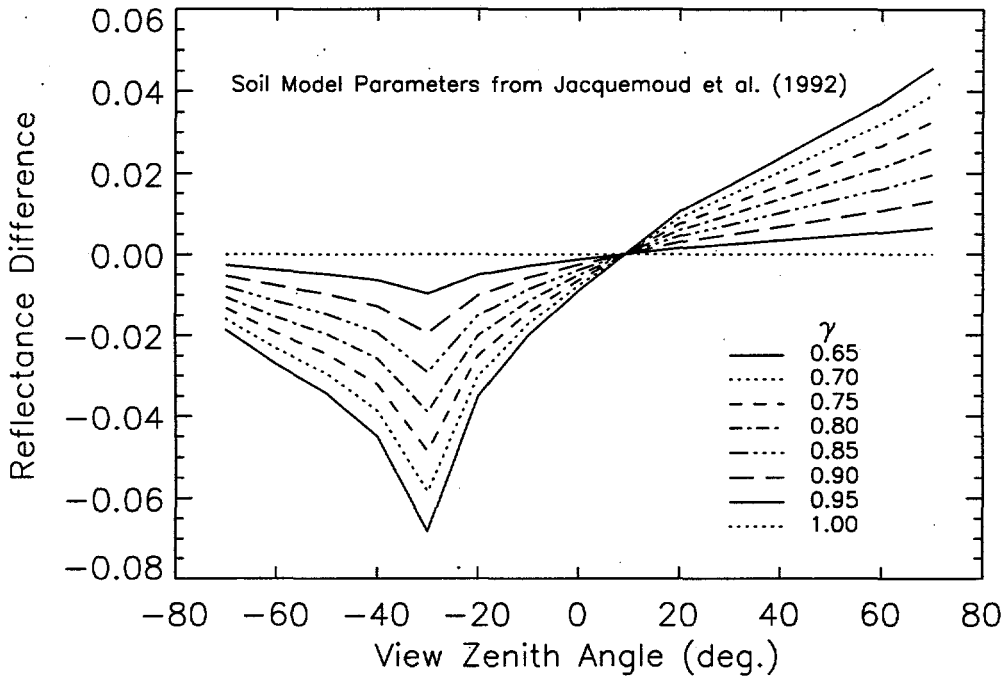

Figure 7.4. Change in principal plane reflectance of soil with γ (ratio of direct-to-total irradiance). Ordinate values represent deviations from the reflectance for 100% direct irradiance (straight line). Diffuse irradiance was isotropic. The SZA was -30°.

H. Inversion Problem Configuration

Due to the dependence of ω_s on moisture level and wavelength, the soil model was inverted by adjusting the parameter set $\{\omega_{s,1}, ..., \omega_{s,N}, h, b, c, b', c'\}$, where N represents the number of independent spectral and temporal data sets. The use of multiple values of ω_s but single values of h, b, c, b', and c' reflects the reported spectral/moisture variance (invariance) of the respective parameters.

Upon testing different optimization routines, the quasi-Newton algorithm E04JAF [Numerical Algorithms Group, 1990] was found to be most efficient with the soil model. This routine requires specification of initial parameter values. As there currently is no way to verify if and when optimization algorithms have found global minimizers (vs. local minimizers), the starting position was prescribed randomly 50 times. One non-random initialization utilized the reported values for

clayey soils [Jacquemoud et al., 1992]. The minimizer that resulted in the lowest merit function value (Equation 2.5) was considered the global minimizer and recorded.

I. Use of Parameter Constraints

Although parameter constraints were not employed by Jacquemoud et al. [1992], they were necessary in this study to prevent errant results. Specifically, without parameter limits, the model occasionally yielded negative reflectance estimates. To demonstrate the impact of constraints, the model was inverted twice with a set of seven MMR samples. In the first case, the parameters were effectively unconstrained. In the second case, the parameters were constrained with the values in Table 7.4. As shown in Figure 7.5, the estimates of principal plane reflectance by the inversion solutions are very similar. However, the unconstrained solution produces some negative estimates in the orthogonal plane (Figure 7.6). This suggests parameter limits can be used to ensure reasonable reflectance in all directions.

Table 7.4. Parameter constraints imposed for inversions.

Parameter	Lower	Upper
ω_s	0.01	1.0
h	0.00	2.0
b	-2.0	2.0
c	-2.0	2.0
b'	-2.0	2.0
c'	-2.0	2.0

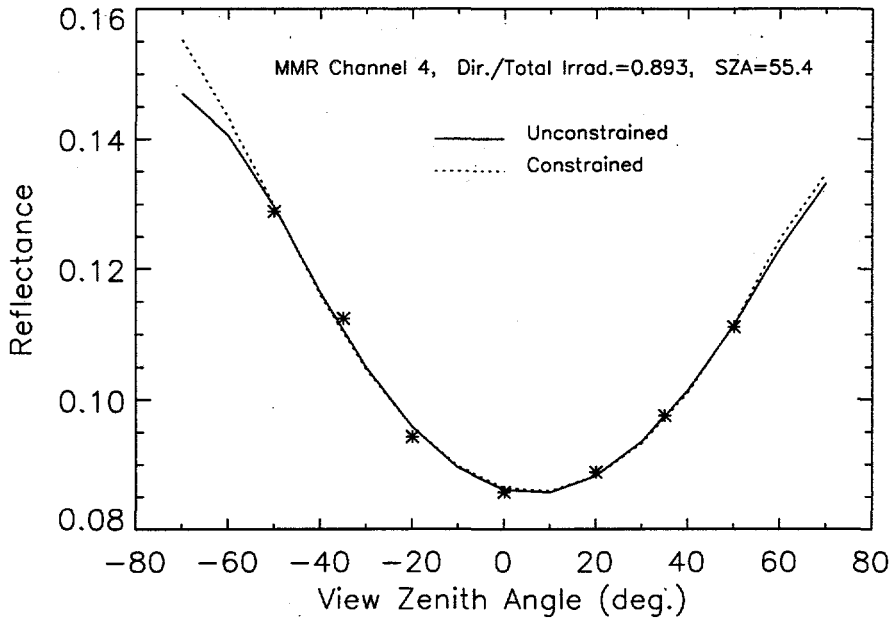

Figure 7.5. Fit of MMR band 4 data (asterisks) in the principal plane using solutions obtained from constrained and unconstrained inversions.

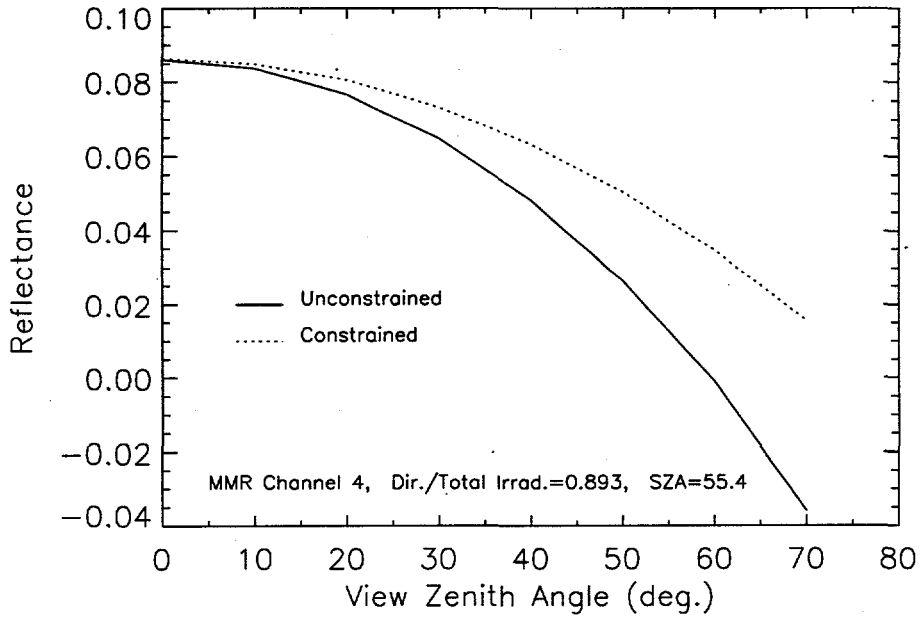

Figure 7.6. Comparison of solutions shown in Figure 7.5, but in the orthogonal plane.

The limits in Table 7.4 were imposed after a review of Jacquemoud et al.'s [1992] results and some experimentation. Nevertheless, since the roughness and phase function parameters are not physical properties, limits on their values are somewhat arbitrary.

J. Inversion Results

Inversions were conducted in three configurations: 1) a single band at a single solar angle, 2) seven bands together at a single solar angle (denoted "7BAND"), and 3) all bands and solar angles together (denoted "ALLDATA"). For increased readability, inversion results determined using the diffuse irradiance approximation are denoted "DIFF", while those determined without the approximation are denoted "NODIFF". The quality of the model fit is indicated by the RMS error,

$$\text{RMS} = \sqrt{\frac{\varepsilon^2}{n - p}}\ , \tag{7.3}$$

where ε^2 is the merit function value from Equation (2.5) with unit weights, n is the number of sample points, and p is the number of parameters adjusted in the inversion ($p = N + 5$). The variables p and n change according to the problem configuration. The values are noted in each case.

Inversions Using Single Bands

Initially, the model was inverted separately for each MMR band at each solar angle. This condition required the determination of six parameters (p) from seven reflectance samples (n). Data sets with shadowed samples were excluded since non-linear least squares problems (Equation 2.5) are not well determined when $n = p$ [Goel, 1988]. Thus, for the five measurement days, only 10 of the 16 available data sets were used.

First, the model was inverted using the diffuse irradiance approximation. This effectively decreased the gradients of the merit function such that minimization proceeded relatively slowly. This follows from Figure 7.4 and the comments in Section G. The mean retrieved values and their standard deviations are shown in Table 7.5. Clearly, the mean parameter values are inconsistent over different bands. Also, the standard deviations are large with respect to the imposed parameter ranges (Table 7.4). Finally, although the RMS differences are rather small, they increase with wavelength. This is probably due to the decrease in diffuse irradiance and the consequent increase in reflectance anisotropy with increasing wavelength (Figures 6.3 and 7.4).

Table 7.5. Mean parameter values with standard deviations retrieved through model inversions of MMR data. Single channel inversions were conducted at individual solar angles. 7BAND denotes the simultaneous inversion of seven MMR bands at single solar angles. ALLDATA denotes the simultaneous inversion of seven MMR bands at all solar angles. Row titles with an asterisk (*) denote use of the diffuse irradiance parameterization.

	h		b		c		b'		c'		RMS
	μ	σ	μ	σ	μ	σ	μ	σ	μ	σ	
BAND 1	0.698	0.907	0.294	1.112	0.483	1.057	0.419	1.405	0.288	0.934	0.001
BAND 2	0.533	0.796	0.516	1.281	0.715	1.026	0.592	1.383	0.477	0.978	0.002
BAND 3	0.780	0.884	0.706	1.162	0.577	1.078	0.872	1.348	0.276	1.062	0.002
BAND 4	0.768	0.805	0.897	1.121	0.576	1.184	0.951	1.389	0.271	1.231	0.003
BAND 5	0.910	0.904	0.871	1.136	0.212	0.966	0.752	1.537	-0.005	0.891	0.007
BAND 6	0.929	0.889	0.702	1.030	-0.002	0.928	0.531	1.499	-0.225	0.869	0.009
BAND 7	0.854	0.854	0.633	0.994	-0.114	0.962	0.629	1.432	-0.366	0.926	0.008
BAND 1*	0.379	0.613	-0.254	0.894	-0.831	0.775	-0.434	1.345	-0.893	0.813	0.001
BAND 2*	0.288	0.606	0.151	1.301	-0.368	1.124	-0.126	1.396	-0.462	1.256	0.002
BAND 3*	0.681	0.884	0.299	1.442	-0.297	0.936	0.186	1.660	-0.483	0.938	0.002
BAND 4*	0.801	0.880	0.620	1.162	0.087	1.211	0.571	1.425	-0.179	1.195	0.003
BAND 5*	0.836	0.904	0.871	0.882	0.357	0.789	0.655	1.295	0.150	0.732	0.007
BAND 6*	1.034	0.902	0.482	1.026	0.151	0.982	0.390	1.548	-0.087	0.929	0.009
BAND 7*	0.827	0.870	0.575	0.988	-0.091	0.997	0.605	1.448	-0.368	0.947	0.008
7BAND	0.485	0.705	0.773	0.618	0.160	0.591	0.520	0.655	0.028	0.652	0.004
7BAND*	0.792	0.854	0.031	0.259	-0.045	0.488	-0.215	0.296	-0.118	0.527	0.004
ALLDATA	1.098		0.294		0.093		0.204		-0.030		0.010
ALLDATA*	0.000		0.345		0.330		-0.015		0.021		0.010

* indicates the inversion was conducted with the diffuse irradiance parameterization.

A second set of inversions was conducted without the diffuse irradiance approximation. The inversions proceeded relatively quickly. Results are shown in Table 7.5. Although some parameters are more consistent over the different bands (e.g., h and b), others remain inconsistent. Furthermore, inconsistency within bands is evident from the large standard deviations. In general, mean parameter values are greater for the NODIFF results. For the roughness parameter h, this implies a smoother surface. This is predictable since a smoother surface tends to have less backscattering and more forward scattering—the same effects produced by diffuse irradiance (Figure 7.4). Finally, the mean RMS values are the same as for the DIFF cases.

To assess the spectral independence of the solutions, the solutions determined from band 7 inversions (DIFF and NODIFF) were used to fit band 1 data for the same SZA. These bands were chosen for comparison since they represent the extremes in wavelength and since local spectral absorption peaks are produced by different molecules (Fe-O charge transfers and H_2O absorption, respectively). The latter consideration reduces bias due to molecularly-correlated behavior. In this comparison, the spectrally-dependent ω_s was readjusted for the best fit. Results are shown in Figure 7.7 for a low SZA (27.4°) and low soil moisture (26%) case. The hot spot area is underestimated while the forward scattering is overestimated by both solutions. Errors are slightly worse for the DIFF solution. Furthermore, the backscatter decreases markedly at large VZAs for both solutions. Subjective observation of all data sets suggests that a reflectance increase in this region is more plausible. These results imply that, for the given inversion configuration, retrieved solutions are not spectrally independent.

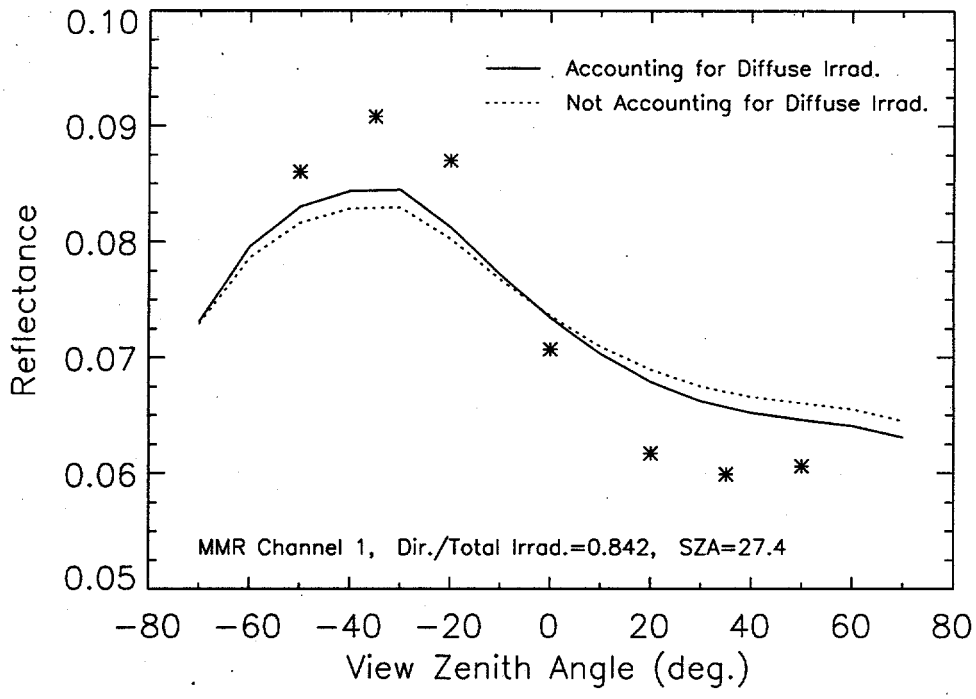

Figure 7.7. Fit of MMR band 1 data (asterisks) in the principal plane using band 7 solutions obtained with(out) the diffuse irradiance parameterization. The data and solutions were obtained at SZA = 27.4°.

Inversions Using All Bands (7BAND)

A possible reason for the inconsistent results above is the poor determination of the least squares problem (a six parameter function determined by seven samples). The sample size can be significantly increased by inverting all seven MMR bands simultaneously [Jacquemoud et al., 1992]. In this scenario, a single set of roughness and phase function parameters are adjusted with seven ω_s variables (one per MMR band). This tacitly assumes the spectral independence of the roughness and phase function parameters. In this study, 49 samples (n) were fit with a 12 parameter (p) model. This oversampling permitted the use of data sets with a sample excluded due to shadow contamination.

Inversions with the diffuse approximation resulted in two non-convergent cases. The mean results for the remaining 14 cases are shown in Table 7.5. The variance of the phase function parameters decreases markedly compared to the single band results. However, the variance of the

roughness parameter is essentially unchanged. The mean RMS error (0.004) is close to the average of the single band cases.

All 16 cases converged in the NODIFF case. Mean results are shown in Table 7.5. Although the standard deviations are lower than for the single band inversions, the values are larger than for the 7BAND DIFF case. The single exception is the roughness parameter. Unlike the DIFF case, the mean parameter values are similar to the mean values retrieved in the single band inversions. This supports the spectral independence hypothesis (Section E). Again, the RMS error is 0.004.

To assess their dependence on SZA, the solutions (DIFF and NODIFF) for the data at SZA = 58.1° (soil moisture = 36%) were used to estimate the data obtained at SZA = 27.4° (soil moisture = 26%). Again, ω_s was readjusted for a best fit. Results are shown in Figure 7.8. As the DIFF solution deviates strongly from the measured data, the parameter set clearly does not embody the fundamental scattering nature of the soil. Thus, the solution is source angle dependent. The NODIFF solution produces a more reasonable fit. Still, the hot spot is underestimated and the forward scattering is overestimated. Moreover, the backscatter at high VZA appears excessive. This may result from the non-independence of soil roughness and phase function effects. Specifically, both may produce increased retro-solar reflectance. Contrary to the findings of Jacquemoud et al. [1992], the comparisons here suggest the solutions vary with illumination angle and/or soil moisture.

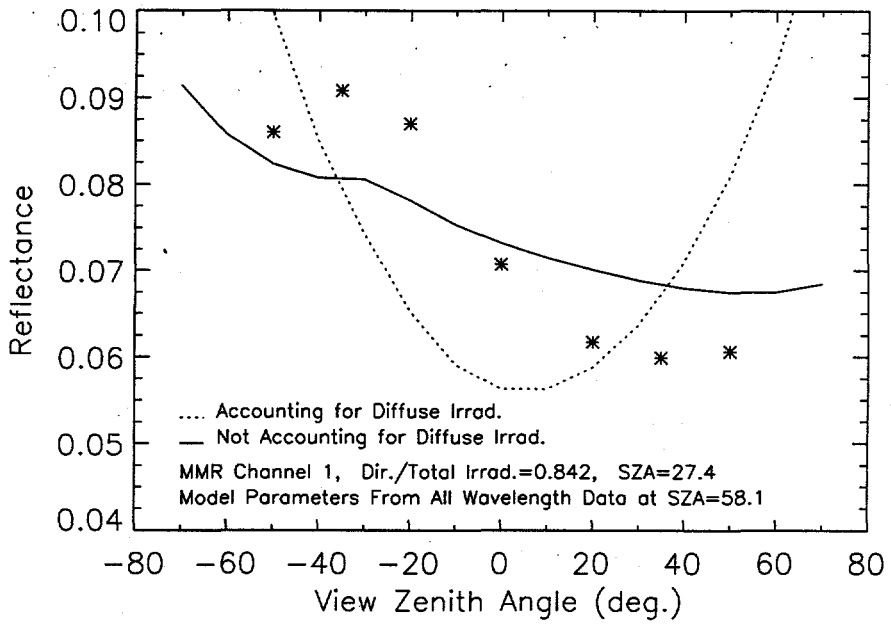

Figure 7.8. Fit of MMR band 1 data (asterisks) in the principal plane using 7BAND solutions obtained with(out) the diffuse irradiance parameterization. The data were obtained at SZA = 27.4°, and the solutions were obtained from data at SZA = 58.1°.

Inversions Using All Data (ALLDATA)

To simplify inversions of the coupled canopy model, a universal set of soil parameters—applicable over all conditions—is desired. Thus, the above results are still unsatisfactory. Nevertheless, the results suggest that a more diverse data set decreases a solution's dependence on sampling conditions. A logical extension is to include all samples (multiple bands, solar angles, and soil moisture levels) in a single inversion. This configuration should allow better discrimination between scattering mechanisms (e.g., backscatter vs. hot spot effects). Moreover, the minimization problem will be highly overdetermined—an advantageous situation given the limited MMR sampling. This generalization also follows Jacquemoud et al. [1992].

To reduce the likelihood of a solar angle bias, some data sets were eliminated so that the resulting SZA distribution would be reasonably even. Specifically, data at three SZAs per 10° interval

between 20 and 60° were used. Data sets with shaded samples were not included when possible. The result was a system of 84 data sets (n = 560 unshaded samples) and 89 independent parameters {$\omega_{s,1}$, ..., $\omega_{s,84}$, h, b, c, b', c'} (p). The inversion was initialized 30 times using randomly chosen sets and the clayey soil solution of Jacquemoud et al. [1992].

Inversions were first attempted using the diffuse irradiance approximation. After more than 100 hours of CPU time (Silicon Graphics Indigo), only 12 of the 30 inversions were completed. The lowest RMS solution is reported in Table 7.5. Clearly the parameter values deviate from the 7BAND values. The RMS error is greater than those of the 7BAND and single band inversions. This reflects the more diverse data set used in the inversion.

In contrast to the DIFF cases, all NODIFF cases converged. The solution resulting in the lowest RMS error is shown in Table 7.5. Most of the retrieved values are outside the range of the mean values found in the single and 7BAND inversions. However, they are within the one standard deviation intervals. The RMS error again equals that obtained in the DIFF case.

To test the generality of the results, reflectances were calculated for 27.4 and 58.1° SZAs using both solutions (DIFF and NODIFF). Comparisons of model results with empirical data are shown in Figures 7.9 (band 1, SZA = 27.4°, soil moisture = 26%) and 7.10 (band 7, SZA = 58.1°, soil moisture = 36%). The NODIFF solution again produced a better fit (Figure 7.9). While the hot spot is underestimated and the forward reflectance is overestimated, the maximum error is less than 10% relative. Comparing Figures 7.8 and 7.9, it is also clear that the ALLDATA solution is an improvement over the 7BAND solution. Again, the DIFF solution does not exhibit a hot spot, although forward scattering is reasonably approximated. In Figure 7.10, the errors are significantly smaller for both solutions. The ALLDATA NODIFF results in Figures 7.9 and 7.10 are representative of those for other bands, solar angles and moisture levels. A comparison of all measured and modeled reflectances (560 points) used in the ALLDATA NODIFF inversion is shown in Figure 7.11. The mean of the absolute values of errors is 0.006 (3.5%). Based on these results, the NODIFF ALLDATA solution was used for inversions of the coupled canopy model. Mean values of ω_s for the NODIFF case are shown in Table 7.6.

Table 7.6. Means and standard deviations of ω_s for the NODIFF ALLDATA case.

Band	μ	σ
1	0.091	0.095
2	0.205	0.046
3	0.259	0.061
4	0.347	0.091
5	0.490	0.132
6	0.603	0.099
7	0.652	0.099

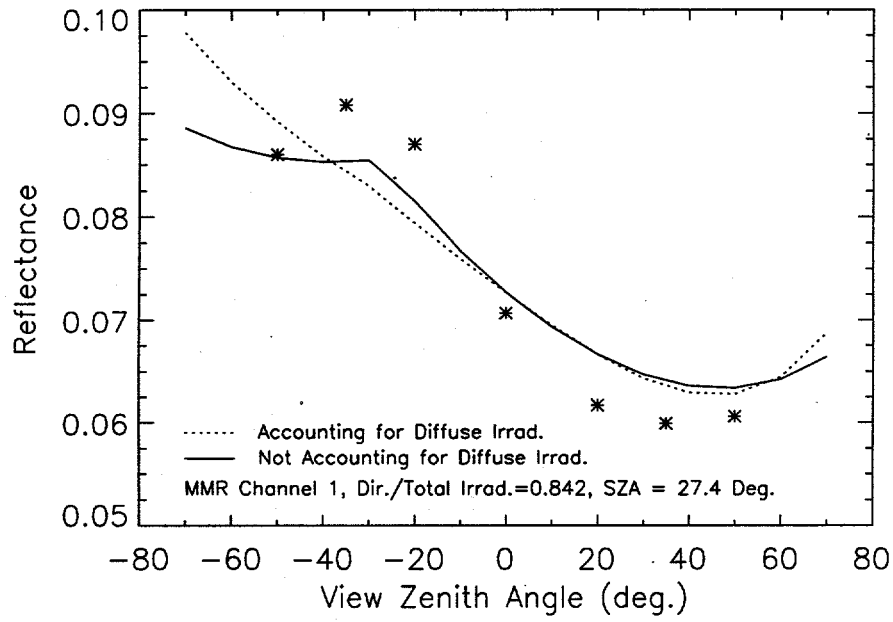

Figure 7.9. Fit of MMR band 1 data (asterisks) in the principal plane using ALLDATA solutions obtained with(out) the diffuse irradiance parameterization. The data were obtained at SZA = 27.4°, and the solutions were obtained over all SZA.

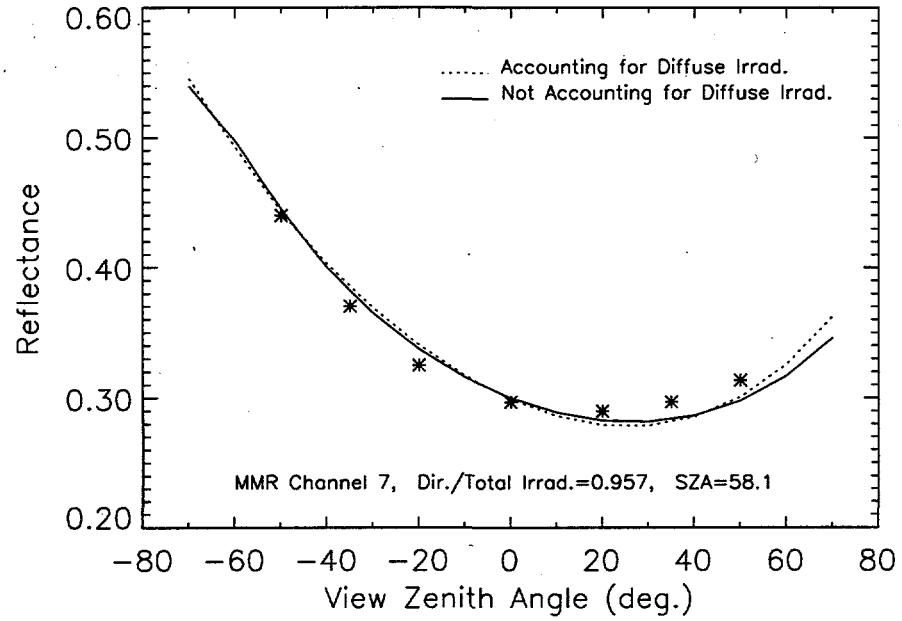

Figure 7.10. Same as Figure 7.9, except data were obtained in band 7 and at SZA = 58.1°.

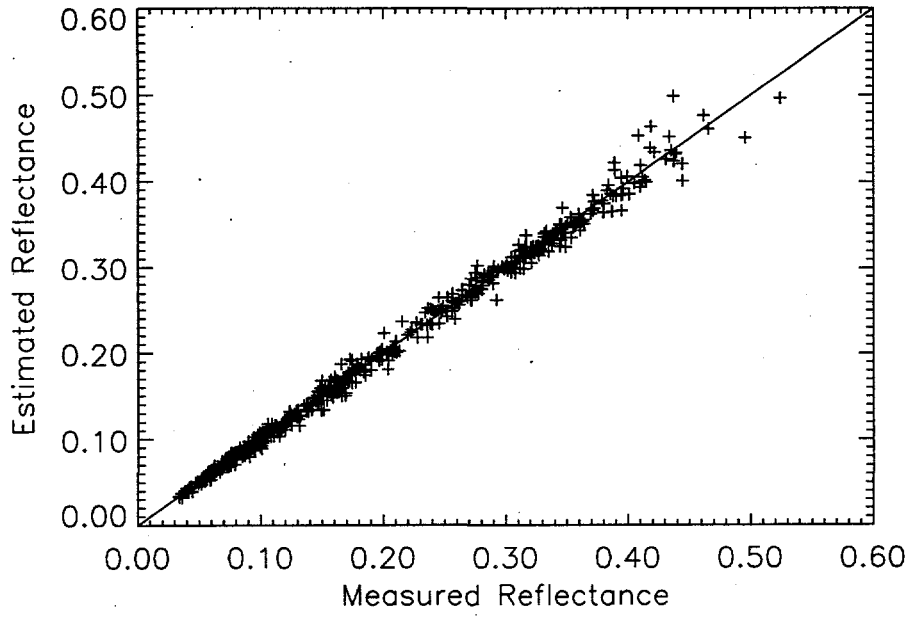

Figure 7.11. Comparison of measured data with model estimates from the ALLDATA solution. The 560 samples are from 7 spectral bands, 7 VZA, and 12 SZA. The 1-to-1 line is shown.

K. Comments on the Diffuse Irradiance Approximation

Although the diffuse irradiance approximation was expected to consistently improve results, its usefulness appears dependent on γ and/or SZA. In Figure 7.9, the atmosphere is relatively transparent ($\gamma = 0.842$). Although both the DIFF and NODIFF solutions fit the empirical data reasonably well in the forward scattering region, only the NODIFF solution exhibits a definite hot spot. In fact, the DIFF solution increases continuously with view angle in the backscatter region. The absence of a hot spot strongly limits the usefulness of this solution in low SZA cases. Results are worse for the 7BAND DIFF case (Figure 7.8). Differences are minimal at high SZAs, however (Figure 7.10).

Sometimes, the DIFF solutions provide a better fit (Figure 7.12). In this thick atmospheric condition ($\gamma = 0.600$, SZA = 58.1°), the two estimates of the data are comparable over most of the principal plane. In fact, the DIFF solution exhibits a better fit at high forward scattering angles. The cases in which DIFF solutions are better appear limited to those in which γ is low (~0.6).

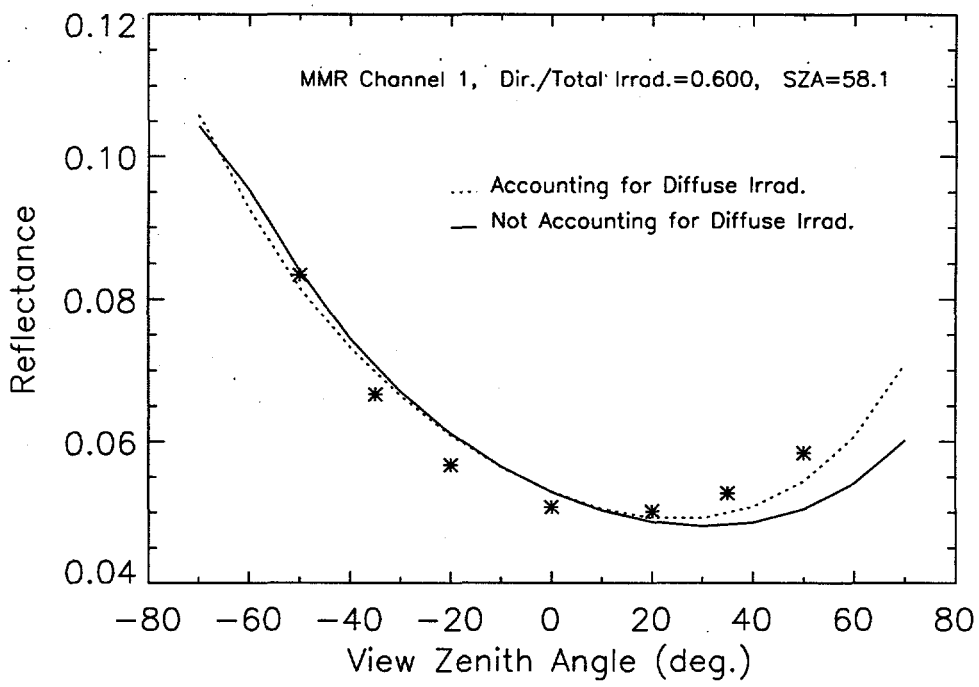

Figure 7.12. Fit of MMR band 1 data (asterisks) in the principal plane using ALLDATA solutions obtained with(out) the diffuse irradiance parameterization. The data were obtained at SZA = 58.1°, and the solutions were obtained over all SZA. Conditions represent the most turbid atmosphere (lowest γ) realized during measurements on five days.

Unfortunately, the diffuse approximation substantially increases optimization time. This may result from a decrease in merit function variance. Specifically, if diffuse irradiance decreases the reflectance anisotropy, the sensitivity of reflectance to soil parameters also decreases (Figure 7.4). This reduces the variance in the merit function, resulting in longer optimization times. The isotropic irradiance assumption may have resulted in these problems. Regardless, the parameterization proved unbeneficial in this study.

L. Model Validity in Directions Absent of Data

The results above demonstrate that inversion solutions depend on the sampling illumination angles (see Figure 7.8). The solutions may likewise depend on the sampling viewing angles. Indeed,

because FIFE MMR sampling was restricted to seven VZA in the principal plane, the validity of the solutions could not be ascertained for directions off the principal plane. Moreover, the accuracy of the solutions for VZA > 50° is unknown. Thus, in an effort to validate the ALLDATA solution, the effects of limited sampling geometries are investigated below.

Comparisons with Solutions from Non-FIFE Data

Assuming most soils scatter similarly, the validity of the ALLDATA solution can be investigated by comparing it to solutions found with non-FIFE data. Although Jacquemoud et al. [1992] utilized a comprehensive set of illumination and view angles, a comparison with their results is not straightforward since MMR measurements were made in the field while those of Jacquemoud et al. [1992] were made in the laboratory.

However, data from Kimes et al. [1985] data were gathered over a plowed field and thus contain effects from diffuse irradiance. Moreover, like the data in Jacquemoud et al. [1992], they were gathered in multiple azimuthal planes and over a large range of VZAs (see Table 7.3). In the study below, Kimes data gathered at three SZAs (26, 30 and 45°) in the red (0.58 - 0.68 μm) and NIR (0.73 - 1.1 μm) bands were used. For discussion purposes, an ALLDATA solution determined with the Kimes et al. [1985] data is denoted "KIMES" while the ALLDATA MMR solution (see Table 7.5) and clayey soil solution from Jacquemoud et al. [1992] are denoted "MMR" and "JAC", respectively.

In this experiment, MMR data gathered at 27.4 and 58.1° SZA were fit with the KIMES and JAC solutions by adjusting ω_s. All other parameters from the respective solutions remained fixed. The diffuse irradiance parameterization was only used with the JAC solution since it was determined from laboratory-measured data. Despite some differences in shape, all three curves depict the general features in the data (Figures 7.13 and 7.14). All show a significant hot spot and relatively low forward scattering. Still, the KIMES and JAC solutions show greater anisotropy. Burn residue at site 916 may be responsible for the more Lambertian nature of the MMR data [Forrest Hall, personal communication].

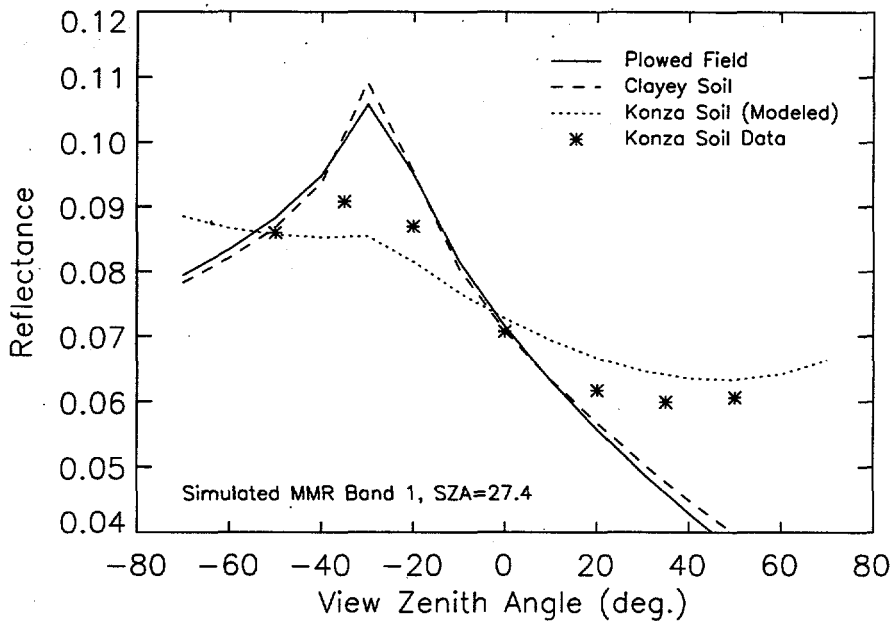

Figure 7.13. Comparison of solutions determined from different data sets to MMR band 1 data (asterisks) in the principal plane. The MMR data were obtained at SZA = 27.4°, and the solutions were obtained over all SZA.

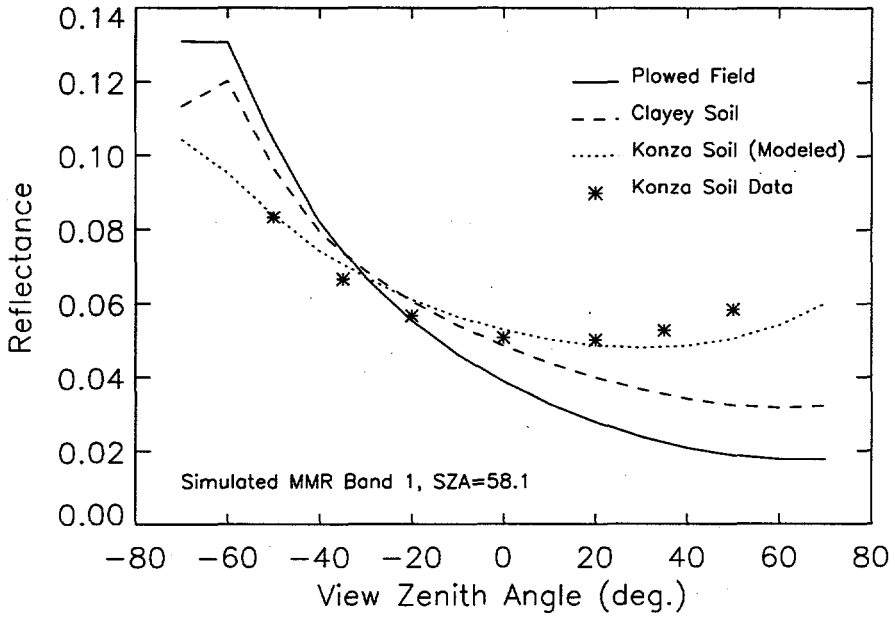

Figure 7.14. Same as Figure 7.13, except MMR data obtained at SZA = 58.1°.

Allowing that the three curves produce similar behavior in the principal plane, the MMR solution off the principal plane can be assessed by again comparing the behavior of the three solutions. Orthogonal plane reflectance (band 1) for the same two solar angles are shown in Figures 7.15 and 7.16. Differences in the mean trends are obvious. Specifically, the MMR reflectance is nearly constant for SZA = 27.4° while the KIMES and JAC solutions show decreasing reflectance with increasing VZA. For SZA = 58.1°, the MMR solution produces increasing reflectance with VZA. The KIMES and JAC solutions, however, show nearly constant reflectance.

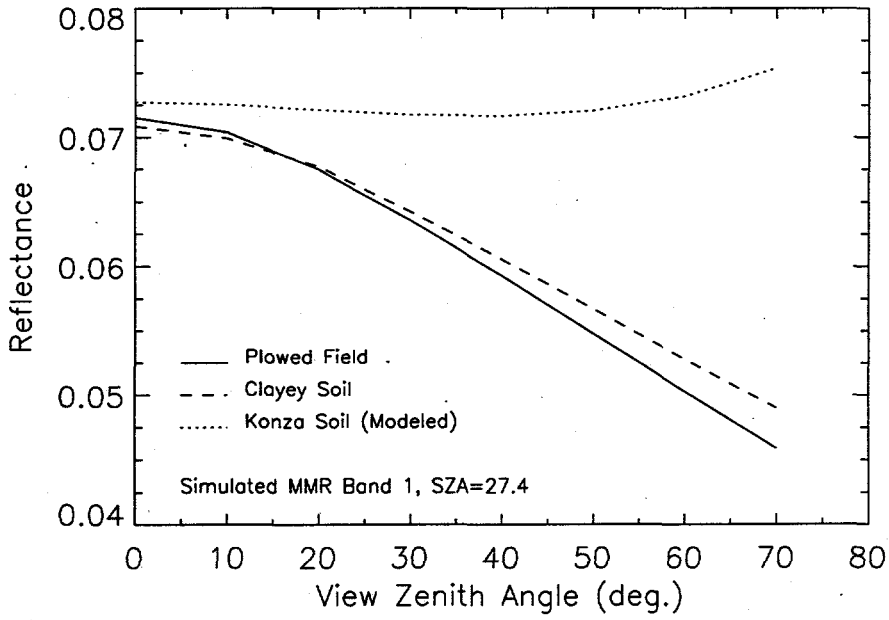

Figure 7.15. Comparison of solutions shown in Figure 7.13, but in the orthogonal plane.

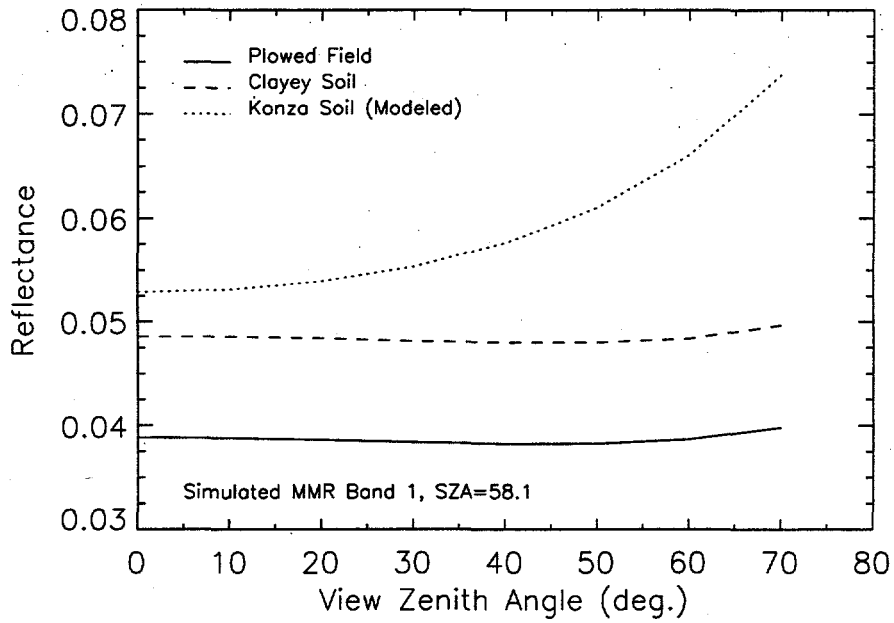

Figure 7.16. Comparison of solutions shown in Figure 7.14, but in the orthogonal plane.

Further comparison is possible using reflectance data from an arid region [Van Leeuwen and Huete, 1993]. The measured surfaces included crusty soil, dry and wet sand, and gravel. Although data at only one SZA per surface were available, the reflectance was sampled at multiple VZA in both the principal and orthogonal planes (Table 7.3). However, the lack of high VZA data (> 50°) is notable. The data were gathered in 46 spectral bands from 450 to 900 nm. Again, ALLDATA solutions were fit to MMR band 1 data (SZA = 27.4°) by adjusting ω_s. Principal plane fits are shown in Figure 7.17. Considering the vastly different surfaces, the estimates are reasonable. In particular, the crust, dry sand and gravel solutions show distinct hot spots. However, the dry sand solutions produce strong backscatter at high VZA whereas other solutions produce more modest backscatter. A decrease in forward scattering is exhibited by all solutions, yet at very high forward VZA, most of the solutions show increasing reflectance. The absence of samples at high VZA prevents validation in this region. Finally, the decorrelation of the wet sand solution from the others is evident.

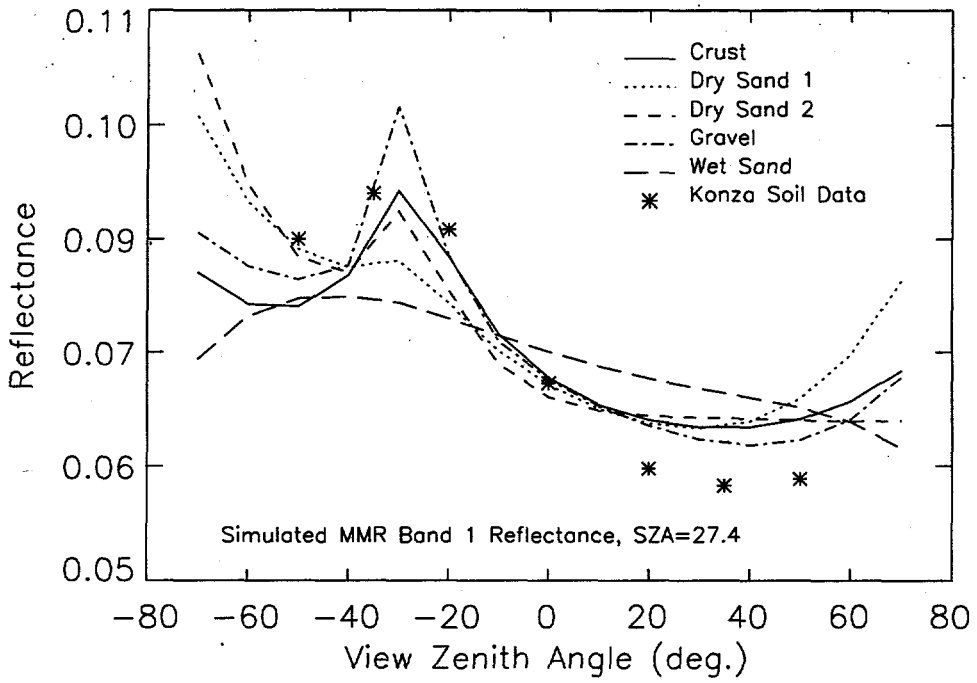

Figure 7.17. Comparison of solutions determined for arid surfaces to MMR band 1 data in the principal plane. The MMR data were obtained at SZA = 27.4°, and the solutions were obtained at different SZA.

The orthogonal plane reflectance is shown in Figure 7.18. Most solutions show slightly decreasing reflectance to about VZA = 45°, followed by sharp increases. This general behavior is similar to the MMR solution (Figure 7.15), although the reflectance increases at a greater rate for some arid soil solutions. Recall the arid soil data were not sampled at large VZAs (> 50°), however. Thus, the accuracy of the model reflectance at these angles is uncertain. The wet sand results again differ from those of the other surfaces.

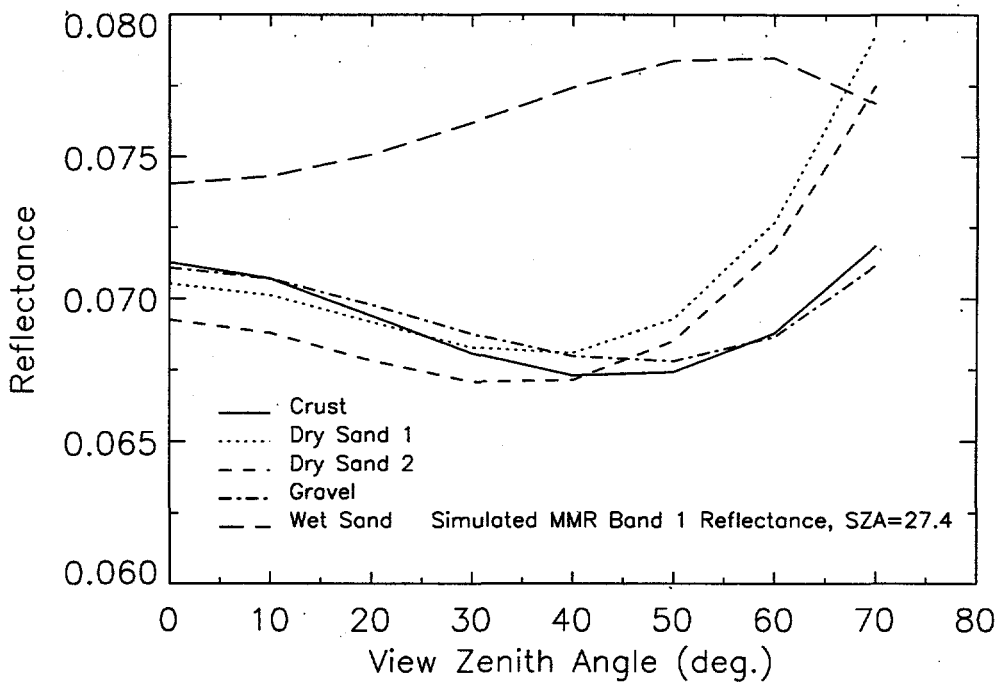

Figure 7.18. Comparison of solutions shown in Figure 7.17, for the orthogonal plane.

Solution Dependence on Sampling Scheme

The above results suggest that the validity of the MMR solution is questionable for some directions (VZA > 50° or orthogonal plane). However, some differences between the various solutions are due to surface differences. To estimate errors due strictly to MMR sampling geometry, the Kimes et al. [1985] data were subsampled to geometrically resemble MMR data. First, samples off the principal plane were eliminated. The reduced data sets contained 11 samples per band per solar angle. Samples suspected of shadow contamination were eliminated as before. Inversions were conducted using data from both bands and all SZA simultaneously (denoted "KIMES2"). Next, measurements at VZA > 50° were also eliminated. The resulting data sets (7 samples each) were used in independent inversions of each band and SZA (denoted "KIMES3").

Principal plane estimates of the Kimes data (SZA = 30°) are shown in Figure 7.19. The KIMES and KIMES2 solutions produce reasonable estimates over all VZA (the sample at -30° was not

used since shadow contamination was suspected). The KIMES3 solution produces reasonable estimates, although it exhibits strong forward scattering at high VZA and appears to overestimate the hot spot. The similarity of the KIMES3 solution to the arid surface solutions (Figure 7.17) at large VZA suggests systematic model behavior in these directions when no data are available.

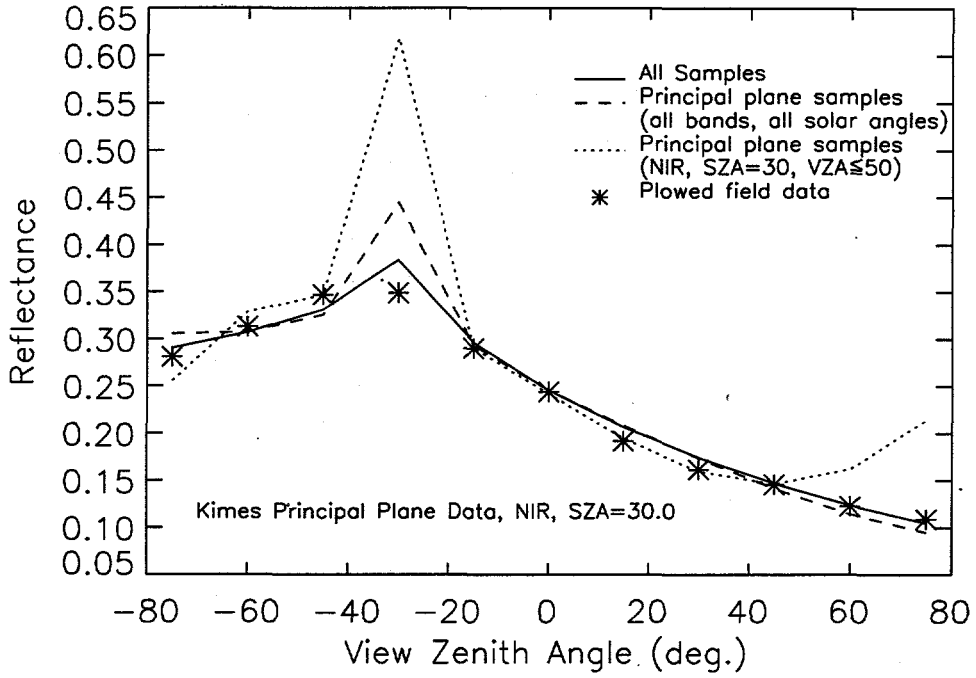

Figure 7.19. Comparison of solutions determined from plowed field data under different sampling schemes to plowed field data in the principal plane. The data were obtained at SZA = 30°, and the solutions were obtained at different SZA.

Results in the orthogonal plane (Figure 7.20) differ significantly. Again, the KIMES solution produces a reasonable fit. However, the KIMES2 solution underestimates the data—the magnitude of error increases with VZA. Greater errors are exhibited by the KIMES3 solution which shows increasing reflectance with VZA. The similarity of the KIMES3 result here and the MMR results in Figures 7.15 and 7.16 suggests that the orthogonal plane behavior for the MMR solution may have resulted from the limited sample sets. This supports the hypothesis that large increases in

reflectance at high VZA, as shown by the arid surface solutions (Figure 7.18), result from model inversions without data in the that region.

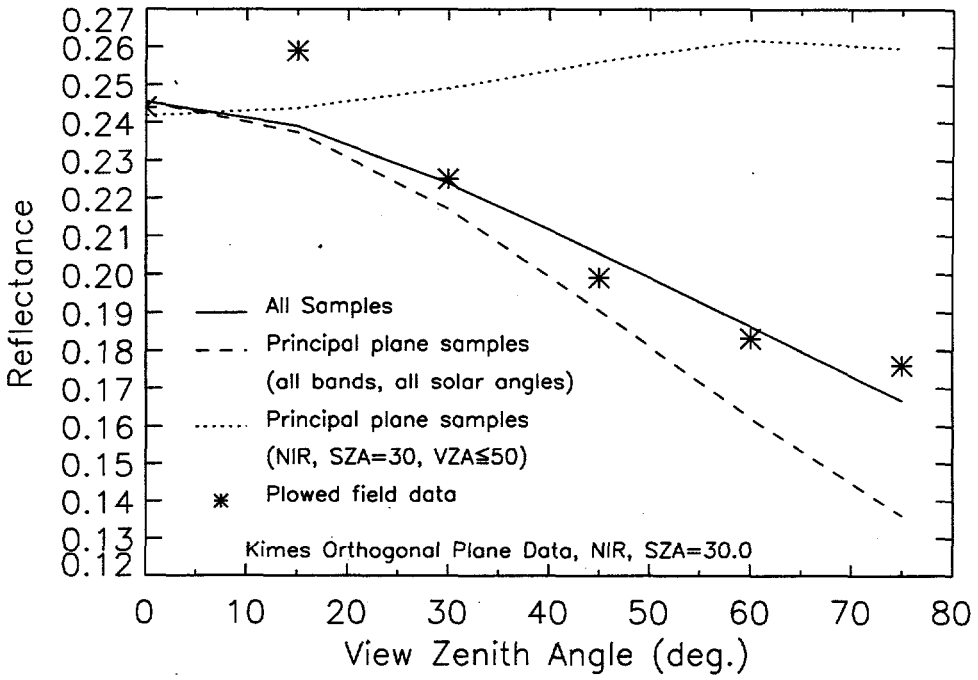

Figure 7.20. Same as Figure 7.19, but for the orthogonal plane.

M. Discussion of Errors

Several sources of errors have been identified that may have affected the MMR results. The reported view angles were accurate to ±10° azimuth and ±2.0° zenith. Also, as noted in the data set documentation, some variable cloud cover could have caused calibration differences since incoming radiation measurements were not simultaneous with surface measurements. As discussed in Section K, the isotropy assumption in the diffuse irradiance formulation introduces some inaccuracy—possibly more than the inaccuracy of neglecting diffuse irradiance.

As shown in Section L, the limited angular sampling of the MMR data may have contributed the largest errors. Not only might this affect the spectral, solar angle and soil moisture invariance of

the inversion solutions, it may have led to unreliable reflectance estimates off the principal plane. Comprehensive sampling may be a greater issue with semi-physically-based models (e.g., the soil model) than with physically-based models, since CANTEQ was successfully inverted using just nine principal plane samples (Chapter V).

Finally, since shaded samples could only occur near the solar direction, the shadow filter may bias the results. Specifically, nadir and forward scattering regions were better sampled than the backscatter region. Thus, forward scattering characteristics would have a greater effect on the parameter values. Furthermore, the trigonometric filter does not eliminate the effects of shading since diffuse irradiance is incident from all directions.

N. Conclusions

Simulations with Lambertian and anisotropic backgrounds revealed that anisotropic soil reflectance affects TOC reflectance for relatively thick (LAI < 8) canopies. Errors were greatest (and negative) in the retro-solar direction. Thus, anisotropic soil reflectance was deemed necessary for accurate modeling of FIFE conditions. Comparisons for different levels of γ suggested that reflectance anisotropy decreases with increasing atmospheric turbidity. A sensitivity study suggested that TOC reflectance (LAI = 1.9) was about twice as sensitive to single scattering albedo as it was to other soil parameters.

Inversions were conducted with FIFE soil data. Soil parameters that were reportedly spectrally-invariant were shown to depend on the data sets used for inversion. However, a relatively invariant solution was determined using data representing a wide range of spectral, SZA and soil moisture conditions. In this case, the mean of the absolute values of reflectance errors was 0.006 (3.5%). An investigation of data sampling geometries was also conducted. Results showed that solutions determined with this soil model may not be accurate for directions in which data are absent during inversion.

Finally, a diffuse irradiance approximation was added to the soil model. However, this approximation did not improve inversion results. Moreover, optimization times increased substantially when this approximation was used. This occurs since soil reflectance becomes less sensitive to model parameters as diffuse irradiance increases.

CHAPTER VIII

POINT INVERSIONS OF THE FIFE CANOPY MODEL

In the following experiments, DISORD was inverted with TOC reflectance data. Only data gathered on 4 August and 8 August 1989 were used. No rainfall occured during this period, and canopy parameters were assumed constant. DISORD was used in 1-D mode with isotropic diffuse irradiance. The fraction of direct-to-total irradiance (γ) was again determined with the 5S model. Despite uncertainty in the accuracy of its non-principal plane behavior, the ALLDATA soil solution from Chapter VII was used to specify the lower boundary condition. After filtering the data for shadow contamination, 23 complete data sets (each defined by seven samples at a given plot and SZA) remained. The range of SZAs for the data was 20 to 60°.

A. Validation of Coupled Model

A partial validation of the coupled (soil + canopy) model was attempted by comparing DISORD reflectance estimates to MMR TOC data. Mean parameter values (Table 6.2) were used together with mean atmospheric properties. Representative plots of red (band 3) and NIR (band 4) reflectance are shown in Figures 8.1 and 8.2. Both TOC and soil reflectance data are shown with model output. Although the model overestimates the red reflectance (absolute errors < 0.02), the differences may be due to soil effects. Specifically, the range of soil reflectance at some angles is more than twice the magnitude of the canopy reflectance. This large variability is probably due to moisture differences. A bright soil may substantially increase TOC reflectance, especially in canopies with high gap probabilities. Since turbid medium theory does not account for canopy gaps, the model may underestimate red reflectance. The NIR estimates (Figure 8.2) are within the range of the empirical data

for all view angles. Although the soil reflectance variability is similar in absolute units to that at red wavelengths, it is lower relative to the canopy reflectance. Therefore, its impact is reduced (see Chapter VII).

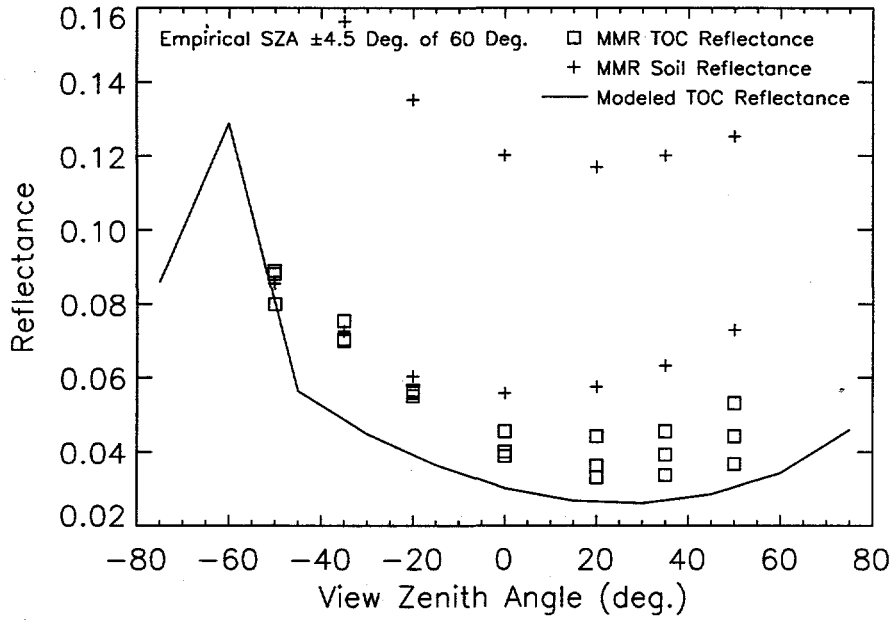

Figure 8.1. Comparison of measured and modeled TOC reflectance in principal plane. Reflectances was determined for band 3 (red) at SZA = 60°. Measured parameter values (Table 6.2) were used. Squares (□) represent TOC data and pluses (+) represent soil data. SZA of measured data were within ±4.5° of 60°.

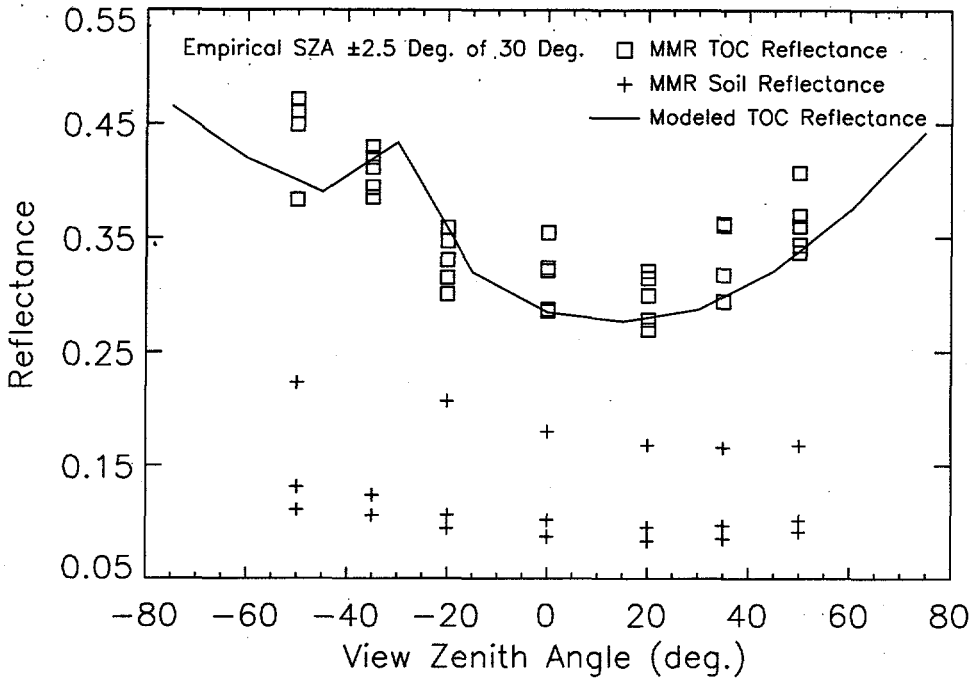

Figure 8.2. Same as Figure 8.1, but for band 4 (NIR) and SZA = 30°. The SZA of measured data were within ±2.5° of 30°.

These comparisons suggest that the method of determining soil and canopy parameters was reasonable and that the model is able to simulate the canopy reflectance with good accuracy. The latter condition is imperative to the success of the inversion problem.

B. Model Sensitivity Study

Although a general sensitivity study was conducted with CANTEQ (Chapter IV), a new sensitivity was required with DISORD due to the change in soil reflectance (Lambertian vs. anisotropic) and LAD (idealized vs. continuous Beta distribution). Moreover, while CANTEQ sensitivity was determined for arbitrary canopies, the following study is catered to conditions at site 916.

The sensitivity study procedure was similar to that used for the soil model, except that the ALLDATA NODIFF solution (Chapter VII) was used rather than the clayey soil solution. Canopy parameters were assigned values as determined from *in situ* measurements (Table 6.2). In cases where a 10% perturbation exceeded theoretical parameter limits, a 5% perturbation was used and the sensitivity value was doubled. Although γ was determined by 5S throughout this study (see Chapter VI), it was included here to assess the impact of errors in its determination.

Sensitivity values (S), found using Equation (7.1), are given in Table 8.1. TOC reflectance is most sensitive to leaf reflectance at both wavelengths. This agrees with results in Chapter IV. This sensitivity increases notably with SZA in the red band. Since leaves strongly absorb red photons, a higher SZA results in a larger path optical depth. The increased path depth decreases the impact of parameters for which the reflectance of a semi-infinite canopy is not sensitive (i.e., soil parameters and LAI). Lower leaf absorption in the NIR results in a smaller effect with SZA. Sensitivity to leaf transmittance is substantially less than to leaf reflectance in the red, however it provides nearly the same effect as leaf reflectance in the NIR. This also agrees with previous findings (Chapter IV). The sensitivity to leaf transmittance at red also increases significantly with SZA. The sensitivity increases most sharply at high SZAs due to changes in TOC forward scattering. Since leaf albedo is relatively high at NIR, there is significant multiple scattering. Hence, changes in leaf transmittance have less effect on forward scattering at these wavelengths.

Table 8.1. Sensitivity (S, from Equation 7.1) of TOC reflectance in principal plane to parameter perturbations. Perturbations equaled 10% of the theoretical or practical ranges. Columns represent different SZAs (30, 45 and 60°) at two wavelengths (red and NIR). Thin lines separate atmospheric, soil and vegetation parameters, respectively. γ is the direct-to-total irradiance ratio, h is the soil roughness parameter, b, c, b', and c' are soil phase function parameters, ω_s is the soil single scattering albedo, HSP is the canopy hot spot parameter, ρ and τ are leaf reflectance and transmittance, and $\mu(\theta)$, $\nu(\theta)$, $\mu(\varphi)$, and $\nu(\varphi)$ are coefficients of the LAD. Base case parameter values are given in Table 6.2.

	Red (Band 3)			NIR (Band 4)		
Parameter	30°	45°	60°	30°	45°	60°
γ	6.95	6.66	5.92	1.80	2.36	3.02
h	0.46	0.41	0.27	0.36	0.31	0.25
b	8.68	6.08	2.50	3.41	2.49	1.59
c	7.92	5.56	2.20	1.77	1.08	0.39
b'	6.57	3.98	2.02	2.90	1.99	1.34
c'	4.91	3.93	1.90	1.08	0.71	0.27
ω_s	14.86	10.66	5.15	6.42	5.19	3.82
HSP	2.73	3.08	1.17	1.00	1.11	0.42
ρ	60.67	71.44	82.34	23.60	24.15	24.33
τ	19.12	28.78	46.57	18.68	19.86	21.38
$\mu(\theta)$	4.62	4.09	5.26	10.10	7.74	7.18
$\nu(\theta)$	1.87	2.45	3.33	3.81	2.57	2.32
$\mu(\phi)$	0.75	0.93	2.66	2.14	2.41	2.87
$\nu(\phi)$	1.74	1.01	2.88	4.27	4.02	4.33
LAI	22.54	22.11	18.08	20.72	20.16	18.09

Relative to the sensitivities to the leaf optical properties, the sensitivity to LAI is significantly lower at red than at NIR. To a lesser degree, this also occurred in Chapter IV results. Due to high leaf absorption, the canopy behaves optically semi-infinite at a lower LAI for red photons. Hence, reflectance becomes relatively insensitive to perturbations in optical depth (LAI). In contrast to leaf optical properties, the sensitivity to LAI decreases with increasing SZA. This results from the increased path optical depth as discussed above. This result differs from that in Goel and Strebel [1983], where sensitivity to LAI increased with SZA. The fourth most influential parameter at red is ω_s, the impact of which decreases with increasing SZA. At NIR, the LAD parameter $\mu(\theta)$ is fourth and ω_s is fifth. The relative brightness of the soil with respect to the canopy causes the differences in parameter sensitivity order between the wavelengths. The sensitivity to the remaining parameters is not significantly different for either wavelength.

For model inversions, one set of adjustable parameters—influential over every band and solar angle combination—was desired. The model clearly is sensitive to the set $\{\rho, \tau, \text{LAI}, \omega_s\}$ at both wavelengths. Although the model is rather sensitive to $\mu(\theta)$ at NIR, its sensitivity to $\mu(\theta)$ at red is

less than its sensitivity to b, c, b', and c' for low SZAs. Nevertheless, $\mu(\theta)$ was kept variable and b, c, b', and c' were fixed. This decision was based both on the sensitivity results and on the results of Jacquemoud et al. [1992]. The latter suggested that $\{h, b, c, b', c'\}$ are essentially invariant with soil moisture and wavelength. Since LAD depends on two parameters ($\mu(\theta)$ and $\nu(\theta)$), both parameters were included in the adjustable set. Thus, for inversion purposes, the set {LAI, ρ, τ, $\mu(\theta)$, $\nu(\theta)$, ω_s} remained adjustable and the set $\{h, b, c, b', c', \mu(\phi), \nu(\phi)\}$ was fixed. Note the adjustable set contains parameters of both vegetation and soil.

C. Inversion Problem Configuration

Inversions were conducted individually for each of the seven spectral bands and 23 data sets. Thus, seven samples (unique VZAs) were used to determine six parameters. This inversion configuration was used based on the redundancy in sampling (each sample represents an average of three measurements), the clarity of the atmosphere, and the high information content in the principal plane (see Chapter V). Equation (2.5) was minimized using a simplex routine (subroutine AMOEBA, [Press et al., 1986]).

To avoid unrealistic results, parameter limits were imposed. The broad ranges were based on both theory ($0 < \omega_s < 1$) and expected results (LAI < 10). The initial AMOEBA simplexes spanned the parameter space but were not necessarily the optimal choices. The AMOEBA routine was modified to permit variable expansion coefficients such that all vertex movements fell within the allowed parameter space. Minimization was terminated when the merit function values (Equation 2.5) of all vertices were to within 10^{-7}. This was found to be a reasonable value in the investigation of optimization routines (Chapter IV). The procedure was restarted once after the initial convergence to avoid local minima trapping. Restart simplexes featured one vertex at the original solution and the remaining vertices extending out from the solution along the respective parameter axes.

D. Inversion Results

Spectral Band and Solar Angle Analysis

Comprehensive analysis of retrieved parameters is possible due to the diverse set of spectral bands and solar angles used. To achieve reasonable statistical significance, SZAs were binned either above or below 40° (approximately the center of the range). Solutions with LAI < 0.1 were eliminated since this condition precludes a reasonable determination of any model parameter. It is assumed that spectral vegetation indices could ascertain whether the target LAI is above this value. The number of cases averaged per band and SZA combination is given in Table 8.2.

Table 8.2. Mean errors (with mean relative errors in parentheses) and standard deviations in retrieved leaf reflectance as a function of band and SZA. Measured values (ρ_o) are also shown. The numbers of samples used to generate means are shown next to standard deviations.

		SZA < 40°			SZA > 40°		
Band	ρ_o	ME (MRE)	σ	no.	ME (MRE)	σ	no.
1	0.101	0.052 (51.5)	0.020	13	0.022 (21.8)	0.007	10
2	0.174	0.100 (57.5)	0.049	10	0.027 (15.5)	0.044	9
3	0.097	0.071 (73.2)	0.031	13	0.053 (54.6)	0.042	9
4	0.452	0.084 (18.6)	0.079	13	0.002 (0.4)	0.033	10
5	0.424	0.054 (12.7)	0.061	13	-0.015 (-3.5)	0.031	10
6	0.320	0.138 (43.1)	0.125	10	-0.006 (-1.9)	0.066	10
7	0.252	-0.115 (-45.6)	0.043	13	-0.113 (-44.8)	0.019	10

Results are indicated as mean errors (ME) and mean relative errors (MRE, in %), where

$$\mathrm{ME} = \frac{1}{N} \sum_{i=1}^{N} (P_i - P_o) , \qquad (8.1)$$

and

$$\mathrm{MRE} = \frac{1}{N} \sum_{i=1}^{N} \frac{(P_i - P_o)}{P_o} \; 100, \qquad (8.2)$$

where P_o is the measured parameter value, P_i is the retrieved parameter value for data set i, and N is the number of data sets.

Errors in leaf reflectance were lowest at high SZA (Table 8.2). Except for band 3, the standard deviations were also lower at high SZA. These observations are consistent with the sensitivity analysis which showed an increased model sensitivity to leaf reflectance with increasing SZA (Table 8.1). They are also consistent with results in Chapter V. This suggests that leaf reflectance is best estimated when the path optical depth for irradiance is large. A large path depth increases photon interaction within the canopy and reduces interaction with the soil. Thus, errors introduced by an incorrectly determined background or LAI are reduced. Leaf reflectance errors are lowest (< 0.006, 1.9%) in the NIR (bands 4 and 6). This may be due to the greater magnitude of canopy reflectance relative to soil reflectance at NIR. This increases the effective signal-to-noise ratio.

Leaf transmittance, in contrast, is most accurately estimated at high SZA for visible bands, but at low SZA for NIR bands (Table 8.3). These trends are predictable given the spectra of soil and vegetation. When the background is relatively bright (as in the visible), results are most accurate when it receives little irradiance (i.e., long path depth due to high SZA). The large increase in model sensitivity to τ with increasing SZA at red (Table 8.1) is consistent with these results. When the background is comparatively dark (NIR), soil effects on TOC reflectance are small and hence canopy downwelling transmittance (soil irradiance) is less important. Thus, although the NIR sensitivity to τ increases with SZA (Table 8.1), it is much less significant than for red. These trends also are consistent with previous results (see Chapter V). The standard deviations are generally lower for all bands at high SZAs. This trend may also be caused by the high sensitivity of canopy forward scattering to leaf transmittance at high SZA.

Table 8.3. Mean errors (with mean relative errors in parentheses) and standard deviations in retrieved leaf transmittance as a function of band and SZA. Measured values (τ_o) are also shown.

		SZA < 40°		SZA > 40°	
Band	τ_o	ME (MRE)	σ	ME (MRE)	σ
1	0.041	-0.015 (-36.6)	0.037	0.009 (21.9)	0.012
2	0.144	-0.028 (-19.4)	0.061	-0.018 (12.5)	0.031
3	0.053	-0.013 (-24.5)	0.067	0.012 (22.6)	0.023
4	0.490	-0.026 (-5.3)	0.078	-0.047 (-9.6)	0.042
5	0.510	0.010 (1.9)	0.057	-0.015 (-2.9)	0.056
6	0.436	0.041 (9.4)	0.054	0.060 (13.7)	0.061
7	0.318	-0.021 (-6.6)	0.130	-0.114 (35.8)	0.036

Errors in ω_s (Table 8.4) are not well correlated with SZA, although standard deviations are mostly lower for low SZAs. The absence of a clear trend with SZA is surprising given the greater sensitivity of TOC reflectance to soil at low SZAs. Nevertheless, a comparison of modeled soil reflectance using the retrieved ω_s is revealing (Figure 8.3). The modeled soil spectrum closely follows the vegetation spectrum for ω_s retrieved at high SZAs. The modeled soil spectrum closely follows the measured soil spectrum for ω_s retrieved at low SZAs. This shows that the inversion correctly adjusts ω_s to "background" spectral behavior for low SZAs, but that it decouples ω_s from background reflectance for high SZAs. Referring again to Table 8.4, estimates of ω_s are low for all bands at low SZAs. The overestimation of leaf reflectance at low SZAs undoubtedly leads to this systematic deviation. Still, it must be reiterated that the "measured" ω_{so} values were not determined from direct measurements (see Chapter VII), and hence may not be correct. In addition, the similarity of the soil from which the measured parameters were determined to the below-canopy soil is not known. Canopy litter was present in the latter case [Dave Schimel, personal communication] which may have impacted results. Soil moisture also may have differed. The relatively low sensitivity of the coupled model (Table 8.1) to soil parameters underscores the difficulty in retrieving soil information from TOC data.

Table 8.4. Mean errors (with mean relative errors in parentheses) and standard deviations in retrieved ω_s as a function of band and SZA. Measured values (ω_{so}) are also shown.

		SZA < 40°		SZA > 40°	
Band	ω_{so}	ME (MRE)	σ	ME (MRE)	σ
1	0.091	-0.043 (-47.3)	0.038	0.111 (122.0)	0.053
2	0.205	-0.129 (-62.9)	0.050	0.084 (41.0)	0.104
3	0.259	-0.098 (-37.8)	0.017	-0.050 (-19.3)	0.078
4	0.347	-0.084 (-24.2)	0.091	0.262 (75.5)	0.130
5	0.490	-0.124 (-25.3)	0.036	0.206 (42.0)	0.127
6	0.603	-0.170 (-28.2)	0.039	-0.086 (-14.3)	0.124
7	0.652	-0.202 (-31.0)	0.138	-0.208 (-31.9)	0.045

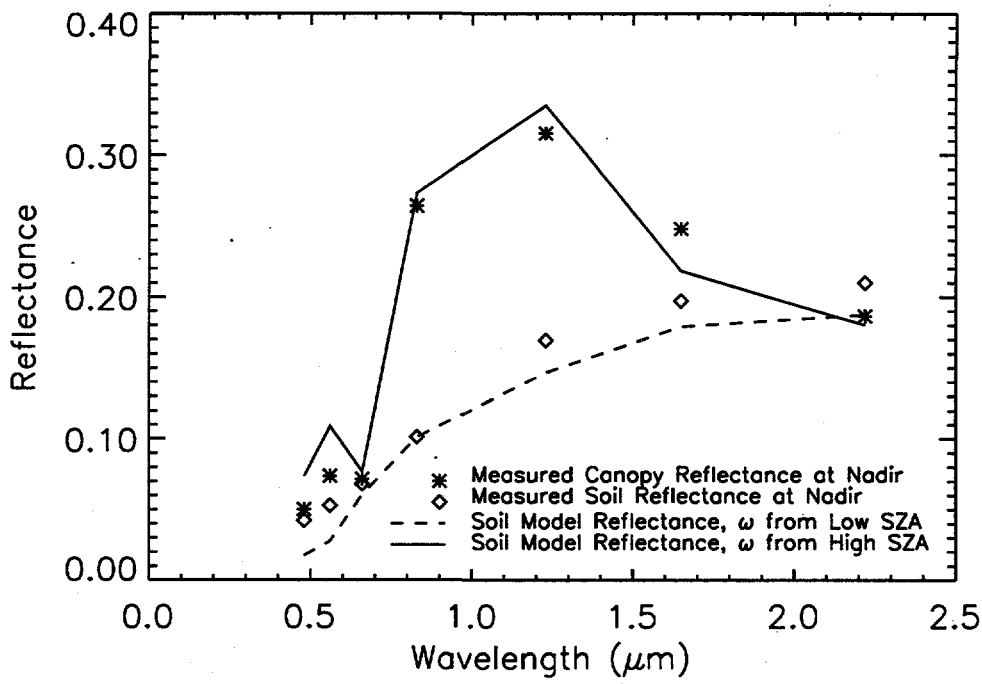

Figure 8.3. Nadir reflectance from the soil model using ω_s retrieved from canopy model inversions. Diamonds (◊) represent soil reflectance as measured by MMR at nadir, and asterisks (*) represent equivalent TOC reflectance. Solid line shows soil model reflectance for ω_s retrieved at high SZA. Dashed line shows the equivalent for ω_s retrieved at low SZA.

The retrieved LAI as a function of SZA and spectral band is shown in Figures 8.4a-g and Table 8.5. The dashed lines (Figures 8.4a-g) represent the mean measured LAI. Several trends are noticeable. First, the means and standard deviations of the errors generally increase with SZA. This is consistent with the sensitivity analysis (Table 8.1) which showed that the model's sensitivity to LAI

decreases with increasing SZA. This results from a longer path length for irradiance with increasing SZA. However, this result is contrary to that of Goel and Strebel [1983]. The best LAI estimates are provided by bands 4 and 5 at low SZAs, where the mean errors are less than 0.16 (8.1%) and the standard deviations are less than 0.35. This error is well within the uncertainty of the measured value. The consistency in bands 4 and 5 is obvious in Figures 8.4d-e. This also follows from the sensitivity study, since the sensitivity to LAI at NIR exceeded the sensitivity to LAI at red, relative to other parameters. The preference of NIR bands for LAI retrieval has been reported in several studies [e.g., Goel and Strebel, 1983]. The superiority stems from the lower leaf absorption at NIR wavelengths. Lower leaf absorption results a greater LAI range for which the canopy behaves optically finite. Excluding outliers in both bands 1 and 3, the visible bands (1-3) consistently underestimate LAI by a small amount for low SZA.

Table 8.5. Mean errors (with mean relative errors in parentheses) and standard deviations in retrieved LAI as a function of band and SZA. The measured LAI value was 1.94 ± 0.61.

	SZA < 40°		SZA > 40°	
Band	ME (MRE)	σ	ME (MRE)	σ
1	0.225 (11.6)	2.382	1.006 (51.9)	1.632
2	-0.641 (-33.0)	0.524	0.466 (24.0)	1.914
3	0.044 (2.3)	2.894	-1.045 (-53.9)	0.658
4	0.157 (8.1)	0.347	5.103 (263.0)	2.587
5	-0.068 (-3.5)	0.331	2.484 (128.0)	3.547
6	-0.590 (-30.4)	2.110	1.027 (52.9)	4.266
7	1.845 (95.1)	3.759	-0.828 (-42.7)	0.395

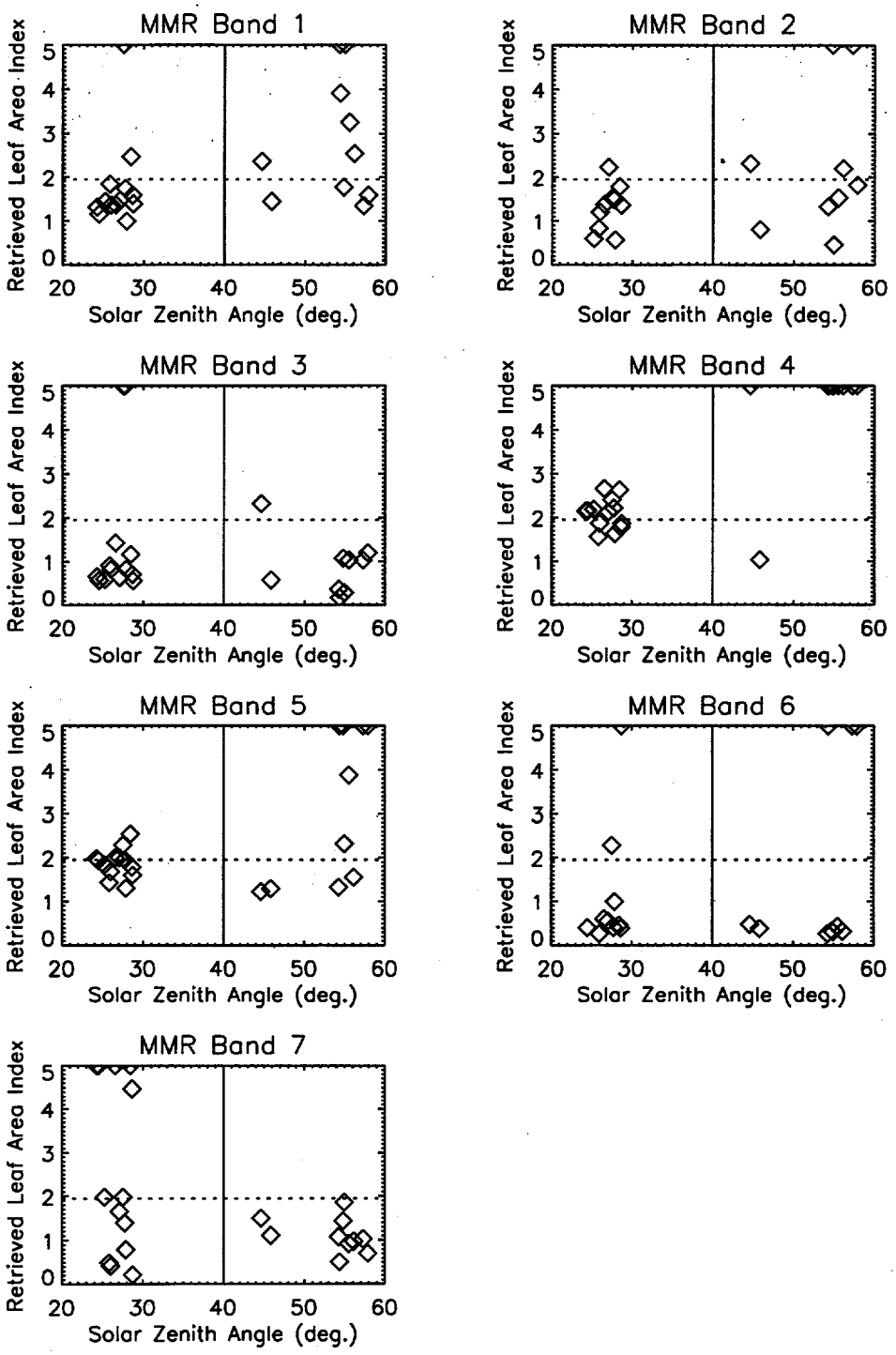

Figure 8.4. Retrieved LAI as a function of spectral band (ordered sequentially from left to right, top to bottom) and SZA. Horizontal dotted line indicates mean measured LAI. Vertical line partitions SZA bins. The accuracy and consistency of inversions with NIR bands (4 and 5) at low SZA is apparent. For graphing purposes, values greater than 5.0 were set equal to 5.0.

To determine the most accurate estimation of LAD, the χ^2 statistic was employed [Press et al., 1986],

$$\chi^2 = \sum_{j=1}^{10} \frac{(f_j^* - f_j)^2}{f_j^* + f_j}, \qquad (8.3)$$

where f_j^* is the estimated fraction of leaf normals in zenith angle bin j, and f_j is the measured fraction. The estimated values were determined at the bin centers and normalized. The estimated distribution is closest to the measured distribution when χ^2 is lowest. The mean estimates of $\mu(\theta)$ and $\nu(\theta)$, their standard deviations, and the associated χ^2 values are given in Table 8.6. High SZAs produce the most accurate estimates for all bands. This may be due to the increased reflectance anisotropy with SZA and the impact of the LAD on that anisotropy. The best estimates are from NIR bands 4 and 5 ($\chi^2 = 0.037$ and 0.008, respectively). Note the latter value is an order of magnitude lower than all others. The average LAD from these two bands ($\chi^2 = 0.020$) matches the true distribution well (Figure 8.5). Band 5 at high SZAs also produces the least variance in $\mu(\theta)$, although $\nu(\theta)$ is more consistently estimated in other bands. Bands 4 and 5 also produce relatively accurate estimates at low SZAs. The preference of NIR bands for the estimation of the LAD is obvious from the sensitivity study results (Table 8.1). Relative to leaf optical properties, the sensitivity to LAD parameters is much greater at NIR wavelengths. Note the NIR sensitivity decreases slightly with increasing SZA. This explains the lack of a strong dependence on SZA in the NIR inversion results. The opposite sensitivity trend with SZA occurs at red (Table 8.1); an SZA dependence is evident in visible band results (Table 8.6).

Table 8.6. Mean errors and standard deviations in retrieved LAD parameters ($\mu(\theta)$, $\nu(\theta)$) as a function of spectral band and SZA. Errors in LAD are characterized by χ^2: lower values indicate fits closer to the measured distribution. The measured values were $\{\mu(\theta), \nu(\theta)\} = \{0.860 \pm 0.063, 2.244 \pm 0.368\}$.

SZA < 40°

	$\mu(\theta)$		$\nu(\theta)$		
Band	ME	σ	ME	σ	χ^2
1	1.183	0.678	2.554	0.265	0.228
2	0.752	0.995	1.801	1.292	0.135
3	0.604	0.864	1.907	1.335	0.100
4	0.119	0.708	0.964	1.452	0.038
5	0.345	0.397	1.261	1.404	0.061
6	0.623	1.621	2.451	0.572	0.102
7	2.366	2.125	2.293	0.707	0.562

SZA > 40°

	$\mu(\theta)$		$\nu(\theta)$		
Band	ME	σ	ME	σ	χ^2
1	0.373	0.395	2.115	0.450	0.076
2	-0.190	0.392	1.724	1.520	0.116
3	0.212	0.838	2.298	0.891	0.085
4	-0.014	0.310	0.924	1.323	0.037
5	-0.189	0.162	-0.100	0.939	0.008
6	-0.180	0.214	1.426	1.583	0.091
7	0.782	1.411	1.806	1.858	0.143

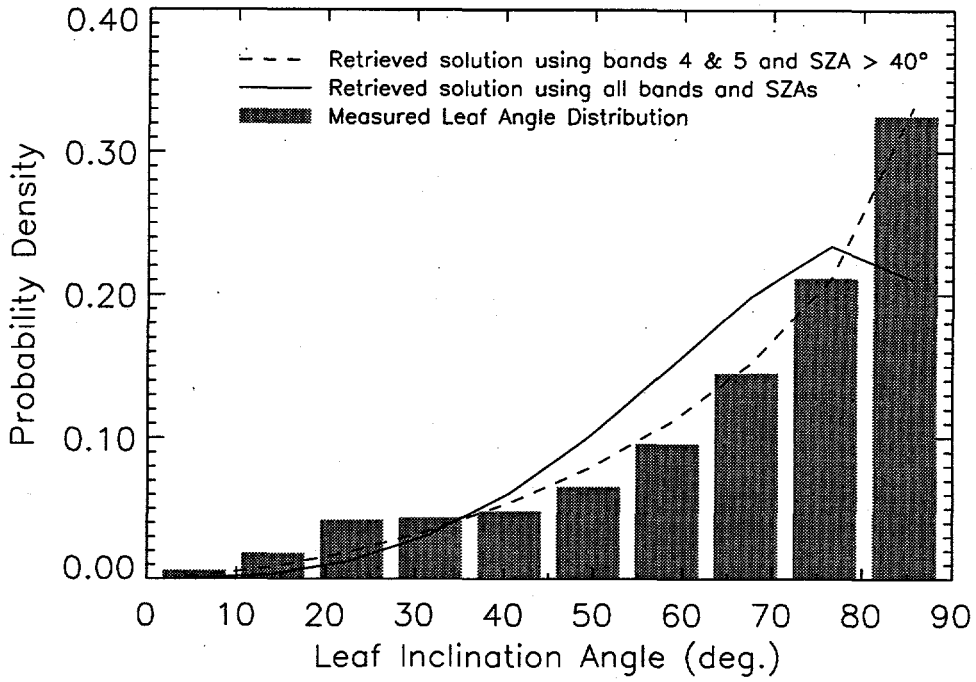

Figure 8.5. Comparison of the mean measured LAD (bars) to retrieved LADs (lines). The dashed line illustrates the distribution determined by averaging over NIR bands and high solar zenith angles. The solid line illustrates the distribution determined by averaging over all bands and solar angles. Retrieved distribution values were determined at bin centers and normalized.

Mean Retrieved Parameters

In previous inversion studies with empirical data, results from multiple bands and SZA were often averaged. To better understand those reports in light of the above analysis, the results obtained here were also averaged.

Spectrally-dependent parameters were determined by averaging over all SZA for each band (19-23 cases per band after LAI > 0.1 filtering). Leaf reflectance is overestimated in all but band 7 (Table 8.7). Leaf reflectance errors in bands 1-6 are as high as 0.066. The tendency for overestimation was reported in Chapter V. Mean errors in leaf transmittance are lower than those in leaf reflectance for all bands (Table 8.7). This result was unexpected due to the greater sensitivity to leaf reflectance (Table 8.1). In part, this is due to the smaller errors in leaf transmittance (compared to leaf reflectance) at low

SZA (Table 8.3). Although errors in ω_s are on the order of those in leaf optical properties, their standard deviations are notably larger in some bands (1, 2, 4, and 5). This indicates the difficulty in retrieving soil parameters from TOC data. It also emphasizes the need for TOC reflectance data at low SZA. Indeed, ω_s may be difficult to assess for canopies at high latitudes. Estimates with bands 6 and 7 are particularly inaccurate.

Table 8.7 Mean errors and standard deviations of retrieved parameters (spectrally-variant) determined from all estimates. Values were averaged over 23 data sets per band. Mean errors in spectrally-invariant parameters were {LAI, $\mu(\theta)$, $\nu(\theta)$} = {0.647, 0.0534, 1.681} and standard deviations were {LAI, $\mu(\theta)$, $\nu(\theta)$} = {2.725, 1.173, 1.341}. Spectrally-invariant parameters were averaged over 7 bands and 23 data sets.

Band	Statistic	ρ	τ	ω_s
1	ME	0.039	-0.005	0.024
	σ	0.022	0.031	0.089
2	ME	0.066	-0.024	-0.028
	σ	0.059	0.048	0.134
3	ME	0.064	-0.003	-0.078
	σ	0.036	0.054	0.055
4	ME	0.048	-0.035	0.067
	σ	0.075	0.065	0.206
5	ME	0.024	-0.001	0.020
	σ	0.061	0.057	0.188
6	ME	0.066	0.051	-0.128
	σ	0.122	0.057	0.099
7	ME	-0.114	-0.062	-0.205
	σ	0.034	0.109	0.106

The spectrally independent parameters (LAI, $\mu(\theta)$ and $\nu(\theta)$) were determined by averaging over all bands and solar angles (153 values). LAI is overestimated by 0.647 (33.3%). As the analysis above (Table 8.5) shows a clear preference for low SZA sampling, it appears that the relatively reasonable estimate here is by coincidence. This is confirmed by the standard deviation, which is more than four times greater than the mean error. This is consistent with results in Chapter V. The LAD parameters are both overestimated, although the distribution remained erectophile ($\chi^2 = 0.089$) (Figure 8.5). The retrieved LAD diverges most notably at large leaf inclination angles.

Surface Albedo

Although the MMR bands are not contiguous over the shortwave frequencies, albedo may be estimated using the "extended band" method of Starks et al. [1991]. In this method, the MMR bandwidths are artificially extended such that all shortwave frequencies are represented (Table 8.8).

Table 8.8. Extended bandwidths used to compute albedo values. Mean weights ($\overline{W_i}$) and standard deviations were determined from 5S results.

Band	Bandpass Limits	Extended Limits	$\overline{W_i}$	σ
1	0.450-0.520	0.300-0.520	0.239	0.005
2	0.520-0.600	0.520-0.615	0.146	0.002
3	0.630-0.690	0.615-0.725	0.144	0.001
4	0.760-0.900	0.725-1.000	0.222	0.002
5	1.150-1.300	1.000-1.360	0.139	0.002
6	1.550-1.750	1.360-1.800	0.067	0.001
7	2.080-2.350	1.800-4.000	0.043	0.001

The fraction ($\overline{W}_i$) of shortwave energy incident in each band is used to weight the broad-band spectral albedo ($\overline{ALB}_i$). The total albedo (ALB) is estimated by summing the spectral products:

$$ALB = \int_{0.3}^{4.0} ALB_\lambda \, W_\lambda \, d\lambda = \sum_{i=1}^{7} \overline{ALB}_i \, \overline{W}_i, \qquad (8.4)$$

where

$$\overline{W}_i = \left[\frac{\int_{\lambda_{a,i}}^{\lambda_{b,i}} I_{o,\lambda} \, d\lambda}{\int_{0.3}^{4.0} I_{o,\lambda} \, d\lambda} \right], \qquad (8.5)$$

and where $\lambda_{a,i}$ and $\lambda_{b,i}$ are the lower and upper limits of extended band *i*, respectively. In DISORD, spectral albedo is determined through quadrature integration of the computed reflectance distribution.

The downwelling energy within an extended band was determined using 5S (see Chapter VI). Exact solar angles and measured atmospheric data were used in each case. Average weights ($\overline{W}_i$) and their standard deviations are given in Table 8.8.

1) Case 1 Equation (8.4) was used to compute albedo for all 23 MMR data sets. In this case, $\overline{ALB}_i$ was calculated separately from the retrieved parameter set for each spectral band and solar angle. Thus, the albedo was effectively determined from seven reflectance samples. This application differs only slightly from Starks et al. [1991], where an average atmosphere was assumed and $\overline{W}_i$ was determined at 10° increments of SZA (0-70°). That study also employed different atmospheric and BRDF models.

Albedo estimates were compared with mean measured values as determined from two pairs of pyranometers. The pyranometer data were gathered at a nearby plot simultaneously with the MMR data. Model estimates exceed the measured albedo in most cases (Figure 8.6a). Differences decrease with increasing albedo, however. The correlation coefficient (r) is 0.89.

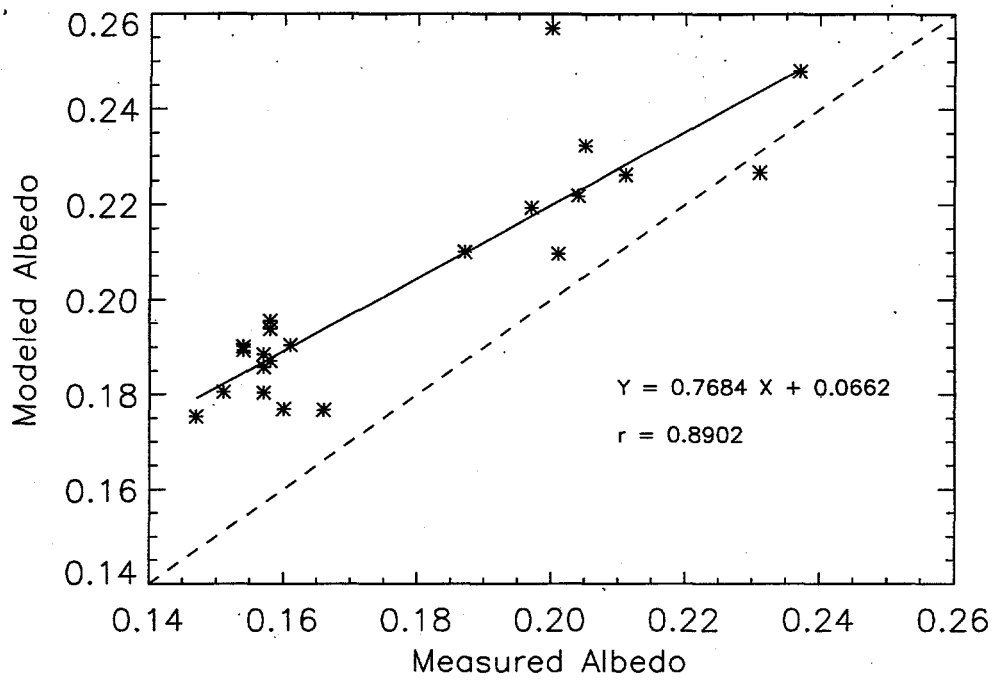

Figure 8.6a. Comparison of measured and modeled albedo. Parameter sets were retrieved for each band and solar angle individually. This follows the method of Starks et al. [1991]. The dashed line is the 1-to-1 line.

Error values were calculated using Equations (8.1) and (8.2), where $(P_i - P_o)$ was replaced with $|ALB_i - ALB_{o,i}|$. $ALB_{o,i}$ is the measured albedo and ALB_i is the estimated albedo for data set *i*. The mean error (ME) is 0.025 and the relative error (MRE) is 14.9%. Errors are not well correlated with either SZA or γ. Starks et al. [1991] report larger errors (MRE = 22.4% for 1987 and 27.6% for 1988) using an empirical model and a more diverse set of MMR data. A significant systematic error—exemplified by the offset of the regression line in Figure 8.6a—was also apparent in their results.

Systematic errors may have resulted from several sources. First, the band extension technique assumes constant average reflectance over the entire extended bandwidth. The lack of data over the full shortwave spectrum prevents validation of this assumption. Second, model or minimization inaccuracies may have produced parameter errors. Given the analysis of parameter errors above, some parameters clearly were not retrieved accurately for some bands and solar angles. Nevertheless, results in Chapter V suggest errors in spectral albedo remain small despite significant errors in retrieved

parameters. Third, the frame supporting the pyranometers caused shading. Starks et al. [1991] found that shading effects increased with SZA, resulting in up to 7% underestimation of measured albedo. Nevertheless, improvements in the results here compared to those in Starks et al. [1991] may be due to the use of a physically-realistic model in this study. This is particularly important in directions for which data were not available, and directions near the hot spot (not accounted for in Starks et al. [1991]). A comprehensive discussion of albedo errors may be found in Starks et al. [1991].

2) *Case 2* In Case 1, the accuracy of the model parameters differed for each band and solar angle. Thus, the exercise demonstrated the model's ability to estimate instantaneous albedo given seven principal plane samples. The operational usefulness of this ability is limited. In a coupled remote sensing-GCM scenario, albedo must be estimated much more frequently than directional reflectance data can be obtained. For example, daylight repeat sample times of polar orbiting satellites are typically regulated to days (e.g., ~1 sample/target/day from AVHRR). The Community Climate Models (CCMs) developed at the National Center for Atmospheric Research (NCAR) have temporal resolutions of 30 minutes. Therefore, a single set of retrieved model parameters must produce accurate albedo values over a broad range of illumination conditions.

To test the potential of a single parameter set, the measured soil and vegetation parameter values (Tables 6.2 and 7.5) were used in DISORD. Spectral albedo was determined through forward model calculations. The total albedo was calculated using Equation (8.4). In this exercise, only the solar angle and atmospheric parameters changed with time. The soil and canopy parameters remained fixed.

A comparison of estimated and measured albedo is shown in Figure 8.6b. The mean difference is 0.022 (13.0% relative)—a small improvement over Case 1. Again, errors decrease as albedo increases. The regression coefficient ($r = 0.95$) indicates a significant reduction in random errors from Case 1. Since Case 2 did not require inversions and its errors were smaller, inversion solution differences must have contributed substantially to the non-systematic errors in Case 1. Systematic error sources noted in Case 1 remain possible here.

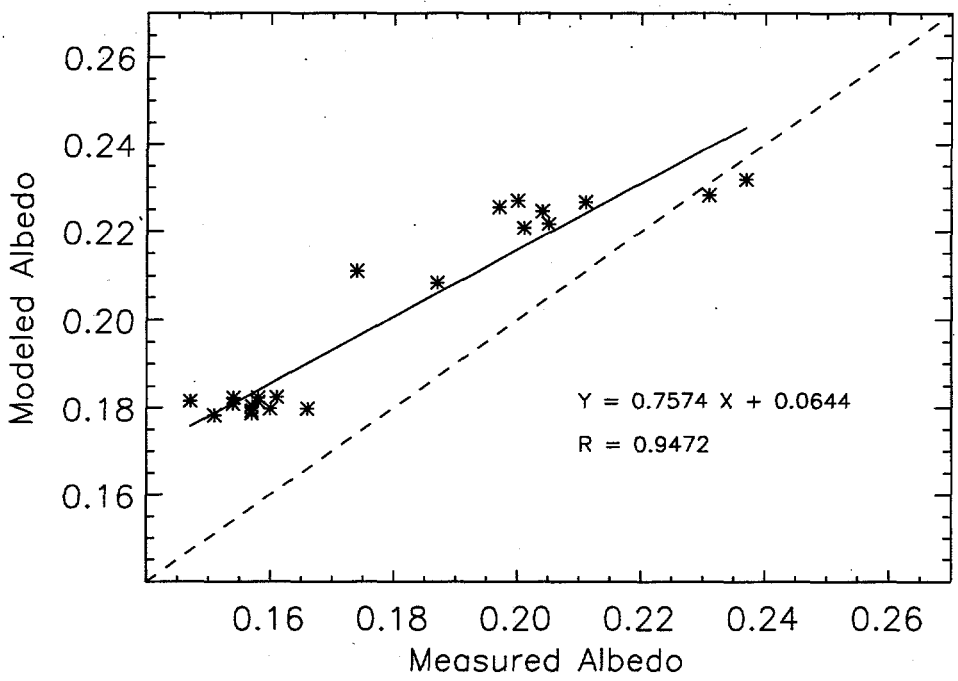

Figure 8.6b. Comparison of measured and modeled albedo. Parameter sets were determined from measured values (Table 6.2). Only atmospheric properties and solar zenith angles were changed between model calculations.

3) Case 3 Cases 1 and 2 suggest that 1) instantaneous albedo can be estimated via inversion given a set of principal plane data, and 2) a single parameter set can produce reasonable albedo values over different times/solar angles. The circle can be completed if the *retrieved* parameters are sufficiently accurate to calculate albedo over different times/solar geometries.

Results from the band/solar angle analysis (Section D) were therefore employed. "Optimal" retrieved parameter values were determined by averaging the results retrieved under preferred solar and spectral conditions. Exceptions were not made for anomalously accurate values (e.g., values of ω_s in bands 2 and 3 at high SZAs). Specifically, leaf reflectance was obtained from results at high SZA (Table 8.2). Leaf transmittance in visible bands was obtained from results for high SZAs, while NIR transmittance was obtained from results for low SZAs (Table 8.3). Soil single scattering albedo was obtained from results at low SZAs (Table 8.4). The LAI (1.985) was obtained by averaging results

from bands 4 and 5 at low SZAs (Table 8.5). Finally, the LAD parameters ($\mu(\theta) = 0.7582$, $\nu(\theta) = 2.656$) were obtained by averaging results from bands 4 and 5 at high SZAs (Table 8.6).

Albedo was determined using the Case 2 method. A comparison of the estimated and measured albedo is shown in Figure 8.6c. Relative to Case 2, the mean error (0.007 or 3.63% relative) decreases by an order of magnitude, although the correlation ($r = 0.94$) is similar. Clearly, a considerable reduction in the systematic bias occurs. Therefore, the measured parameter values—or method of determining canopy averages (Chapter VI)— probably introduced a bias into the Case 2 results.

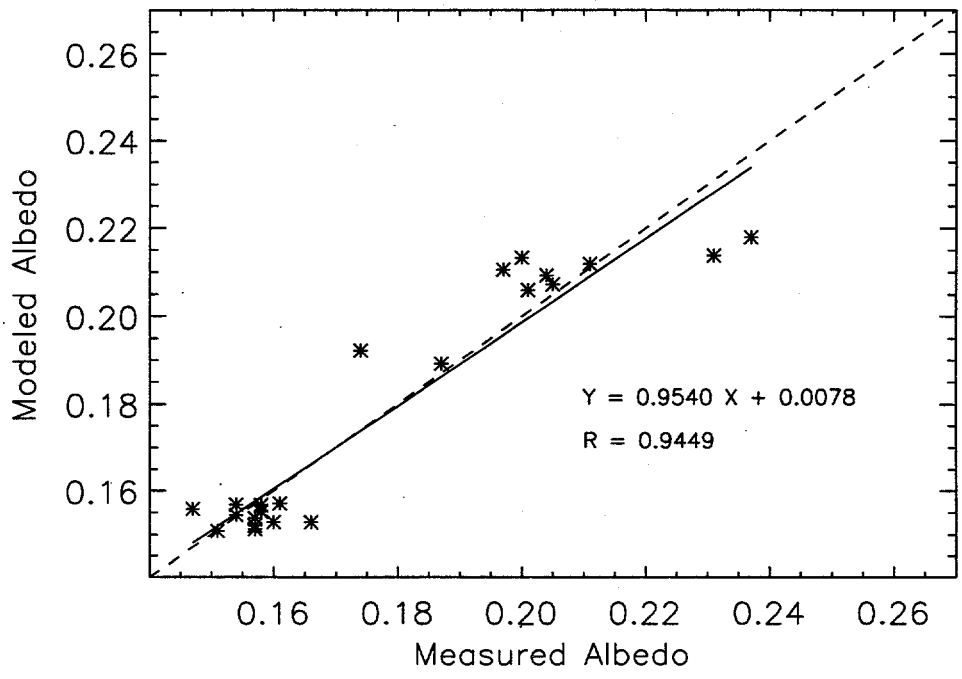

Figure 8.6c. Same as Figure 8.6b, but parameter sets were determined from retrieved values at preferred wavelengths and solar zenith angles.

Two additional observations deserve comment. First, results determined with variable parameter sets (Case 1) are less accurate than those computed with fixed parameter sets (Cases 2 and 3). This suggests that inversions with a single band and SZA may yield unrealistic parameter sets. Then, despite fitting seven samples well, the model may provide poor reflectance estimates in directions

where data were absent during inversion (in this study, off the principal plane and at high VZA). Angular reflectance errors lead to erroneous spectral albedo upon integration. Some bands may be more prone to this problem than others. This points to the advantage of using the preferred wavelengths and SZA for parameter retrieval (Section D). It also suggests that physically-based models may be more useful for albedo calculations than other models. This assumes that physically-based models can better relate measured reflectance data in given directions to reflectance estimates in other directions. Second, albedo results obtained with retrieved canopy parameters are superior to those obtained with measured parameters. As this may indicate inaccuracies in the BRDF model or parameter measurements, it underscores the potential for determining radiation variables (e.g., albedo) from radiation data (e.g., angular reflectance). Essentially, inverse methods may compensate for model inaccuracies. Such inaccuracies can worsen results despite the use of accurate (measured) parameter values.

Although this study had the advantage of ground-based, principal plane measurements, these results indicate the potential for accurately estimating albedo from a small number of remotely sensed samples. Such accuracy would not normally be possible with Lambertian approximations.

Fraction of Absorbed Photosynthetically Active Radiation (fAPAR)

Before proceeding with the fAPAR results, a brief review of previous work is in order. Studies have suggested that fAPAR may have a near-linear relationship with some vegetation indices [Asrar et al., 1989]. Nevertheless, applications with FIFE fAPAR data have revealed limitations. Walter-Shea et al. [1992] showed that the fAPAR-NDVI relationship depended strongly on the sensor view angle. Demetriades-Shah et al. [1992] concluded that even VIs determined from near-ground sensors were not well correlated with measured fIPAR (fraction of Intercepted PAR). Hall et al. [1992] showed that fAPAR-VI relationships depended on soil spectra—a significant factor even over the limited FIFE area. Hall et al. [1992] also showed that Green fAPAR, determined by weighting the measured fAPAR by the ratio of live-to-total canopy biomass, provided a more linear relationship with

NDVI. Several theoretical studies (e.g., Goward and Huemmrich [1992]) have shown that the fAPAR-VI relationship is also dependent on canopy optical and morphological properties.

Below, a different method for retrieving fAPAR is outlined. Results in Chapter V suggested that spectral fAPAR could be accurately estimated from BRDF model inversions despite some errors in retrieved parameters. The potential of this method was therefore tested using a series of experiments similar to those for albedo.

In field applications, fAPAR and fIPAR are defined, respectively, as:

$$\text{fAPAR} = \frac{I_o - R_c - (T_c - R_s)}{I_o}, \text{ and} \tag{8.6}$$

$$\text{fIPAR} = \frac{I_o - T_c}{I_o}, \tag{8.7}$$

where I_o is the incident photon flux density (PFD), R_c is the exitant PFD above the canopy, T_c is the PFD transmitted through the canopy, and R_s is the PFD reflected by the soil. PFD is the number of photons (0.4-0.7 μm) incident per unit time on a unit surface (mol m^{-2} s^{-1}). Photon counts rather than energy units are used since photosynthetic rates are essentially independent of the energies of the absorbed photons [Pearcy, 1989]. PFD quantities were measured during FIFE with line quantum sensors.

Although Equation (8.6) requires four sensors for determination, a reasonable approximation is possible by letting $R_s = T_c R_c I_o^{-1}$. This effectively assumes the soil and surface (soil + canopy) albedos are equal. With this substitution, Equation (8.6) requires just three sensors (as used in FIFE) and can be expressed as [Walter-Shea et al., 1992]:

$$\text{fAPAR} = \text{fIPAR} \left[1 - \frac{R_c}{I_o} \right]. \tag{8.8}$$

For modeling purposes, fAPAR is [Myneni et al., 1992]:

$$\text{fAPAR} = \int_{0.4}^{0.7} F_{a,\lambda}\, W_\lambda\, d\lambda, \tag{8.9}$$

where $F_{a,\lambda}$ is the fraction of radiant energy absorbed by the canopy at λ, defined as,

$$F_{a,\lambda} = \int_V [F^o_{a,\lambda} + F^d_{a,\lambda} + F^c_{a,\lambda}]d\vec{r}, \tag{8.10}$$

and W_λ is the fraction of incident solar energy at λ, defined as,

$$W_\lambda = \left[\frac{I_{o,\lambda}}{\int_{0.4}^{0.7} I_{o,\lambda}\, d\lambda}\right]. \tag{8.11}$$

In these equations, V is the volume of the canopy, $I_{o,\lambda}$ is the irradiance at λ, and $F^o_{a,\lambda}$, $F^d_{a,\lambda}$, and $F^c_{a,\lambda}$ are the fractions of absorbed uncollided sunlight, diffuse, and scattered fluxes, respectively. For the inversion problem, Equation (8.9) must be approximated since the reflectance data are from broad spectral bands. A band extension method, similar to that used to compute albedo, was used here. Band intervals and weights are shown in Table 8.9.

Table 8.9. Extended bandwidths used to compute fAPAR and $\text{fAPAR}_{\text{total}}$. Mean weights ($\overline{W_i}$) were computed by the 5S model. Also shown are the normalized weights after conversion from energy units to quantum units. Standard deviations were negligible in each case.

Band	Bandpass Limits	Extended Limits	$\overline{W_i}$ [energy]	$\overline{W_i}$ [photons]
1	0.450-0.520	0.400-0.520	0.410	0.345
2	0.520-0.600	0.520-0.615	0.330	0.342
3	0.630-0.690	0.615-0.700	0.261	0.313

The standard deviations of the band weights were negligible. Equation (8.9) for MMR data can then be expressed as,

$$\text{fAPAR} = \sum_{i=1}^{3} \overline{F}_{a,i}\, \overline{W}_i , \tag{8.12}$$

where $\overline{F}_{a,i}$ is the mean fraction of radiant energy absorbed by the canopy in band *i*, and

$$\overline{W}_i = \left[\frac{\int_{\lambda_{a,i}}^{\lambda_{b,i}} I_{o,\lambda}\, d\lambda}{\int_{0.4}^{0.7} I_{o,\lambda}\, d\lambda} \right], \tag{8.13}$$

where $\lambda_{a,i}$ and $\lambda_{b,i}$ are the lower and upper limits of extended band *i*, respectively. The fraction of absorbed energy ($\overline{F}_{a,i}$) is evaluated directly by DISORD. This quantity is determined from computed canopy and soil albedo using energy balance arguments (Equation 8.6). In this application, $\overline{F}_{a,i}$ gives the effective broadband absorption since MMR reflectance data were used to determine the model parameters. The weighting function, $\overline{W}_i$, is composed of integrals that are computed directly from the 5S model. However, 5S determines irradiance in W m^{-2}. Therefore, a correction based on Planck's Law ($K_\lambda \propto \lambda$) must be used to convert W to mol s^{-1}. The neglect of this correction biases the weights towards shorter wavelength (higher energy) bands (see Table 8.9). To facilitate the use of standard 5S output, $\overline{W}_i$ was simplified as follows:

$$\overline{W}_i = \left[\frac{\int_{\lambda_{a,i}}^{\lambda_{b,i}} I_{o,\lambda}\, K_\lambda\, d\lambda}{\int_{0.4}^{0.7} I_{o,\lambda}\, K_\lambda\, d\lambda} \right] = \left[\frac{\int_{\lambda_{a,i}}^{\lambda_{b,i}} I_{o,\lambda}\, d\lambda\, \bar{\lambda}_i}{\sum_{j=1}^{3} \bar{I}_o} \right], \tag{8.14}$$

$$\bar{I}_0 = \int_{\lambda_{a,j}}^{\lambda_{b,j}} I_{0,\lambda}\, d\lambda\, \bar{\lambda}_j \qquad (8.15)$$

where $\bar{\lambda}_i$ is the center wavelength of extended band *i*.

1) Canopy fAPAR Equation 8.12 was used to estimate fAPAR in two cases. First, the measured canopy parameters (Table 6.2) were used in DISORD. Atmospheric data collected near the time of the fAPAR measurements were used to estimate $\overline{W}_i$. The fAPAR data—measured in eight periods over the two days—spanned a range of SZAs from 22 to 56°. Typically, five values were recorded within each period. Unlike the albedo data, however, fAPAR data were not collected simultaneously with the MMR measurements. Thus, only MMR data sets collected closest in time to the fAPAR data acquisitions were used.

Modeled fAPAR values are plotted against mean fAPAR data in Figure 8.7a. Error bars indicate the maximum and minimum values per measurement period. The modeled fAPAR consistently exceeds the measured values. The mean error is 0.174 (37.14% relative). The correlation coefficient is 0.906, which suggests the largest errors are systematic. The predominance of systematic errors and decreasing errors with increasing fAPAR (and SZA) are the same trends observed for the Case 2 albedo (measured parameters). Errors are worse with Green fAPAR [Hall et al., 1992], which reduced measured values by 19.5%.

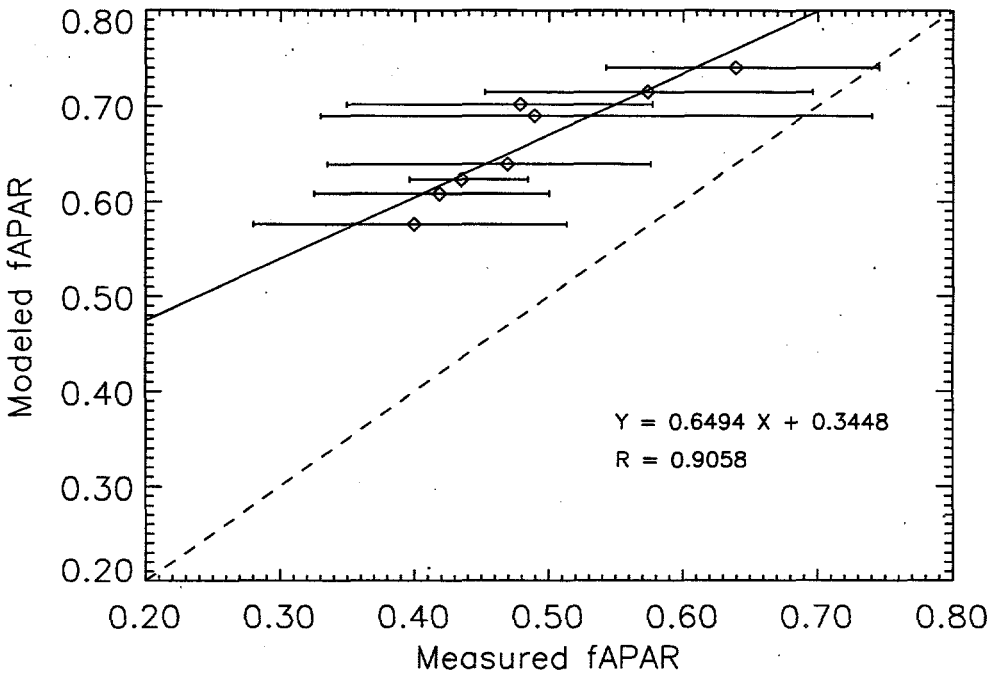

Figure 8.7a. Comparison of measured and modeled fAPAR. Canopy parameters were determined from measured data (Table 6.2). Only atmospheric properties and solar zenith angles were changed between model calculations. Error bars represent the minimum and maximum values per measurement period. Note that fAPAR was not measured simultaneously with MMR reflectance. The dashed line is the 1-to-1 line.

Second, the preferred canopy parameters—explained in the Case 3 albedo study—were used (Figure 8.7b). Again, the model values exceed the measured values. However, the mean error is reduced by nearly 20% to 0.142 (30.17% relative). The correlation coefficient (0.899) is similar to the case above. As in the albedo calculations, the model clearly is more accurate when retrieved parameters are used. In addition, errors decrease with increasing fAPAR (SZA). The lack of simultaneity in the MMR and fAPAR data acquisition may contribute some of the non-systematic errors. Systematic errors may arise from differences in vegetation between the sampling areas of the MMR and line quantum sensors.

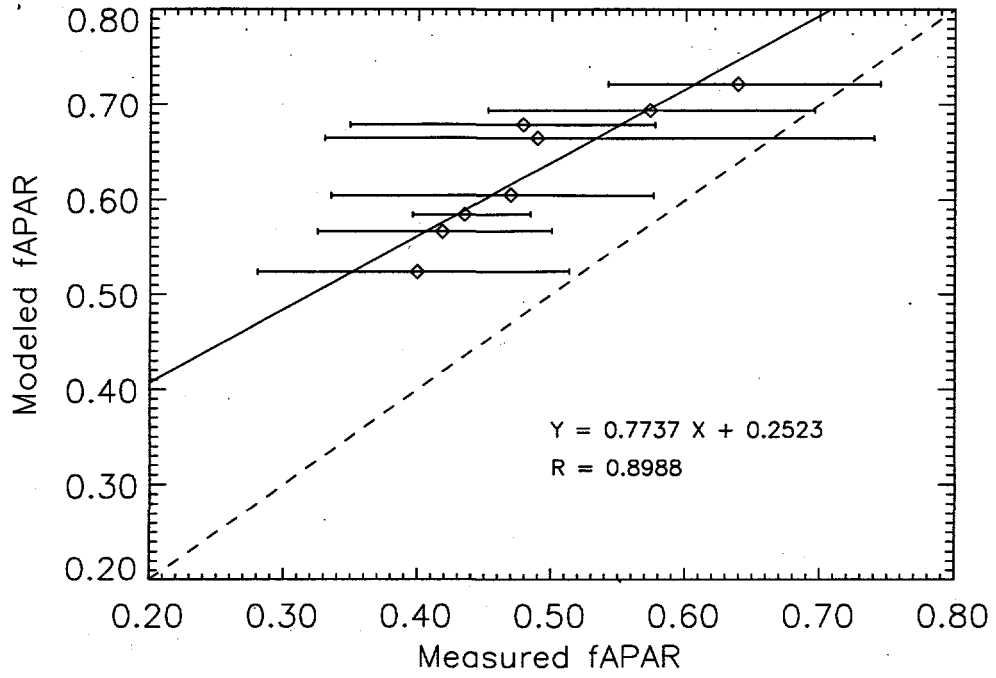

Figure 8.7b. Same as Figure 8.7a, but canopy parameters were determined from retrieved values at optimal wavelengths and solar zenith angles.

2) *Surface fAPAR* Clearly, the errors in fAPAR significantly exceed those encountered in the albedo study. To help isolate the primary sources of these errors, total (canopy + soil) fAPAR values were compared. Empirical $fAPAR_{total}$ values were determined by,

$$fAPAR_{total} = I_o - R_c. \tag{8.16}$$

In DISORD,

$$fAPAR_{total} = fAPAR + fASOIL \tag{8.17}$$

$$= 1 - ALB_{PAR},$$

where fASOIL is the fraction of solar radiation absorbed by the soil. Thus, $fAPAR_{total}$ was determined by replacing $\overline{F}_{a,i}$ in Equation (8.12) with $\overline{ALB}_i$, and subtracting the result from 1.0 (Equation 8.17). Again, both the measured and preferred retrieved parameters were used (Figures 8.8a-b, respectively).

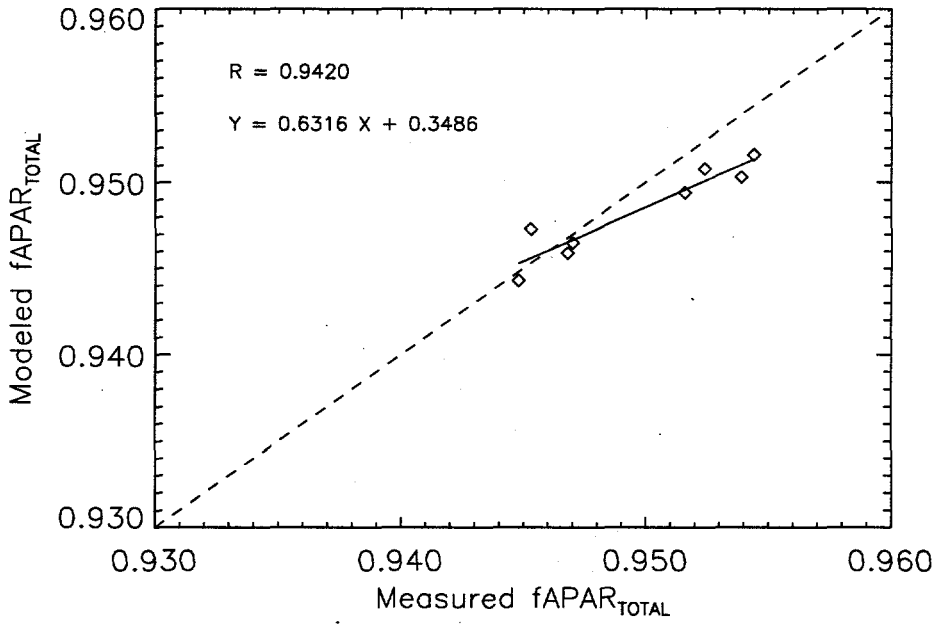

Figure 8.8a. Comparison of measured and modeled $fAPAR_{total}$. Canopy parameters were determined from measured values (Table 6.2). Only atmospheric properties and solar zenith angles were changed between model calculations. Note that $fAPAR_{total}$ was not measured simultaneously with MMR reflectance.

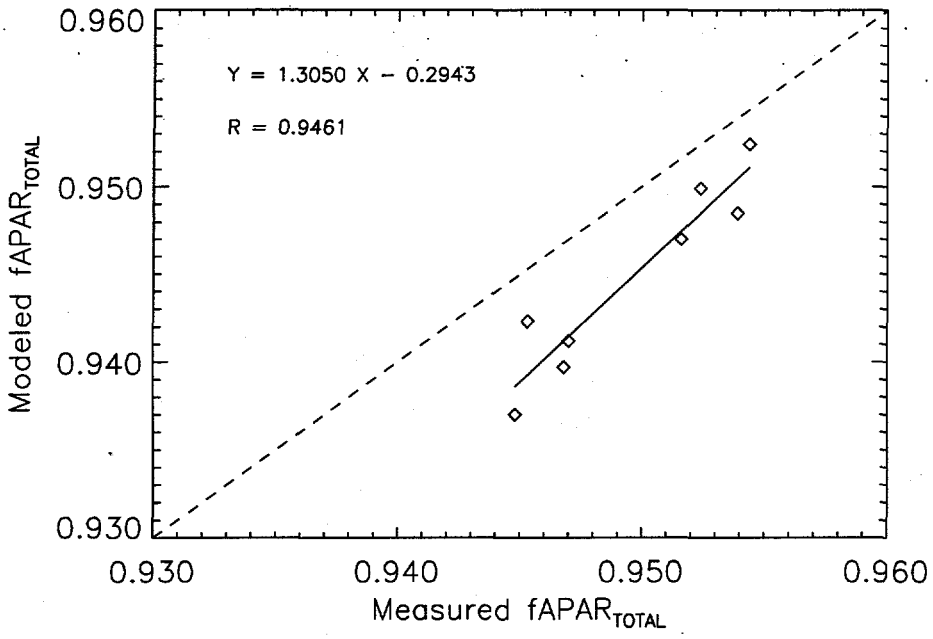

Figure 8.8b. Same as Figure 8.8a, but canopy parameters were determined from retrieved values at preferred wavelengths and solar zenith angles.

Estimates of $fAPAR_{total}$ are within 0.04 (measured parameters) and 0.09 (retrieved parameters) of the measured values. The measured parameter values result in a mean error of 0.002 (0.185% relative), and the preferred retrieved parameters produce a mean error of 0.005 (0.503% relative). Both parameter sets underestimate $fAPAR_{total}$. The correlation coefficients are 0.942 and 0.946, respectively. Thus, both systematic non-systematic errors are relatively minor. Unlike for albedo and canopy fAPAR, errors in $fAPAR_{total}$ are larger when the retrieved parameters are used. In addition, errors increase with increasing $fAPAR_{total}$ in the measured parameter case.

3) Discussion and Error Analysis Overestimation of canopy fAPAR must be due to errors in the modeled fAPAR and/or the "measured" fAPAR. Errors in the modeled fAPAR may be further broken down into errors in the band extension method (Equation 8.12) and errors in the spectral fAPAR calculations (Equation 8.10).

First, errors in the band extension method were estimated using directional reflectance data gathered with an SE590 Spectroradiometer (Spectron Engineering, Denver, CO). Reflectance data were determined at every 5 nm of the PAR spectrum for canopy, litter (thatch), and soil. Thatch was loosely defined as the discernible mat of dead vegetation on the soil surface. The canopy and soil data were obtained at site 916 during IFC-5. The thatch data were obtained at various sites on 15 September 1993. Only thatch data obtained over previously burned sites were used. SZAs ranged from about 20-60°. The SE590 reflectance data were averaged over all solar angles for both the true and extended MMR bandwidths (Table 8.9). Only the maximum VZA (50° backscatter) was used to reduce contributions from underlying media.

Mean relative errors (MRE) were determined using Equation (8.2), where P_i was replaced with the average MMR bandwidth reflectance (determined from SE590 data), and P_o was replaced with the average extended bandwidth reflectance (also determined from SE590 data). MRE values for each band and the PAR spectrum (using quanta weights from Table 8.9) are shown in Table 8.10. Errors are greatest in band 1, however the weighted PAR errors are less than 3.3% for each component. The PAR reflectance error for the total soil, litter and canopy system is 2.53% (σ = 0.36%) as determined from nadir reflectance data. Errors are generally correlated with the variability of the spectra in a given band. These errors should be regarded as rough estimates of band extension errors since MMR spectral sensitivity and BRDF effects were ignored. For analysis of errors in absorbed radiation, optically semi-infinite media must also be assumed (i.e., albedo must be considered the complement of the absorbed fraction). The relatively small errors in Table 8.10 were expected since the actual MMR bands cover about 70% of the PAR spectrum. This is considerably more than the 26% coverage of the shortwave spectrum (0.3-4.0 μm), for which the band extension method provided reasonable albedo estimates. Moreover, since the same band extension (Equation 8.12) was used to determine both fAPAR and $fAPAR_{total}$, significant errors in this technique would cause significant errors in $fAPAR_{total}$. This clearly did not occur (see Figures 8.8a-b). This analysis implies the PAR spectral coverage and the conversion from energy-based weights to quantum-based weights (Equation 8.14) are acceptable.

Table 8.10. Mean relative errors in extended band reflectance due to the assumption of constant reflectance outside MMR bandwidths. To reduce effects from other components, the maximum VZA (50° in backscatter) was used. Results were averaged over multiple SZAs. Reflectance errors over the full PAR spectrum were determined using the quantum band weights in Table 8.9.

	MRE (%)			
Component	Band 1	Band 2	Band 3	Weighted PAR
Canopy	15.2	2.51	-10.7	2.75
Litter (Thatch)	12.4	-1.72	-1.41	3.27
Soil	9.3	-2.03	0.12	2.55

The second source of modeled fAPAR errors may be deduced from the energy balance relationship (Equation 8.17) and soil model results. If fAPAR is significantly overestimated and $fAPAR_{total}$ is reasonable, Equation (8.17) requires that fASOIL be significantly underestimated—i.e., the modeled soil must be considerably brighter than the true soil. When compared to soil reflectance data, soil model estimates were reasonable (see Chapter VII). However, though prairie soils are relatively dark, data suggest thatch is darker. Thus, if thatch were present below the canopy, the soil model would overestimate the combined soil and thatch albedo (and underestimate fASOIL) for the measured parameter case (Figure 8.8a). The absence of top-of-thatch reflectance data from IFC-5 makes quantification of this error impossible. Since soil model parameters were determined from exposed soil data, soil albedo errors may also occur due to moisture differences between the exposed soil and below-canopy soil. In the retrieved parameter case, however, ω_s should adjust to any background. Thus, errors with the retrieved parameters (Figure 8.8b) should have been lower than those with the measured parameters (Figure 8.8a). This did occur to some degree. Finally, the soil model probably overestimated reflectance off the principal plane (see Chapter VII). This, too, would reduce fASOIL. Unfortunately, errors off the principal plane could not be evaluated due the absence of measured reflectance there. The decrease in fAPAR errors with increasing SZA (increasing fAPAR) is as would be expected for a soil error source.

The last source of differences between modeled and measured fAPAR is the "measured" fAPAR. Two points are noteworthy. First, high variance in the fAPAR data (see error bars in Figures 8.7a-b) and low variance in $fAPAR_{total}$ data indicate significant variability in the transmitted flux (T_c).

Sources of this variability include instrument problems, canopy gaps and heterogeneity. Gaps and heterogeneities may have increased due to wind effects. Moreover, the availability of PFD data from just eight periods substantially impacts the statistical significance of these results. At best, these concerns suggest caution in the interpretation of fAPAR results. Second, Equation (8.8) assumed that the surface albedo equaled the soil albedo. Although soil albedo was not measured, soil directional reflectance exceeded TOC reflectance in some bands and directions. If the true soil albedo exceeded the TOC albedo, Equation (8.8) would underestimate the measured fAPAR. Since this error source would decrease with increasing fAPAR (increasing SZA and decreasing soil contribution), the trend in fAPAR errors is consistent with its presence. The assumption of equal soil and canopy albedo was not necessary in Equation (8.16); therefore, it would not have affected the $fAPAR_{total}$ results. This is consistent with $fAPAR_{total}$ errors. Quantitative assessment of these error sources will be addressed in future work.

E. Other Sources of Errors

Although error sources have been identified in the sections above, several general error sources deserve review. First, the minimization algorithm may not have converged at the global minimum of Equation (2.5). Presently, there is not a method to insure global minimization in multiple variable problems. Second, the MMR data were measured with a 15° IFOV instrument, yet the model assumes a unit steradian IFOV. This effect is more important in visible wavelengths where the angular reflectance varies more in proportion to the mean. In addition, the measurement angles were accurate to ±2° zenith and ±10° azimuth. Third, soil parameters $\{h, b, c, b', c'\}$ were determined using data obtained over a bare plot. This surface may not have represented the below-canopy conditions. This is particularly important if litter existed below the canopy or if the moisture regimes were different. Finally, turbid medium models are not ideally suited to low LAI conditions. Still, for grassland model inversions, turbid medium models are probably the most reasonable.

F. Conclusions

Using measured parameter values (Chapter VI), a partial validation of the coupled soil and canopy model was attempted. Reflectance estimates agreed well with measured TOC values. A sensitivity study suggested that TOC reflectance was most sensitive to leaf optical properties at both red and NIR wavelengths. The third most influential parameter was LAI, however relative effects varied with wavelength. At red, LAI is significantly less influential than leaf optical properties; at NIR, sensitivity to LAI and leaf optical properties is nearly equal. Sensitivity to leaf optical properties increased with SZA, however sensitivity to LAI decreased with SZA. All other parameters were substantially less influential.

Inversions were conducted with field measured data. Results were binned according to SZA (above or below 40°). Leaf optical properties were generally retrieved more accurately at high SZA, although leaf transmittance was better determined at low SZA for NIR bands. LAI was most accurately determined at low SZA with NIR data. LAD was accurately determined with NIR data for all SZA. Soil single scattering albedo, determined from low SZA data, exhibited appropriate spectral behavior.

Shortwave albedo was estimated by weighting spectral albedo with the fraction of irradiance in each band. Agreement with pyranometer-measured values was greatest when "preferred" canopy parameters were used. These parameters were determined using retrieved values from select SZA and spectral bands. Using a similar technique, fAPAR and $fAPAR_{total}$ were also determined and compared with measured values. Values of fAPAR were overestimated in all cases, however there was significant variability in measured data. Values of $fAPAR_{total}$ were highly accurate.

CHAPTER IX

INTEGRATED INVERSION SCHEME AND APPLICATION TO SATELLITE DATA

A. Introduction

Results in Chapter VIII confirm that model inversions with ground-based radiometer data can produce reasonable estimates of surface parameters. However, some process models require surface data at regional or global scales. As noted in the Chapter I, satellites currently provide the only practical method by which such data can be obtained with a single, consistent sensor in a reasonable time frame.

Naturally, new issues arise in moving from ground based, point data to satellite data. These include the differences in temporal, spatial and spectral resolution, the impact of more limited sun-target-sensor geometries, and the modulation of upwelling radiance by the atmosphere. While different approaches may be used to resolve these issues, the method described below is based on the results from Chapters V-VIII. In addition, it is designed to facilitate production of regional or global data sets.

B. Satellite Sensor Selection

Presently, environmental satellite sensors do not collect data at the spatial resolution of ground-based instruments. Indeed, the resolution of continuously orbiting sensors extends from the High Resolution Visible (HRV) instrument of Systeme Probatoire d'Observation de la Terre (SPOT), at 10 m (panchromatic mode), to AVHRR Global Area Coverage (GAC) at 4 km.

High spatial resolution sensors (HRV, Landsat Thematic Mapper and MultiSpectral Scanner) typically have low temporal resolution (10- to 20 days). As the presence of clouds renders samples useless to the inversion problem, the effective temporal resolution can be significantly lower. And,

since multiple samples of a target are necessary for inversions of multiparameter models, the data collection period for a single inversion may be several months. Obviously, a canopy may undergo significant changes in such a period. In contrast, lower spatial resolution sensors (AVHRR, Visible and Infrared Spin Scan Radiometer (VISSR)) have substantially higher temporal resolution (0.5 hours to 1 day). Therefore, the probability of acquiring a sufficient number of cloud-free samples before surface conditions change is much higher. For this reason, AVHRR and VISSR represent the only practical instruments for acquiring data useful in model inversions.

AVHRR and VISSR operate under very different sampling strategies. VISSR is onboard Geostationary Orbiting Environmental Satellite (GOES). Geostationary satellites orbit above an approximately constant geographic position. This limits their FOV coverage to less than one hemisphere. Furthermore, the target-sensor geometry remains approximately constant for each target. The quasi-fixed orientation allows frequent observations of land targets. In practice, VISSR collects a sample over each 0.9 km of earth in its FOV every 0.5 hours.

In contrast, AVHRR is onboard the National Oceanic and Atmospheric Administration (NOAA) polar orbiters [Kidwell, 1991]. NOAA polar orbiters are launched into sun-synchronous orbits with an inclination angle of about 99°. Sun synchronicity implies that a satellite's orbital plane maintains a constant orientation with respect to the sun-earth vector by precessing 360° yr^{-1}. Together with AVHRR's wide FOV, this orbit ensures global coverage since the orbital plane bisects the rotating earth. It also ensures that the satellite crosses the equator at the same local solar time (LST) on every orbit. NOAA satellites are in one of two orbits depending on the direction of satellite travel on the sunlit side of earth. The morning descending orbit (north to south) is utilized by all even-numbered NOAA satellites. The afternoon ascending orbit (south to north) is utilized by all odd-numbered satellites. Nominal equator crossing times are 0730 and 1330 LST (1430 for NOAA-9 and before), respectively. Due to these differences, some AVHRR sensors collect their daytime samples in the morning while others collect them in the afternoon.

AVHRR scans ±55.4° from nadir at a rate of 6 scans s^{-1}. At nadir, the ground instantaneous field of view (GIFOV) is 1.2 km^2. At the edge of the scan, the GIFOV increases to about 15.6 km^2.

Each scan line contains 2048 samples from a 2700 km wide swath. This sampling strategy results in at least one observation of every earth position each day and night. The rate increases with latitude—surface targets at 60° N are sampled at least three times each day and night. Since NOAA satellites complete about 14.1 orbits day^{-1}, consecutive observations of a given land target occur at different geometries.

Although AVHRR makes repeat measurements less frequently than VISSR, its data were utilized in this study for several reasons. First, AVHRR data have a significantly larger range of sun-target-sensor geometries. For example, Figures 9.1a-c show the NOAA-11 AVHRR (afternoon ascending orbit) geometries for three latitudes. In contrast to the minimal variation of target-sensor geometry (per target) of VISSR, AVHRR data are collected over a large range of VZAs and a fairly large range of SZA. The azimuth angle of the sensor relative to the principal plane also varies significantly. Moreover, the AVHRR collects some data in or near the principal plane at most latitudes during summer. This was shown to be advantageous in Chapter V. Second, at least two active AVHRR instruments typically orbit earth at all times. Although multiple sensors may present calibration problems, they also provide higher effective sampling frequency and hence increased probability of daily cloud-free samples. Third, VISSR has just one optical band (0.55-0.70 μm) compared to two on AVHRR. In addition to the demonstrated superiority of NIR data for inversions (see Chapter VIII), the extra AVHRR band provides more complete coverage of the shortwave spectrum. This permits more accurate estimation of surface albedo. Finally, AVHRR satellites provide global coverage in contrast to the VISSR sub-hemispherical coverage. Global coverage is clearly required if data sets are to be produced for GCM usage.

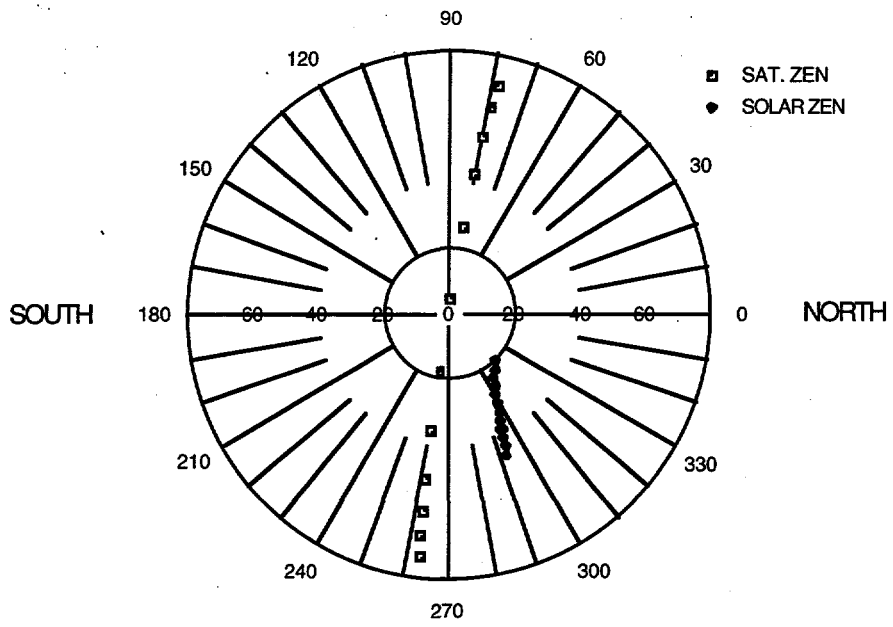

Figure 9.1a. Polar plot of solar and NOAA-11 AVHRR geometries relative to earth target (represented by origin) for nine days in early July, 1990. Diamonds represent position of sun, squares represent positions of AVHRR. Zenith angles are represented by distance from origin. Azimuth angles increase from north (0°) to east (90°). Latitude of target is 10° N.

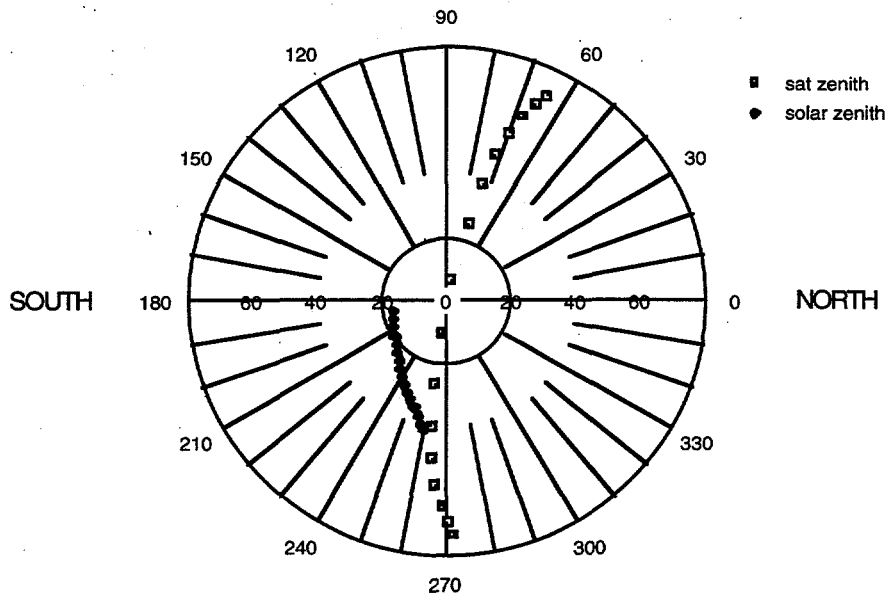

Figure 9.1b. Same as Figure 9.1a, except latitude of target is 40° N.

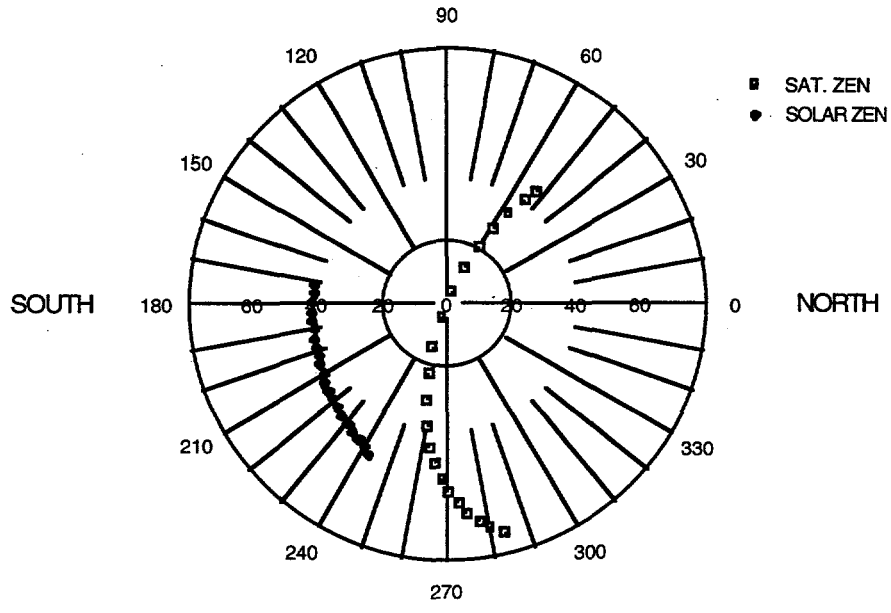

Figure 9.1c. Same as Figure 9.1a, except latitude of target is 65° N.

For this initial investigation, only band 2 (NIR) data from AVHRR were used. NIR data were found to be superior for the estimation of LAI and LAD in Chapter VIII. Nevertheless, the inversion methodology developed below is general and can accommodate data from VISSR and the planned instruments of the Earth Observing System (EOS) (e.g., MISR, Moderate-Resolution Imaging Spectrometer (MODIS)) [NASA, 1993].

C. Issues in Using AVHRR vs. Ground Radiometer Data

Unlike ground-based radiometers, the relatively low spatial resolution of AVHRR implies that large scale horizontal heterogeneity may exist in each GIFOV. Such heterogeneity may include both topographical and land cover variations; consistent mixtures of surface media (small scale heterogeneity) are not included in this definition. Significant variation in AVHRR scan angles can amplify heterogeneity due to changes in GIFOV. In this case, surface heterogeneity at a given target may not be consistent among repeat samples. Since 1-D BRDF models assume horizontal homogeneity, inversion results obtained with data from heterogeneous targets may be inaccurate. Interpretation of results may also be difficult. Finally, it may be impossible for the model to replicate the measured data.

Effects of atmospheric processes on surface reflectance present another complication [Lee and Kaufman, 1985; Holben et al., 1986]. First, the atmosphere modifies the quantity and angular distribution of irradiance striking the canopy. These effects, which increase with SZA, were investigated with the soil model (Figure 7.4). Second, the atmosphere modulates the surface-reflected radiation as it travels from target to sensor [Simmer and Gerstl, 1985]. Absorption and scattering processes decrease the magnitude and reduce the angular differences in surface reflectance. These effects increase with VZA. In NIR wavelengths, water vapor and aerosols are the primary culprits of this attenuation. Finally, the atmosphere scatters radiation from non-target directions into the sensor. These directions include those of the sun, atmosphere and non-target surface points. This is

particularly problematic at red wavelengths, where the addition of Rayleigh and aerosol path radiance causes top-of-atmosphere (TOA) radiance to exceed TOC radiance. This effect increases with SZA and VZA.

The net result of atmospheric effects is apparent in Figure 9.2. The plots depict simulated reflectance at ground, 5 km, and satellite levels for a typical surface. The model atmosphere is relatively turbid (optical depth = 0.587). The hot spot decreases significantly with altitude, however reflectance increases at most other directions—especially in the forward and orthogonal scattering directions. The nadir reflectance remains nearly constant. Overall, anisotropy decreased with altitude.

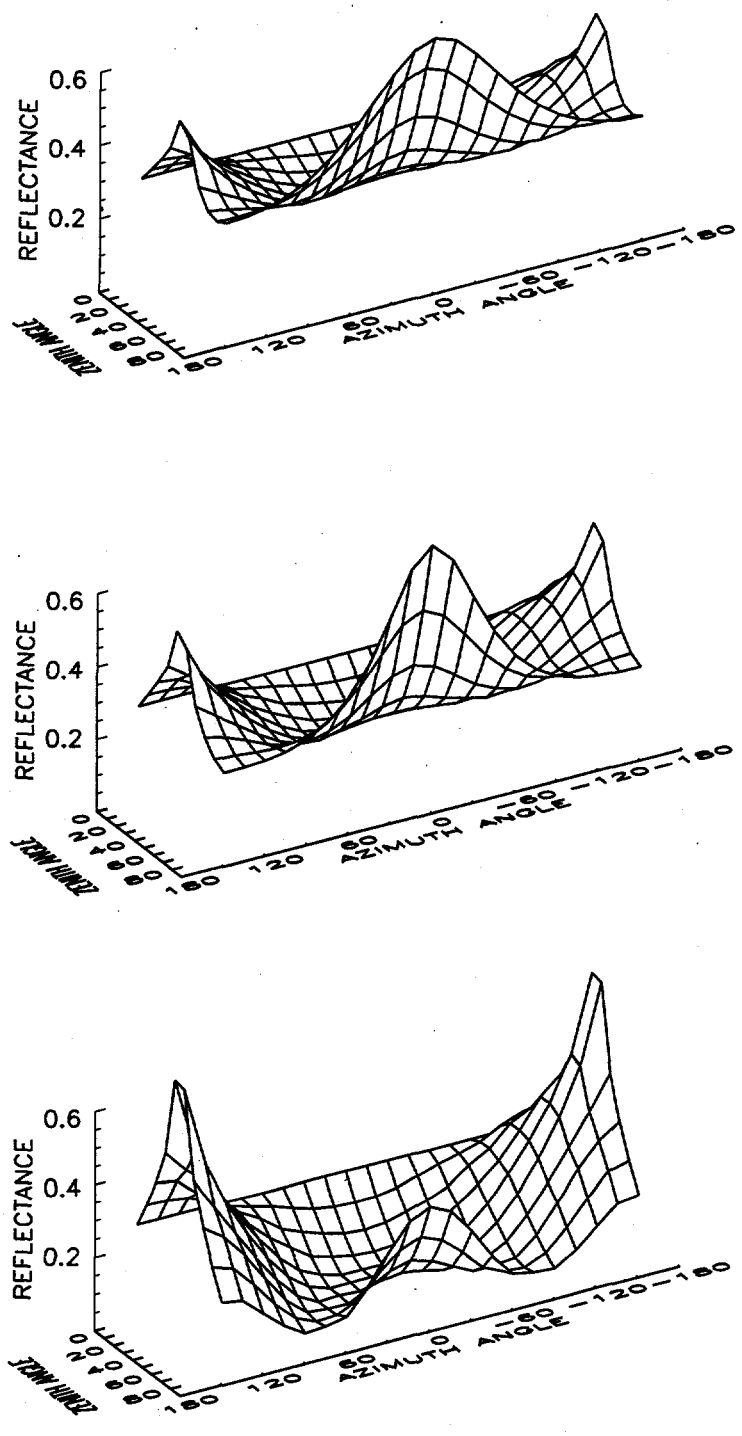

Figure 9.2. Atmospheric effects on surface signal for different altitudes. Reflectance generated for satellite (top), 5 km (middle) and surface levels (bottom). The solar azimuth angle = ±180°; the solar zenith angle = 45°.

Although such effects may be simulated and "removed" using appropriate models, accurate corrections require knowledge of the atmospheric state at the time of the sampling. Complete atmospheric information is difficult if not impossible to obtain. Moreover, atmospheric models introduce other uncertainties. Hence, the correction algorithms may reduce data errors, but cannot eliminate them.

Other sources of errors in satellite data include those of geolocation and sensor drift. Geolocation errors originate both from orbital models used to navigate the data and ephemeris data used to initiate the orbital models. Modern navigation algorithms can reduce AVHRR geolocation errors to about 180 m for non-extreme scan angles [Baldwin et al., 1995]. Sensor drift errors occur because AVHRR spectral sensitivity changes with time. Hence, pre-launch calibration values become inaccurate. AVHRR is not equiped for on-board calibration of its optical bands. Various attempts have been made to determine post-launch coefficients from empirical data, however these values have large uncertainties (ironically in part due to unknown surface anisotropy) [e.g., Kaufman and Holben, 1993].

The additional sources of error in satellite sensor data, compared to ground-based sensor data, imply that surface reflectance cannot be determined as accurately. Hence, some variability in reflectance, previously attributed to changes in surface scattering, must now be regulated to data uncertainty (i.e., the noise equivalent change in reflectance [$NE\Delta\rho$] is increased). This reduces the accuracy of retrieved parameters. Two methods may be employed to combat this problem. First, various models (atmospheric, sensor drift, etc.) may be used to reduce errors in data. Second, the number of BRDF model parameters adjusted during inversion may be reduced. In this study, atmospherically corrected AVHRR data processed by FIFE Information System (FIS) staff were used. Therefore, no additional data corrections were attempted. A reduction in the model parameters was attempted, however.

D. Reduction in Model Parameters

With respect to the goals and limitations outlined above, several new criteria may be used to determine the most suitable parameters to hold constant during model inversions. First, some parameters may be reasonably estimated based on ancillary data (e.g., LAD for grasslands may be assumed erectophile). Second, some parameters change more rapidly. For example, soil reflectance changes immediately during a precipitation event, whereas leaf optical properties normally do not [Walter-Shea et al., 1992]. Third, some parameters may be correlated with other parameters for particular vegetation classes. In this case, only one parameter needs to be adjusted by the optimization algorithm—the correlated parameter value can be a function of this parameter. Fourth, some model parameters (e.g., LAI) may be more difficult to estimate via other techniques. Therefore, model inversions may be the only reasonable method for their quantification. Finally, some BRDF model parameters (e.g., LAI) are more critical to the accuracy of process models [Collins and Avissar, 1994]. Thus, their retrieval may be of greater priority. Note that all parameters held constant in the Chapter VII and VIII inversions remained fixed here.

Results in Chapter VIII suggested that LAI, leaf optical properties, LAD, and ω_s are the model parameters which most affect tallgrass prairie reflectance. Of these, LAD parameters ($\mu(\theta)$ and $\nu(\theta)$) and ω_s were least influential. However, ω_s is important to the determination of canopy fAPAR. In contrast, LAD is less important to the estimation of albedo and absorbed radiation. LAD also requires two parameters. Hence, it is a particularly beneficial property to hold constant during inversion.

Due to the extensive *in situ* data collected during FIFE, a site-wide LAD could be reasonably estimated. Although LAD was measured on both a mixed canopy and a per species basis, the mixed canopy data were considerably more comprehensive in both space and time. Plant canopy analyzer (LAI-2000, LI-COR Inc., Lincoln, NE) data were collected from June to August, 1989 (68 data sets) and June and September, 1993 (7 data sets) by researchers from the Universities of Nebraska and Kansas State. In the present study, mean leaf tilt angle data (determined by indirect methods within the LAI-

2000 processor) were averaged over the site and day for each data set. Using the empirical equations of Welles and Norman [1991], the mean leaf angle (58.27°) was used to estimate $\mu(\theta)$ (1.083) and $\nu(\theta)$ (1.933) for the entire FIFE site. Standard deviations were 0.063 and 0.368, respectively. LADs, determined for all 75 site-day values of mean tilt angle, are shown in Figure 9.3. Nearly all LAD profiles tend toward erectophile. Note that measurements were not made over cropland or wooded areas. However, together these cover classes composed just 15% of the FIFE area. The mean values for $\mu(\theta)$ and $\nu(\theta)$ were therefore fixed in DISORD, reducing the number of adjusted parameters from six to four.

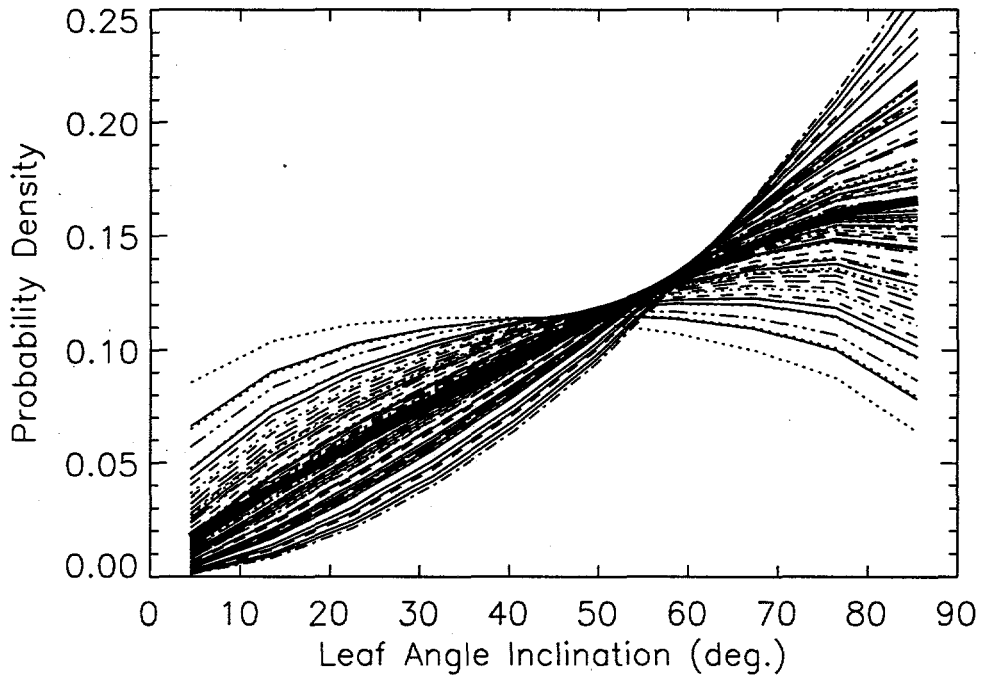

Figure 9.3. LADs determined from mean tilt angles for 75 site-days of FIFE. Tilt angle estimates were determined by LAI-2000 using indirect methods. The mean LAD is indicated with the thicker line.

Although DISORD is relatively sensitive to both leaf reflectance and transmittance (see Chapters V and VIII), these parameters are not entirely independent. Indeed, these quantities vary similarly throughout the visible and NIR wavelengths [e.g., Walter-Shea et al., 1992]. If the relationship between these parameters can be reasonably estimated, then only one parameter needs to be

varied by the optimization algorithm. An empirical relationship was therefore found based on leaf optical data from an SE590 field spectrometer. The data were collected from June to September in 1989 and 1993. Eleven species were sampled. Using spline interpolation, FIFE investigators determined values at 5 nm intervals from 400 to 1000 nm (4991 data points). In the present study, the variation of leaf transmittance with reflectance for all available data were fit using a linear least-squares model (Figure 9.4). Although some scatter exists (r = 0.984), the data are clearly correlated. If this relationship is utilized in the inversion process, then adjustment of leaf reflectance effectively adjusts leaf albedo. However, unlike models in which leaf albedo is adjusted without regard to reflectance and transmittance, this method allows a reasonable estimation of each parameter. Hence, this method should be more accurate.

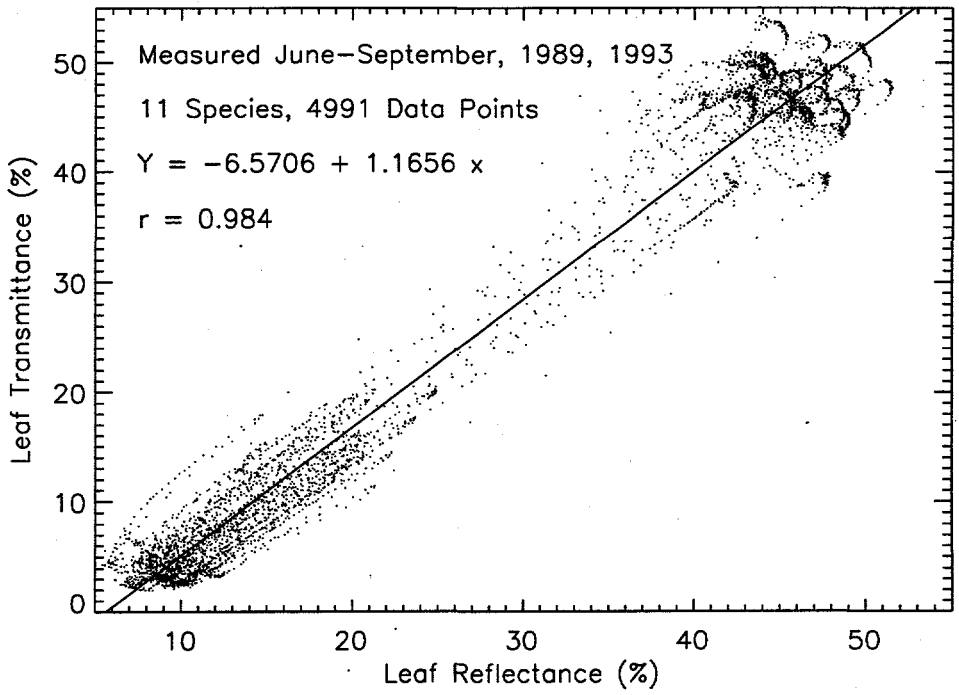

Figure 9.4. Regression fit of leaf optical data from SE590 spectrometer. Data were measured over 11 tallgrass prairie species during FIFE.

E. Estimation of Variable Model Parameters from *In Situ* Data

For validation purposes, the variable model parameters (LAI, leaf optical properties, ω_s) were also estimated. Since mean site-wide values were not available in FIS, manipulation of *in situ* data was necessary. Below, the manipulations are described.

In Chapter VII, the spectrally invariant parameters of the soil model were determined over seven spectral bands and a wide range of solar angles and moisture conditions. Hence, assuming the reflectance anisotropy of the Dwight Series is representative of all FIFE soils, these parameters are probably applicable to AVHRR data. In reality, large limestone outcrops create widely varying "background" reflectance. Morever, the applicability of the MMR NIR (0.76-0.90 μm) ω_s to AVHRR NIR (0.60-1.12 μm) is not known. The temporal variability of ω_s was also not assessed. This may be important since the mean MMR value was determined from reflectance data gathered in late July and early August 1989, yet corrected AVHRR data extends from May through October, 1987. Since some FIFE areas had burn residue on the surface in the early summer, ω_s was probably lower during that period. Nevertheless, a better estimate of ω_s was not possible since *in situ* bidirectional reflectance data were not measured over the AVHRR NIR bandwidth. Thus, a value of 0.4 was used. (Recently, a limited set of bidirectional reflectance data, collected with the SE590 spectrometer, became available [Betty Walter-Shea, personal communication].)

Similarly, leaf optical properties were not measured with an instrument having AVHRR spectral sensitivity. However, high spectral resolution data, interpolated to 5 nm intervals, were available. These data were obtained for a select set of grasses and forbs; tree and agricultural leaf optical properties were not measured. In this study, only data from big bluestem (*Andropogon gerardii* Vitman) and little bluestem (*Andropogon scorparius* Michx) leaves were used since these were predominate species. Data from 11 green leaves were available. Leaf reflectance data were convolved with AVHRR spectral sensitivity functions and solar spectral irradiance data to obtain the effective broadband reflectance. Leaf transmittance was found using the linear relationship described above. Since the AVHRR NIR band extends to longer wavelengths (1.08 μm) than those for which data were

available (1.00 μm), the reflectance at 1.00 μm was used to represent values at longer wavelengths. The mean leaf reflectance and transmittance for AVHRR band 2 were thus estimated to be 0.4322 and 0.4380, respectively. The ranges of values were [0.4022, 0.4652] and [0.4031, 0.4766], respectively.

Finally, site-wide LAI estimation was achieved by weighting LAI estimates for 10 topographical classes by the fractional coverage by each class. Live biomass data for each topographical class were available for the first day of each IFC (28 May, 29 June, and 13 August 1987) [Schimel et al., 1991; Kittel et al., 1990; Turner et al., 1992]. October IFC data were not used since very little green biomass remained by that time. Using the equations of Schimel et al. [1991], mean live biomass data were converted to LAI estimates. Since neither biomass nor LAI data were available for cropland and wooded classes, LAI estimates of 5 and 10 were used, respectively. A topographical stratification was developed based on the results of Davis et al. [1992]. Classes included uplands, bottomlands, moderate (3-7°) and steep (>7°; non-North and North facing) slopes for burned and unburned prairie, cropland and wooded. Fractional proportions were 0.095, 0.096, 0.116, 0.023, 0.083, 0.116, 0.080, 0.128, 0.024, 0.084, 0.083, and 0.072, respectively. Although this stratification considers only topography and burn treatment, these variables result in most of the spatial variability. Grazing is also a significant factor, however its extent is difficult to assess [Davis et al., 1992]. Upon linearly summing the products of class LAI and class fractional coverage, a second order polynomial was fit to the results such that LAI estimates were available throughout the summer.

F. Improving Inversion Accuracy via a Directional Sensitivity Method

As shown in Chapters V and VIII, some sun-target-sensor geometries are more beneficial to model inversions than others. For instance, the most accurate estimates of LAI were achieved with samples in the principal plane and at low SZA. While sampling geometries of ground-based sensors can be arranged conveniently, those of AVHRR are determined by orbital and sensor characteristics. In fact, while some AVHRR samples may be collected at more preferable geometries, others will be

collected at less preferable geometries. Clearly, if an inversion scheme is to benefit from preferential sampling geometries, a general method applicable to all geometries must be developed.

The characteristics of beneficial sampling geometries can be found by analyzing merit function behavior. Based on results for MISR sampling (Chapter V), two different sampling geometries (principal plane and orthogonal plane) were compared. Eleven equally-spaced VZA were used for each. Synthetic reflectance data were generated for a series of equally-spaced parameter sets around the "true" set. The latter was determined by the mean FIFE parameter values. Only leaf reflectance/transmittance and LAI were varied; ω_s was held constant. Merit function values were determined for each parameter set and both sampling schemes via Equation (2.5). In this case, the empirical data were represented by the model reflectance for the true parameter set. Results (Figure 9.5) suggest that the merit function for the principal plane data has a steeper gradient near the minimizer (i.e., closer contour lines). This creates a steeper "bowl" shape which facilitates a more rapid and accurate inversion.

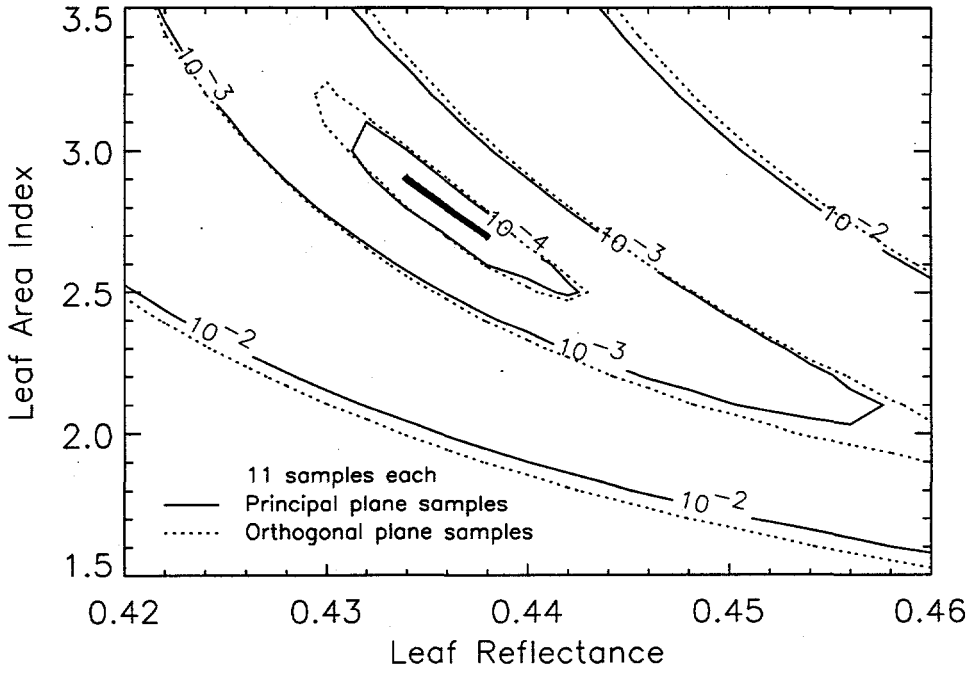

Figure 9.5. Contour plot of merit function variability over select range of LAI and leaf reflectance. Solid lines indicate merit function values for principal plane samples, dotted lines represent merit function values for orthogonal plane samples. All reflectance values were determined through forward modeling.

Mathematically, a merit function gradient simply expresses the change in reflectance for a unit change in parameter values. Hence, the results above are consistent with intuition: if the reflectance does not change over a parameter space, the merit function remains constant and all solutions are equally viable. Conversely, if the reflectance changes substantially for small parameter changes, the merit function changes significantly and the minimizer is well defined.

This information was incorporated into a general, continuous scheme for weighting AVHRR samples. Assuming quasi-linear behavior, determining the merit function gradient for a single sample is equivalent to determining the partial derivatives of reflectance with respect to the parameters. These derivatives will be referred to as "directional sensitivities" (in publication, we termed them "derivative weights" for better description). The results above, combined with those in Chapter V, reveal that optimization is most accurate when the gradient is large. Therefore, if reflectance errors in the merit function are weighted by the directional sensitivities of the respective geometries, then samples gathered at geometries with greater directional sensitivity will exhibit more influence on the merit function than samples gathered at geometries with less directional sensitivity. Hence, the merit function gradients will increase.

In an effort to make this method practical, the scheme below was developed. If a merit function is,

$$\varepsilon^2 = \sum_{j=1}^{n} [R_j - R_j^*]^2, \tag{9.1}$$

then

$$\frac{\partial \varepsilon^2}{\partial P_i} = \sum_{j=1}^{n} 2\,[R_j - R_j^*]\,\frac{\partial R_j^*}{\partial P_i} \tag{9.2}$$

is the partial derivative of the merit function with respect to parameter i. The first factor in Equation (9.2) (2 $[R_j - R_j^*]$) is the difference between the AVHRR-measured reflectance and model reflectance. This factor is determined by the proximity of the minimizer estimate to the actual minimizer. However, this factor already exists in the original merit function and hence provides no additional information. The second factor, $\frac{\partial R_j^*}{\partial P_i}$, is the partial derivative—i.e., directional sensitivity—of the model reflectance with respect to parameter i. Although this factor cannot be analytically determined for numerical models, it can be approximated with finite differences,

$$\frac{\partial R_j^*}{\partial P_i} \sim \frac{\Delta R_j^*}{\Delta P_i}. \tag{9.3}$$

In a typical data set for model inversion, each sample will have been acquired at a unique SZA. Because bidirectional reflectance varies significantly with SZA, the directional sensitivity ($S_{i,j}$) could be normalized by the mean TOC reflectance, e.g.,

$$S_{i,j} = \frac{\frac{\Delta R_j^*}{\Delta P_i}}{\overline{R^*}} \tag{9.4}$$

$$\text{where } \overline{R^*} = \frac{1}{LK}\sum_{l=1}^{L}\sum_{k=1}^{K} R_{lk}^* \cos(\theta_{v,k}), \tag{9.5}$$

K is the number of samples (R_{lk}^*) per SZA used to estimate the mean reflectance, L is the number of SZA, and $\theta_{v,k}$ is the VZA of sample k. To insure non-negative values, $S_{i,j}$ may need to be squared.

$S_{i,j}$ depends both on the sun-target-sensor geometry of the sample and position in parameter space. If only positions near the solution are considered, then $S_{i,j}$ can be assumed to depend on geometry only. In this case, $S_{i,j}$ may be determined before the inversion if reasonable estimates of parameter values are available.

In operation, Equation (9.4) requires two forward executions of the model for each parameter (i) and sample (j) in an inversion data set. For most numerical models, this is computationally expensive. However, directional sensitivity information may be efficiently stored *a priori* in a look-up table (LUT). In the present study, reflectance values were computed at every 5° of VZA between 0 and 75°, every 15° of view azimuth angle between 0 and 180°, and every 5° of SZA between 0 and 75° for the "nominal" canopy conditions. Representative values of γ were used. The nominal conditions were then perturbed by changing each variable parameter by 10% of its range, one at a time. The reflectance was recomputed for each perturbation, and $S_{i,j}$ was determined for each geometry according to Equation (9.4).

Directional sensitivity data for negative perturbations (-10%) of each parameter (LAI, leaf reflectance/transmittance and ω_s) are shown in Figures 9.6-9.8 for two SZA (20 and 65°). Despite some spurious anomalies due to graphical interpolation, several observations may be made. First, the retro solar direction is the most sensitive to changes in LAI and ω_s (Figures 9.6 and 9.8). This occurs because the hot spot formulation reduces the canopy optical depth, allowing parameters which determine soil scattering (i.e., LAI and ω_s) to strongly affect TOC reflectance. Second, low VZA reflectance is more strongly affected by LAI and ω_s than is high VZA reflectance. Similar to the hot spot situation, this results from smaller canopy path lengths at low VZA. At high VZA, the longer path length decreases sensitivity to parameters affecting soil scattering. For analogous reasons, changes in leaf reflectance/transmittance strongly affect reflectance at high VZA, but have comparatively little effect at low VZA (Figure 9.7).

As SZA increases, the sensitivity of the hot spot decreases for LAI and ω_s (Figures 9.6b and 9.8b) and increases for leaf reflectance/transmittance relative to other directions (Figures 9.7b). The average directional sensitivity increases with increasing SZA for leaf reflectance/transmittance and decreases for ω_s. Changes with SZA are not significant for LAI. These results are consistent with sensitivity results in Chapter VIII. Results for positive perturbations were qualitatively similar, although the sensitivity to LAI was less invariant at low VZA (i.e., the surface was more curved) than

for negative perturbations. Quantitatively, directional sensitivity was greater for positive perturbations of LAI and ω_s and for negative perturbations of LAI.

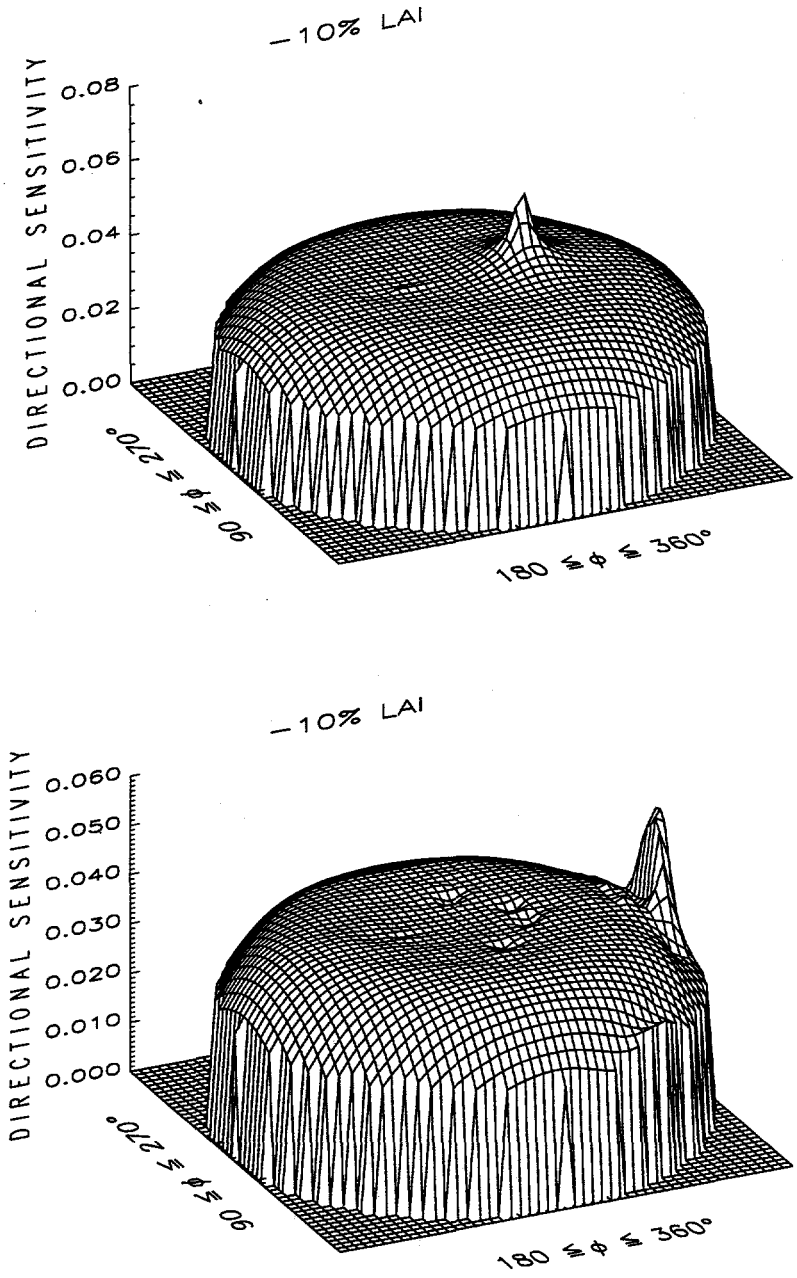

Figure 9.6a-b. Polar plots of directional sensitivity for 10% decreases in LAI. VZAs increase away from center of plot. SZA = 20° (top) and 65° (bottom).

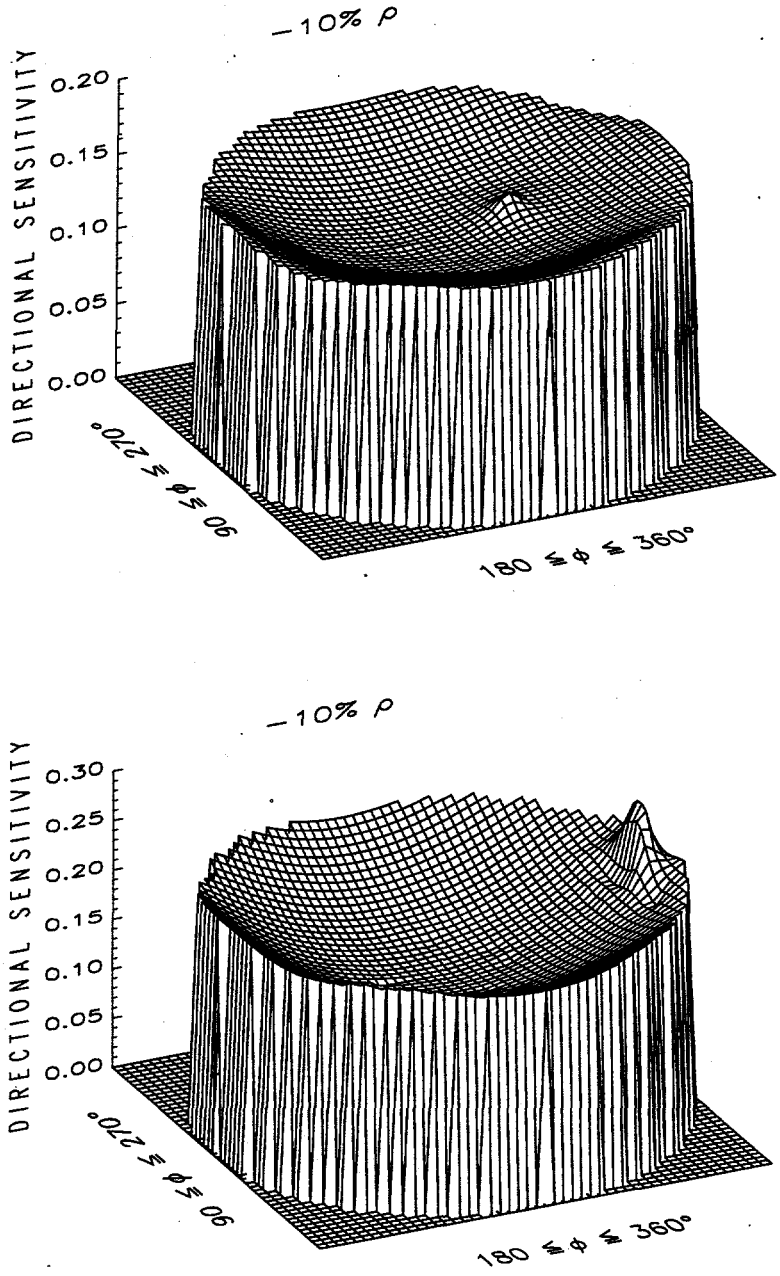

Figure 9.7a-b. Polar plots of directional sensitivity for 10% decreases in leaf reflectance/transmittance. VZAs increase away from center of plot. SZA = 20° (top) and 65° (bottom).

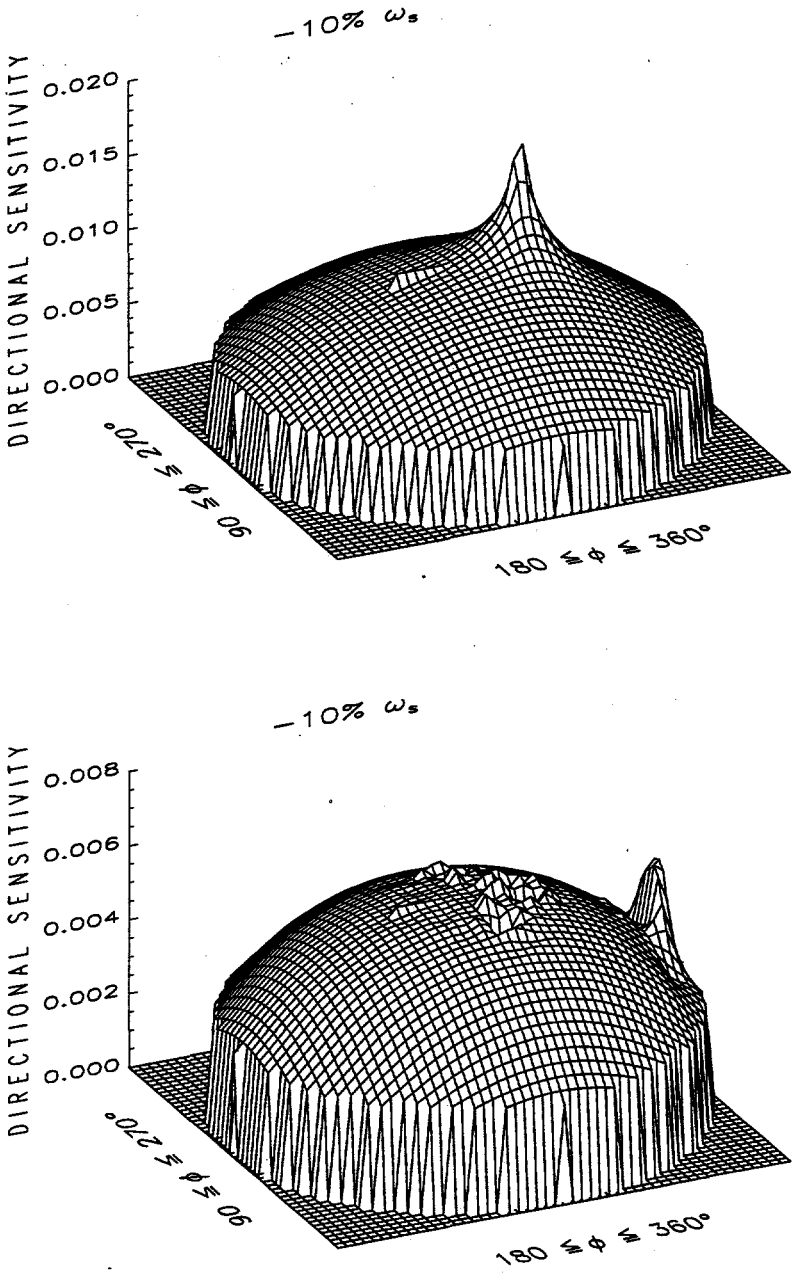

Figure 9.8a-b. Polar plots of directional sensitivity for 10% decreases in ω_s. VZAs increase away from center of plot. SZA = 20° (top) and 65° (bottom).

G. Validation of Directional Sensitivity Method

The directional sensitivity method can be incorporated into the merit function via the weighting variable w_j, such that Equation (2.5) may be rewritten as

$$\varepsilon^2 = \sum_{j=1}^{n} S_{i,j} [R_j - R_j^*]^2. \qquad (9.6)$$

This formulation uses the directional sensitivity of just one parameter, denoted by the subscript *i*. Presumably, this is the parameter for which the highest retrieved accuracy is desired. Still, all parameters may be accurately retrieved regardless of *i*.

The validity of the directional sensitivity theory can be assessed by comparing the surface of a two parameter merit function before and after the application of directional sensitivity weights. Using the site-wide FIFE parameter values found above, reflectance data were generated at every 15° zenith (0 - 75°) and 45° azimuth (0 - 180°) angles (26 total). These were considered the "true" parameter and reflectance values, respectively. As in Section E, the merit function (with $w_j = 1$) was evaluated at equally spaced positions in the parameter space around the true parameters.

Next, weights determined for LAI and leaf reflectance were applied separately. To emphasize differences, the fourth power of each weight was determined. The resulting values were normalized. A comparison of the weights for the respective parameters (Figure 9.9) illustrates differences. The LAI weights apply greatest emphasis on hot spot errors. In addition, the LAI weights decrease substantially for increasing VZA. In contrast, the leaf reflectance weights increase substantially for increasing VZA. The weight for VZA = 75° is about 10 times larger than the analogous LAI weight. Although the leaf reflectance weights also emphasize the hot spot direction, the emphasis was significantly less than for LAI. In general, both weighting schemes have decreasing values for increasing azimuth angle (where 0° azimuth is defined by the projection of the solar vector onto the horizontal plane) such that backscatter errors are emphasized more than forward scatter errors.

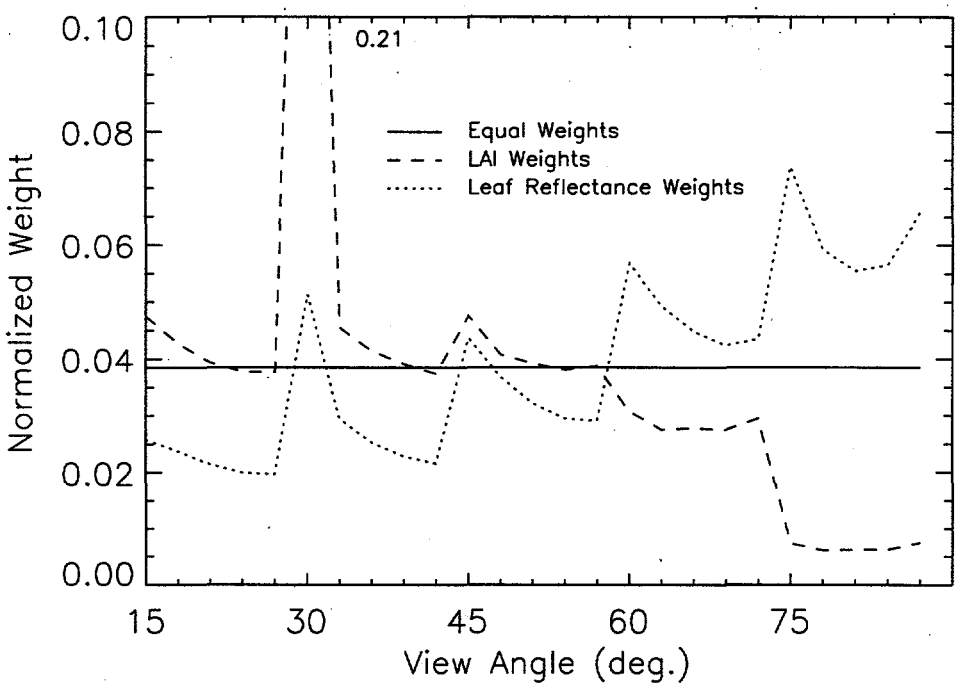

Figure 9.9. Weights used to compare effects of different directional sensitivity sets. Major ticks represent VZA from 15-75° by 15° intervals. Minor ticks represent view azimuth angles, from 0-180° by 45°, per major tick interval.

The merit functions for the different weighting schemes are shown in Figure 9.10. First, several general trends unrelated to the weighting schemes can be noted. For example, the minimizer "valley" sweeps from high LAI, low leaf reflectance to low LAI, high leaf reflectance. This illustrates the fact that increasing LAI has the same general effect as increasing leaf reflectance—it increases TOC reflectance. Second, there is some ambiguity as to the correct minimizer position. Specifically, the 10^{-6} contour line spans about 0.2 LAI and 0.003 leaf reflectance. Since the gradient of the merit function is small within this contour, an optimization algorithm would have difficulty determining the true minimizer. If empirical reflectance data had been used, random errors would serve to lengthen and broaden this valley. This would possibly result in smaller gradients and poorer inversion results (see Chapter V).

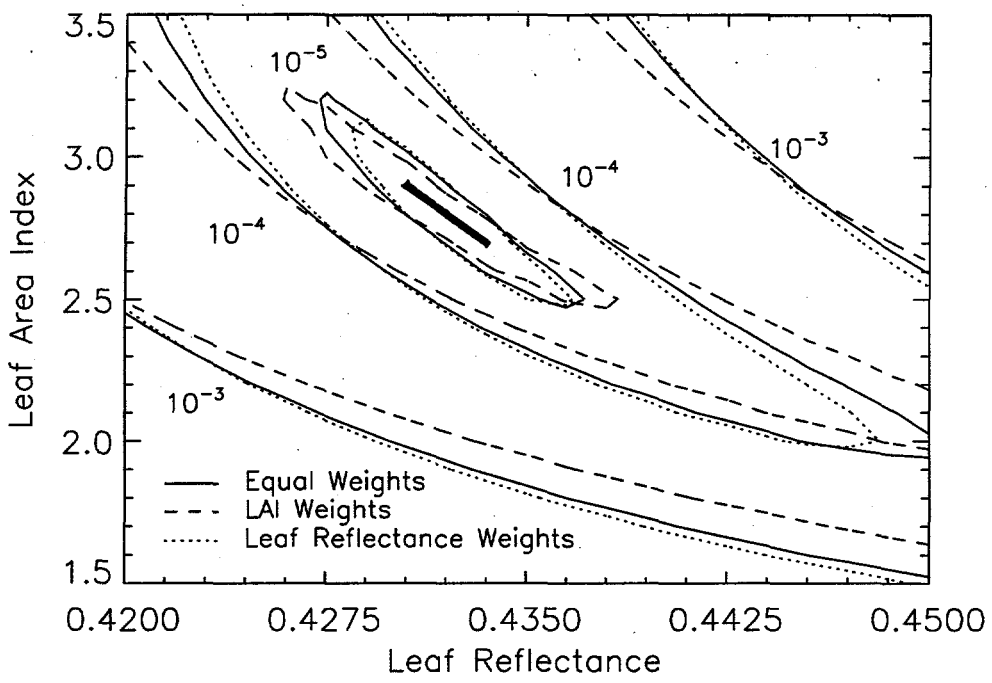

Figure 9.10. Variation in merit function due to directional sensitivity weights from different parameters. Weights are indicated in Figure 9.9.

Inspection of weighting effects reveals important differences. Application of the LAI weights causes contours to become more perpendicular to the LAI (ordinate) axis. In effect, this increases the gradient along lines determined by constant leaf reflectance. As noted above, steeper gradients allow more computationally efficient minimization. Moreover, it decreases the ambiguity in the LAI minimizer value since the lowest ε^2 contour extends over a smaller LAI range. It also effectively increases the range of leaf reflectance values spanned by the lowest ε^2 contour. Thus, greater errors in leaf reflectance could be tolerated while still retrieving a correct LAI. In the limit of weighting effects, the contour lines would be perpendicular to the LAI axis such that the correct LAI could be ascertained for a large range of leaf reflectance estimates. In practice, however, such a severe change could not be achieved since the angular regions over which the respective parameters influence reflectance are not independent.

Likewise, when leaf reflectance weights are applied, contours become more perpendicular to the leaf reflectance axis (abscissa). This increases the gradient along constant LAI lines such that the optimization algorithm can more efficiently determine leaf reflectance. Again, the range of leaf reflectance spanned by the smallest contour line is reduced while the range of LAI is increased. This suggests that larger errors could be tolerated in LAI without sacrificing accuracy in leaf reflectance estimation.

These results show that the directional sensitivity method allows advantageous manipulation of the merit function surface. While basic trends in merit function behavior are defined by the influence of respective parameters on reflectance, more subtle yet distinct changes can occur by employing a directional sensitivity weighting scheme. Although the fourth power of $S_{i,j}$ was used here, other exponent values would emphasize/de-emphasize reflectance differences at various geometries. Further experimentation may reveal an optimal exponent. While future methods may have more direct impact on the merit function shape, the directional sensitivity method is reasonably simple and easily implemented—important characteristics for operational use.

H. Application of Directional Sensitivity Method to AVHRR Data

Although $S_{i,j}$ varies smoothly over most directions (cf., Figures 9.6-9.8), it varies sharply near the hot spot. Therefore, despite the relatively high angular resolution of the LUTs, the rounding of sun-target-sensor angles to the nearest LUT element may produce errors in directional sensitivity. To rectify this condition, a 2-D cubic spline was fit to the $S_{i,j}$ data for each SZA. To eliminate anomalous results near their edges, the splines were determined over angular ranges (-30 to 210° azimuth, -30 to 75° zenith) larger than the necessary ranges (0-180° azimuth, 0-70° zenith). The continuous splines allow the interpolation of $S_{i,j}$ for any view zenith and azimuth angle.

In operation, the SZA of an AVHRR sample is rounded to the nearest 5° interval. The resulting value is used to determine the appropriate spline. With the viewing geometry of the sample, the spline is used to interpolate $S_{i,j}$. This method assumes that $S_{i,j}$ varies relatively slowly in SZA,

such that SZA differences of up to 2.5° have minor effect. Qualitative inspection suggests this assumption is reasonable.

The directional sensitivity method also provides a convenient method for selecting an optimal set of samples for inversion. Specifically, since the directional sensitivity indicates the relative usefulness of a particular sample, it is reasonable to choose a sample set for which the mean directional sensitivity,

$$\overline{S} = \frac{1}{n} \sum_{j=1}^{n} S_{i,j} , \tag{9.7}$$

is maximum, where $S_{i,j}$ is the directional sensitivity for a given sample and n is the number of samples in the subset ($n > p$).

In the present study, inversion of DISORD was attempted with FIFE AVHRR data from 1987. Although previous inversions (Chapters VII and VIII) utilized data from 1989, ground truth data were more comprehensive in 1987. AVHRR data from both NOAA-9 (morning) and NOAA-10 (afternoon) were utilized. In an attempt to decrease sampling errors from subpixel heterogeneity and georegistration, mean site-wide AVHRR values were used. A filter eliminated passes for which the FIFE area was cloudy. The resulting data were relatively sparse (68 reflectance values between 9 May and 22 October 1987).

Because the number of samples collected over the FIFE area per satellite pass depends on the VZA, the statistical significances of the "average" values differ. Moreover, the average value for a given pass may not be the same as any measured value due to the large spatial heterogeneity at FIFE. Specifically, large limestone outcrops are evident in high resolution images of the area. Other issues, such as the varying amounts of overlap between adjacent pixels for different passes, or the differential spatial weighting due to the sensor point spread function, further complicate the interpretation of a site-wide average reflectance. These complicating issues were not addressed in this study.

Because canopy conditions changed throughout the summer, subsets of the 68 AVHRR samples were used for inversions. Although more samples can improve the determination of the model parameters, all samples in a subset must be gathered within a time frame for which the target vegetation is likely to be invariant. In practice, this time frame depends on many variables including vegetation type and condition, climatology, and soil moisture. Inspection of FIFE data suggests that the tallgrass prairie may normally be regarded as invariant for 11-day periods.

Optimal subsets were thus found as follows. First, the directional sensitivity of each cloud-free AVHRR sample was determined. The $S_{i,j}$ values for samples within every 11-day period were sorted according to magnitude. The mean directional sensitivity ($\overline{S}$) of the p samples with the highest $S_{i,j}$ was determined for each period. Results in Figure 9.11 clearly show that the logical selection of periods can result in a substantially larger $\overline{S}$ compared to other periods. Thus, all periods with mean sensitivity values exceeding a user-defined threshold were used in inversions, while those with values below the threshold were rejected. In using this strategy, inversions were conducted only with the most promising 11-day periods (i.e., those identified via directional sensitivity to contain the most information about the model parameters).

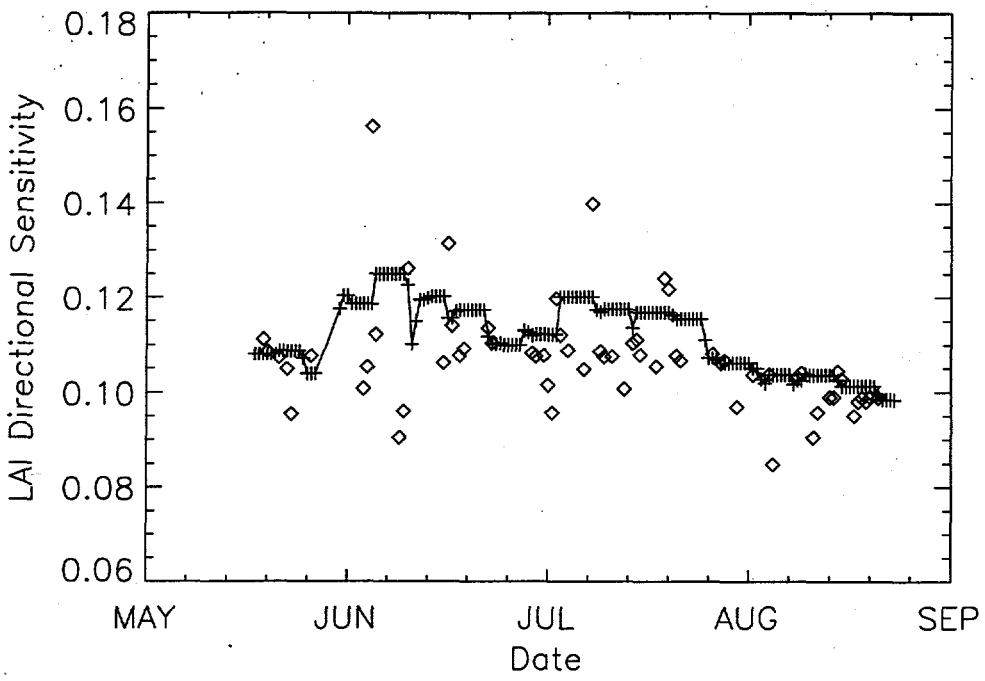

Figure 9.11. Directional sensitivity values for 68 AVHRR samples from 1987. Diamonds represent weights for individual samples, pluses (+) represent mean weights for three most highly weighted samples per 11-day period.

I. Atmospheric Correction of AVHRR Data

The Local Area Coverage AVHRR data (Level-2a) from FIFE were corrected for atmospheric effects by Goetz (1995) using the 5S+ model of Vermote et al. [1994]. 5S+, and it successor 6S, are extensions to 5S and feature increased spectral, spatial, and angular resolution. The 5S+ model was used to estimate surface reflectance given the atmospheric conditions and observed TOA reflectance. The thermodynamic profile of the atmosphere was assumed to follow the US62 model, and the aerosol distribution for mid-continental areas was used. The atmospheric precipitable water was estimated from the brightness temperature difference between AVHRR bands 4 and 5 [Eck and Holben, 1994]. The aerosol optical depth at 550 nm was fixed with the median value observed in 1987. Although this parameter is not constant in nature, sensitivity studies [Tanré et al., 1992] suggest the AVHRR band 2 reflectance is not highly sensitive to it.

The correction scheme above yields an estimate of the TOC reflectance. Nevertheless, DISORD still requires an estimate of γ, the ratio of direct-to-total irradiance. For the inversions described in Chapters VII-VIII, 5S was used to estimate γ based on *in situ* data from sun photometer (557 nm) and radiosonde measurements near the time of MMR sampling. However, these measurements were not conducted throughout 1987. Thus, atmospheric data were determined as described below.

Aerosol optical depth data at 500 nm were obtained from sun photometer observations. The data extended from 9 April 1987 to 31 October 1989. Using the FIS-supplied Angstrom exponent, the optical depth at 550 nm was calculated for each observation. Mean morning (0800-1130 local time) and afternoon (1230-1630 local time) values were then determined for each observation day. Fourth order polynomials were fit to these data. Although the data are highly variable, results (Figure 9.12) suggest that afternoon optical depth exceeds morning optical depth. Moreover, both morning and afternoon optical depths are greatest during the summer. These results are somewhat intuitive since rural aerosols generally evolve from atmospheric convection. Convection varies with insolation and hence season.

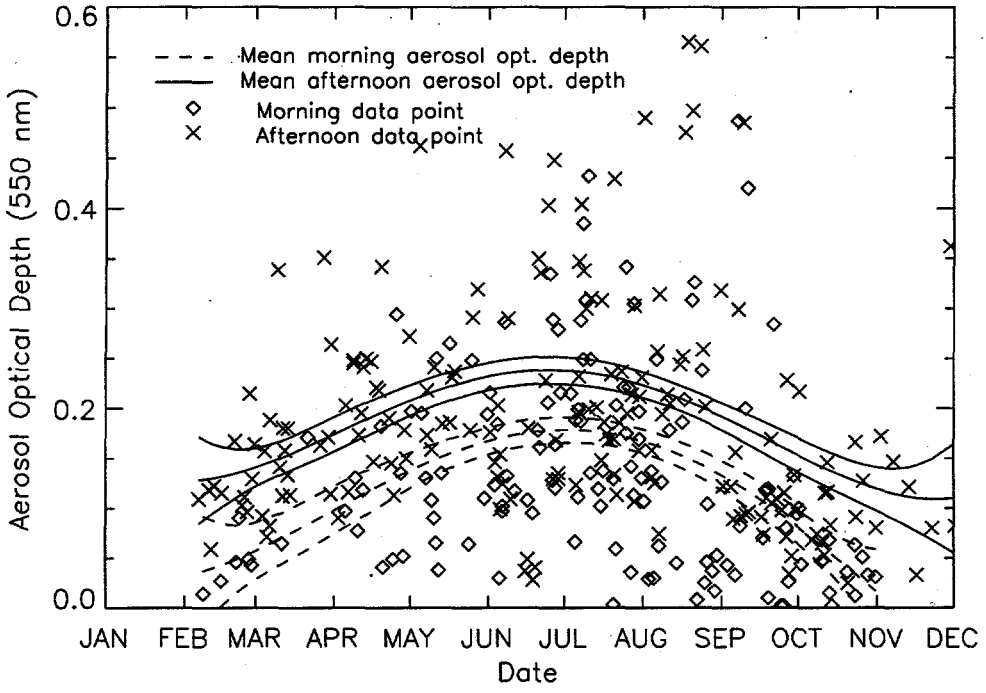

Figure 9.12. Variation in aerosol optical depth with date during FIFE. Values were determined from sun photometers. Curves represents 4th order polynomial fits, and their confidence intervals, of morning and afternoon values.

Ozone abundance was available from High Resolution Infrared Sounder-Version 2 (HIRS-2) data sets. HIRS-2 is part of the Tiros Operational Vertical Sounder (TOVS) system onboard NOAA-9 and -10. These data were available for 1 January 1987 through 31 December 1987. Again, a 4th order polynomial was fit to the data. Results (Figure 9.13) suggest that ozone abundance is highest and most variable in winter and early spring.

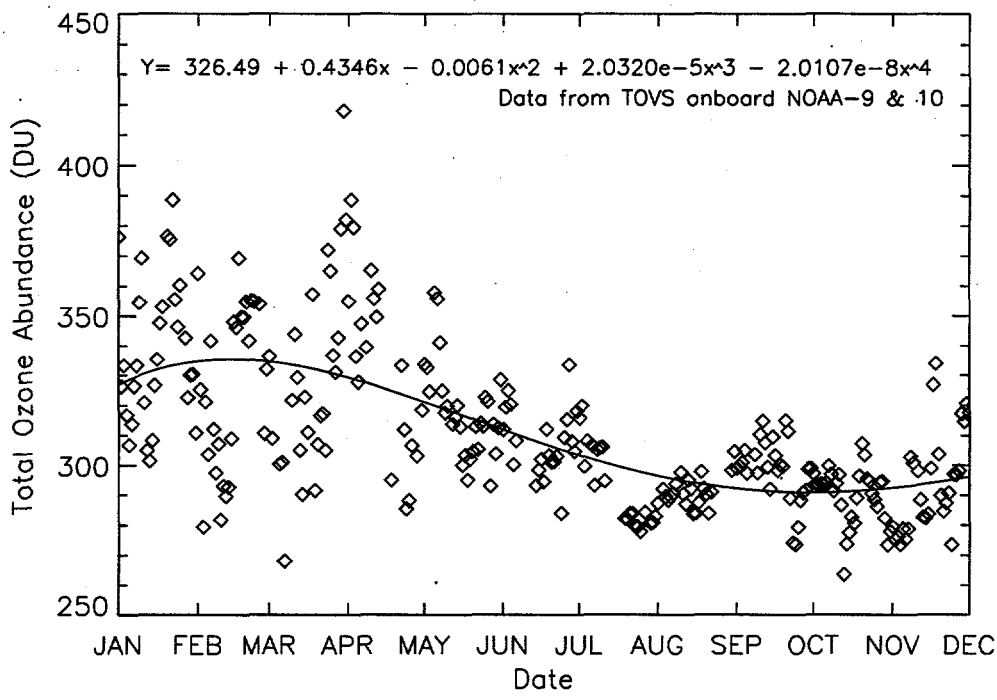

Figure 9.13. Ozone abundance estimates over FIFE from TOVS HIRS-2 data. Curve represents a 4th order polynomial fit of the data.

Finally, column water vapor was available from the TOVS HIRS-2 (1987). It was also determined from radiosonde data (1987 and 1989). Only data collected between 0700 and 1700 local time were used. No appreciable differences were evident between morning and afternoon values. A 4th order polynomial was again fit to the data. Results (Figure 9.14) suggest that column water vapor is highly variable, especially during summer months. Moreover, summer values may be more than twice the magnitude of winter values. This reflects the impact of temperature on the ability of the atmosphere to hold water.

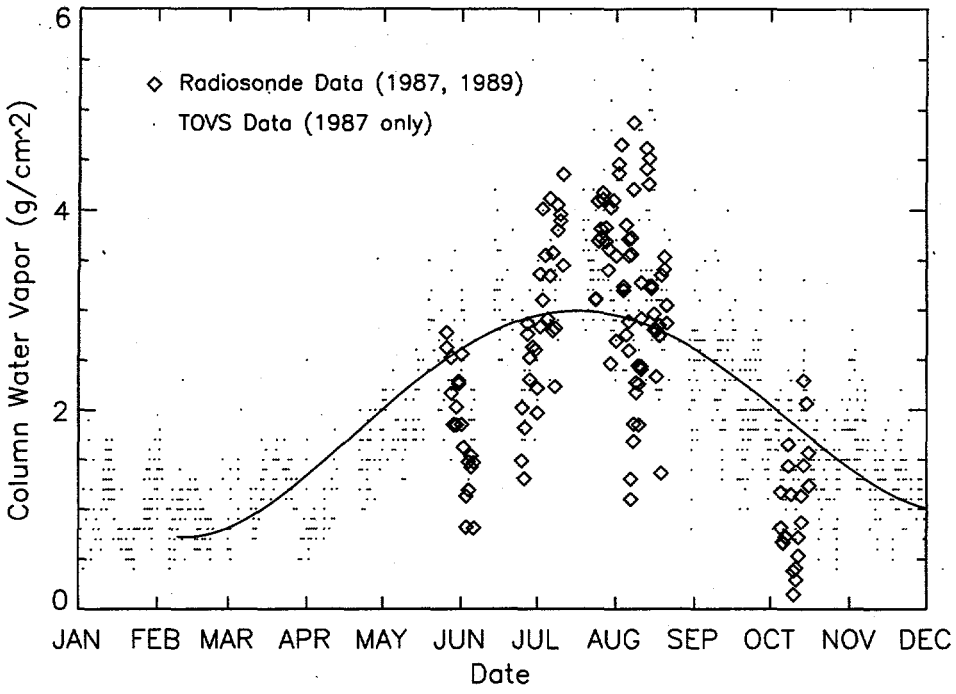

Figure 9.14. Column water vapor estimates over FIFE from TOVS HIRS-2 and radiosonde data. Curve represents a 4th order polynomial fit of the data.

The polynomial equations for these atmospheric properties were programmed into the 6S code. This allowed determination of γ directly from sun-target-sensor geometry and Gregorian Day. Although this method relies on statistical fits, it is undoubtedly superior to methods which assume constant atmospheric properties throughout the year. Assuming the data are typical for the FIFE area, this modified model may be used to atmospherically correct FIFE AVHRR data for any date.

J. Comparison of Model Estimates to AVHRR Data

Before model inversions were attempted, the atmospherically corrected AVHRR data were compared to DISORD estimates. Excluding LAI, the model parameters were fixed with the mean values described above. LAI was determined individually for each date using polynomial interpolation (also described above). While a comparison of AVHRR data with model estimates does not provide

true validation of either data set, it does indicate the potential success of model inversions. Specifically, if the values match well, it is likely that the merit function minimum will occur when model parameters assume reasonable values.

Results in Figures 9.15a-b reveal several interesting phenomena. First, the largest errors occur during the early and latter parts of this period (Figure 9.15b). In those cases, the model consistently underestimates the measured reflectance. While the general green up and senescence periods are obvious in the modeled data, they are less obvious in the measured data. In specifying parameters, however, the model was intended to simulate mature, healthy canopies. For example, only live biomass data were used to calculate LAI, and only green leaves were used to determine leaf optical properties. These conditions did not exist in late spring due to the prescribed burning of some areas on or near 15 May 1987. Moreover, transect biomass data suggest that little or no live biomass was present by 12 October 1987. Hence, it is probable that the canopy was progressively senescing during the latter part of the AVHRR measurement period. Moreover, the model LAI was not permitted below 0.5 since the LAI polynomial was considered inaccurate in such cases. Thus, accurate modeling of spring and autumn conditions should not be expected.

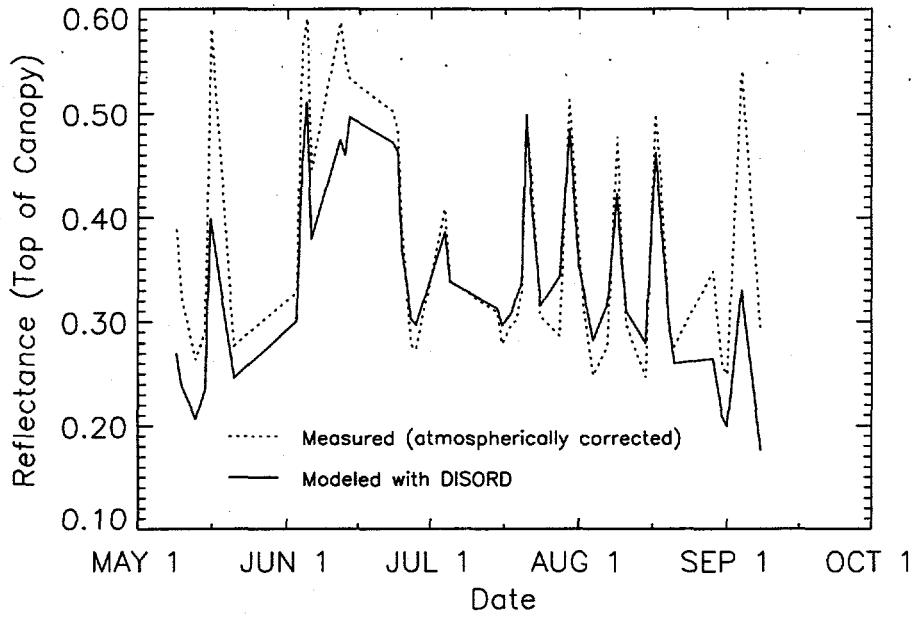

Figure 9.15a. Comparison of atmospherically corrected measurements and BRDF model estimates of AVHRR band 2 reflectance.

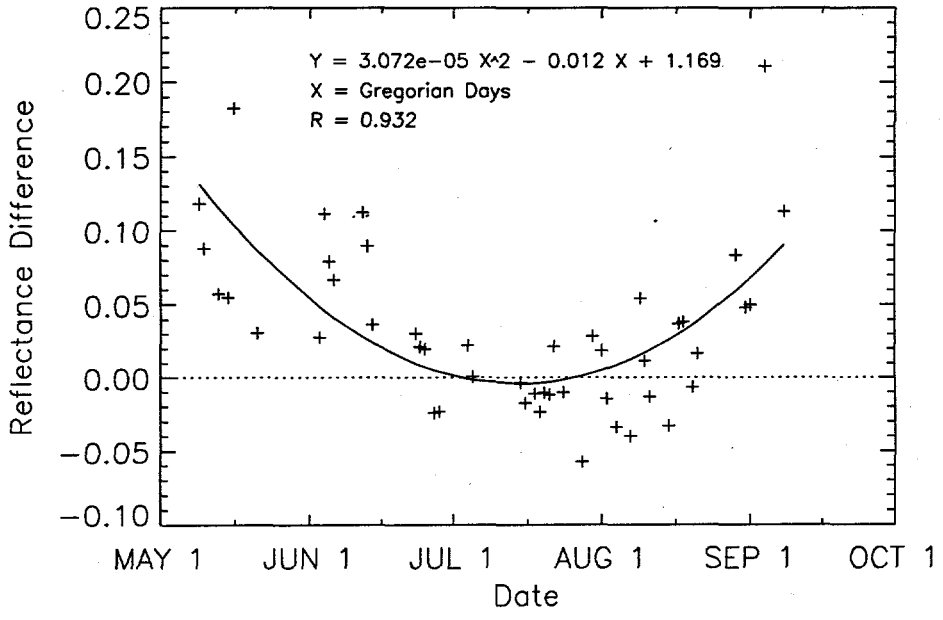

Figure 9.15b. Errors, as a function of date, between measured and modeled reflectance of AVHRR.

For mid-June through mid-August, the measured and modeled values agree reasonably well (mean of absolute values of errors = 0.022). Still, the model estimates vary less than the measured values. The opposite was expected since model estimates depict the reflectance per unit steradian, whereas AVHRR measures reflectance over about 1.99 μsr. Reasons for this inconsistency are not clear. Figure 9.15c suggests no significant correlation of errors with VZA. This implies that the turbid medium model is able to adequately represent the actual canopy. If this were not true, some correlation would be expected since canopy gaps visible to the sensor would decrease with increasing VZA. Figure 9.15d, however, suggests the reflectance errors are somewhat correlated with SZA. Although SZA was higher during the early and later parts of the measurement period (where canopy conditions were not suited for this model), it is possible that the atmospheric correction was less accurate for high SZA. Improved modeling and atmospheric corrections will be considered in future work.

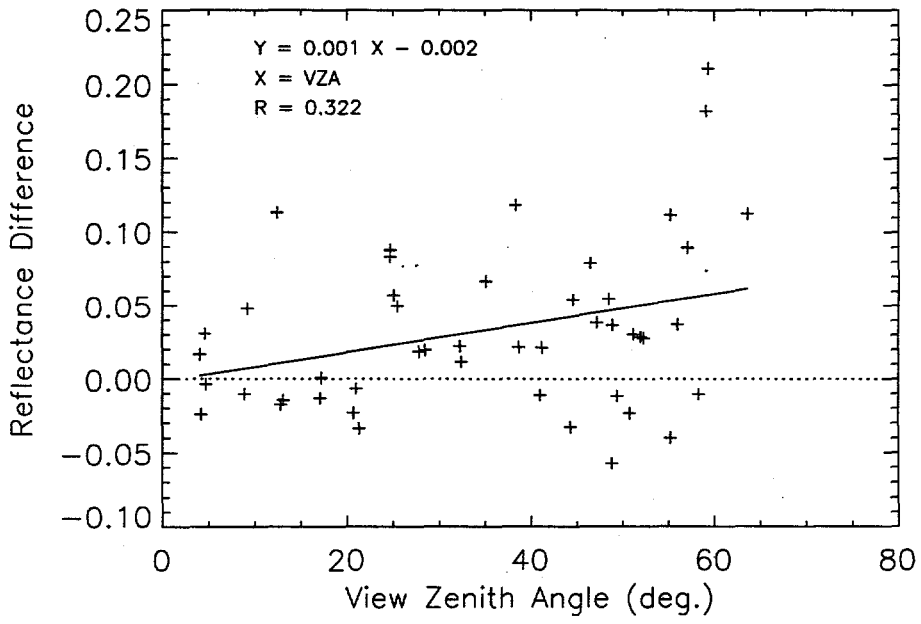

Figure 9.15c. Errors, as a function of VZA, between measured and modeled reflectance of AVHRR.

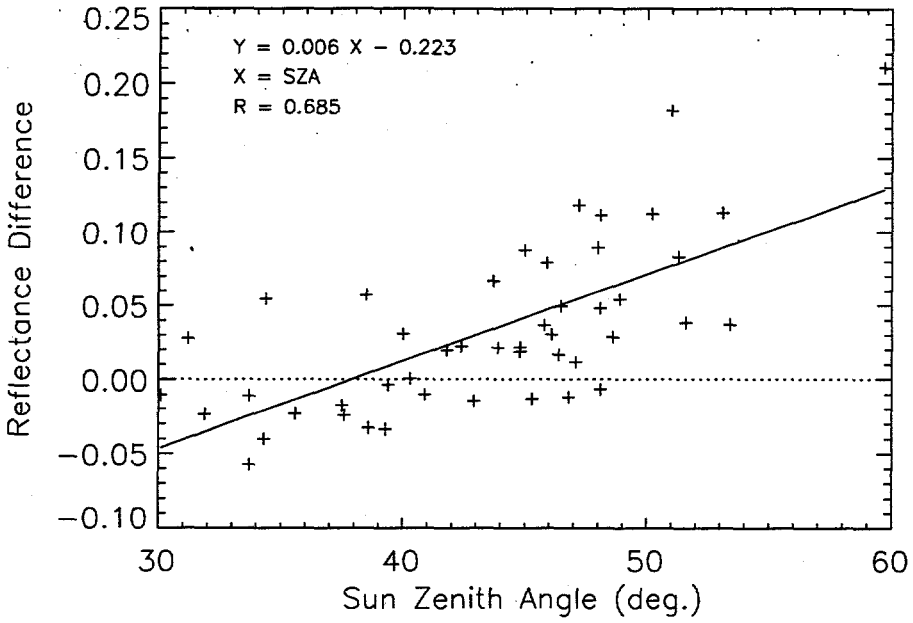

Figure 9.15d. Errors, as a function of SZA, between measured and modeled reflectance of AVHRR.

K. Inversions with One Adjustable Parameter

Due to the significant differences between data measured by ground-based and space-based sensors, only one parameter was initially adjusted in the inversion. Since LAI is one of the most useful parameters [Collins and Avissar, 1994] and the most difficult to obtain [Goel and Thompson, 1985], it remained adjustable. Leaf reflectance/transmittance and ω_s were held constant using the values determined in Section G. The LAI directional sensitivity data were used to weight the reflectance errors. Only 11-day periods where $\overline{S} > 0.11$ were used. Inverse parabolic interpolation (subroutine BRENT [Press et al., 1988]) was used to adjust LAI.

Results are shown in Figure 9.16. Although errors are large for early June, this is not unexpected based on results above. Specifically, the inversion increased LAI such that model estimates would match the high reflectance data (cf. Figures 9.15a-b). Errors from mid-June through mid-August are significantly smaller. Indeed, the retrieved LAI matches the *in situ* curve (see Section E) relatively well during this period. Of particular note is the decrease in retrieved LAI during the latter part of the

period. The same trend is obvious in the measured data. This undoubtedly reflects the decrease in green vegetation in late summer.

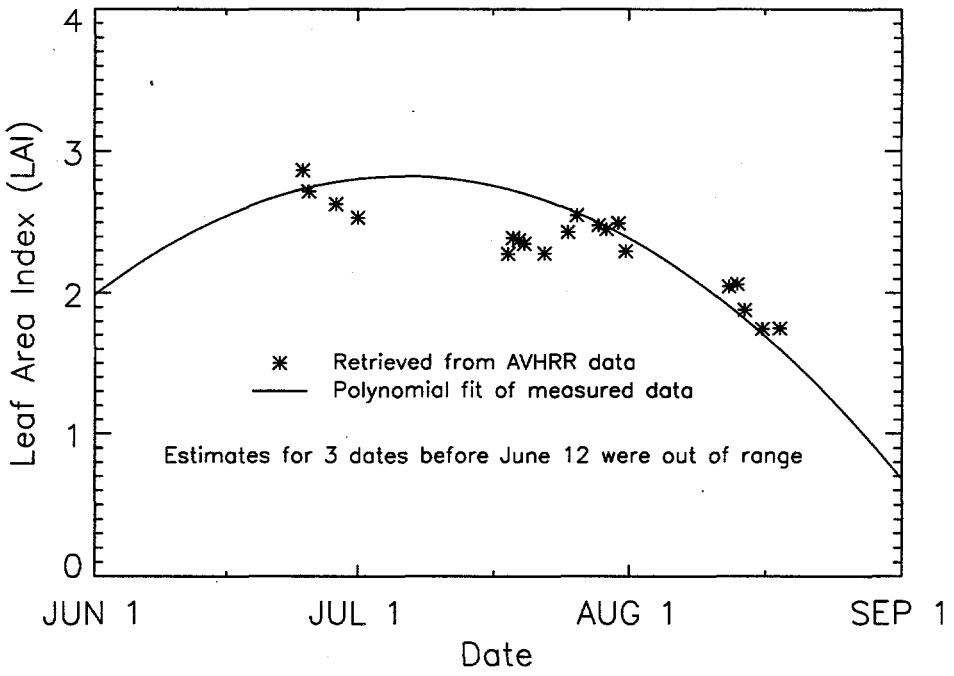

Figure 9.16. Comparison of AVHRR-retrieved and measured LAI over FIFE during 1987. BRDF model was inverted for one parameter. Measured data are discussed in Section E.

Inversions were also attempted by adjusting leaf reflectance/transmittance. LAI was fixed at 2.8. The directional sensitivity weights for leaf reflectance/transmittance were used in the merit function. Results in Figure 9.17 show the retrieved reflectance is higher than the mean measured value through mid-June, although it is within the range of the measured data. From mid-June through early September, differences between the retrieved and mean measured values are significantly smaller. By mid-September, the retrieved leaf reflectance is consistently lower than the mean measured value for green leaves. However, the differences between the retrieved and mean measured values for senescing leaves is small. In all cases, the retrieved values are within the range of measured data. This suggests that, given a reasonable value of LAI, inversion of DISORD allows an accurate estimation of mean leaf reflectance throughout the tallgrass life cycle.

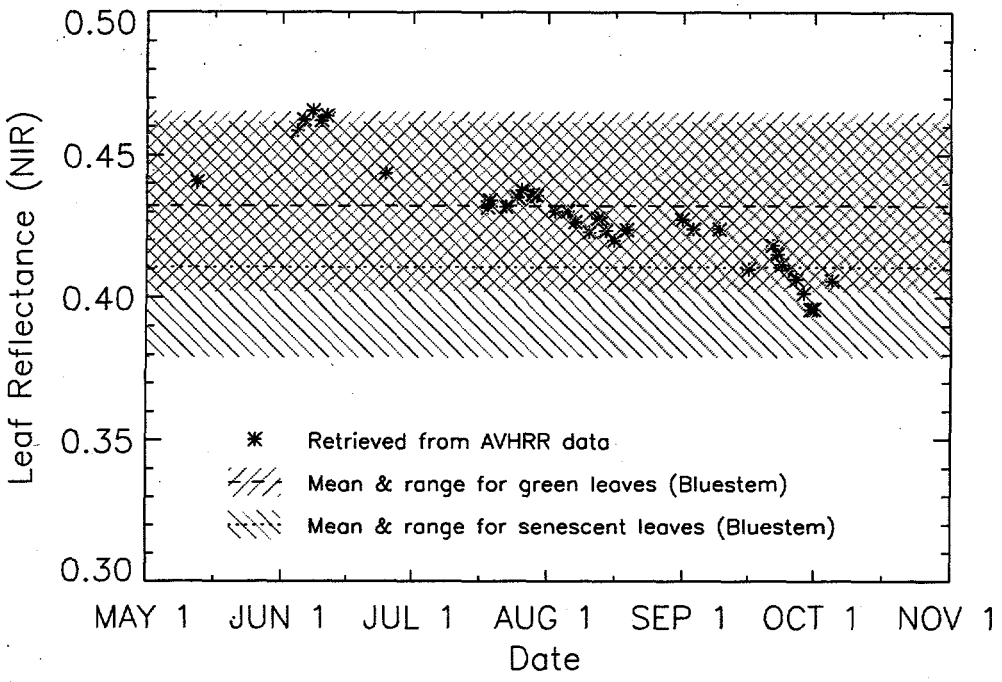

Figure 9.17. Comparison of AVHRR-retrieved and measured leaf reflectance over FIFE during 1987. BRDF model was inverted for one parameter. Measured data are discussed in Section E.

L. Inversions with Two Adjustable Parameters

Based on the success of the one parameter inversions, two parameter inversions were attempted. In this case, the simplex routine described in Chapter VIII was used to determine LAI and leaf reflectance. All other parameters were held constant at the values used in Section J. Assuming LAI is the more useful retrieved parameter, the LAI directional sensitivity values were used. As noted above, this choice presumably means that LAI can be determined more accurately despite possibly larger errors in leaf reflectance.

Results with two adjusted parameters were clearly less successful (Figures 9.18a-b). Although some retrieved LAI values near the middle of July and middle of August were in the range of the measured LAI values, the remaining LAI estimates were too low. In contrast, the corresponding leaf reflectance/transmittance were too high. The potential to overestimate leaf albedo and underestimate

LAI is a result of the merit function behavior (cf. Figure 9.10). Indeed, in cases where the leaf reflectance was reasonably estimated (leaf reflectance error < 0.03), the canopy LAI was more reasonably estimated (Figure 17a). These data (corresponding to reasonable ρ) correctly show the decrease in LAI during the late summer.

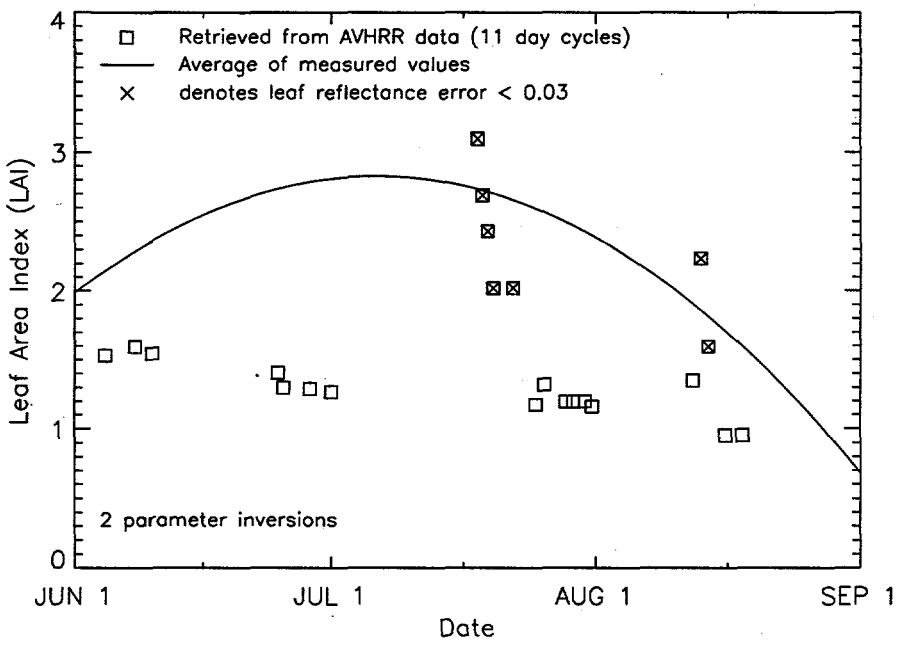

Figure 9.18a. Comparison of AVHRR-retrieved and measured LAI over FIFE during 1987. BRDF model was inverted for two parameters.

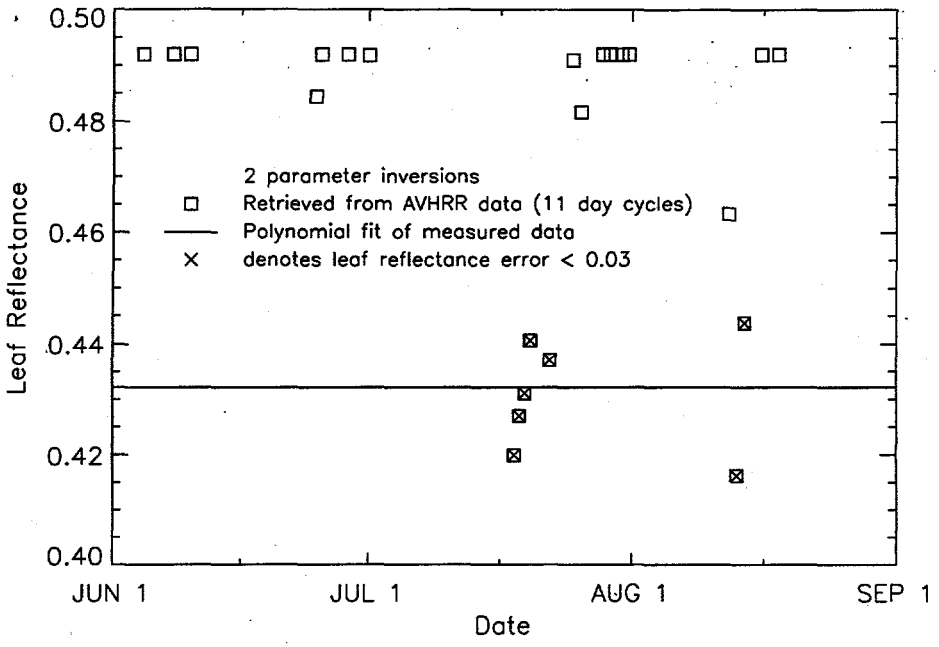

Figure 9.18b. Comparison of AVHRR-retrieved and measured leaf reflectance over FIFE during 1987. BRDF model was inverted for two parameters.

In an effort to decrease these errors, the period over which AVHRR data were collected per inversion was extended to 18 days. In this case, consecutive 18-day periods from 26 April 1987 were considered rather than every possible 18-day period. It was hoped that by increasing the number of samples, the model parameters could be better determined and hence more accurate. In practice, however, errors were significantly larger than for the 11-day cycles. In most cases, the leaf albedo was estimated to be the theoretical upper limit (1.0). Due to the inverse relationship between retrieved leaf albedo and LAI, this resulted in low estimates of LAI. The increased errors probably resulted for two reasons. First, since successive rather than all 18-day cycles were used, the magnitude of $\overline{S}$ was not considered. Thus, there was no discrimination between promising and non-promising data sets. Second, by extending the data collection periods to 18 days, it is likely that all periods contained some samples for which the measured and modeled reflectances were very different (cf. Figure 9.15a).

M. Inversions with Three Adjustable Parameters

Despite the limited success with two parameter cases, inversions with three adjustable parameters (LAI, leaf reflectance/transmittance and ω_s) were also attempted. Again, an 11-day cycle was used with the LAI directional sensitivity weights. Results in LAI and leaf albedo were similar to those above (Figures 9.19a-c). Specifically, LAI was underestimated and leaf albedo was overestimated in most cases. When leaf albedo errors were less than 0.03, however, LAI errors were reasonable in all but one case. There was no obvious correlation of ω_s errors with errors in the other parameters. In nearly half of the cases, ω_s assumed the value of either the upper or lower limit (0.2 and 0.7, respectively). This suggests that ω_s of grasslands may be very difficult to retrieve from satellite data.

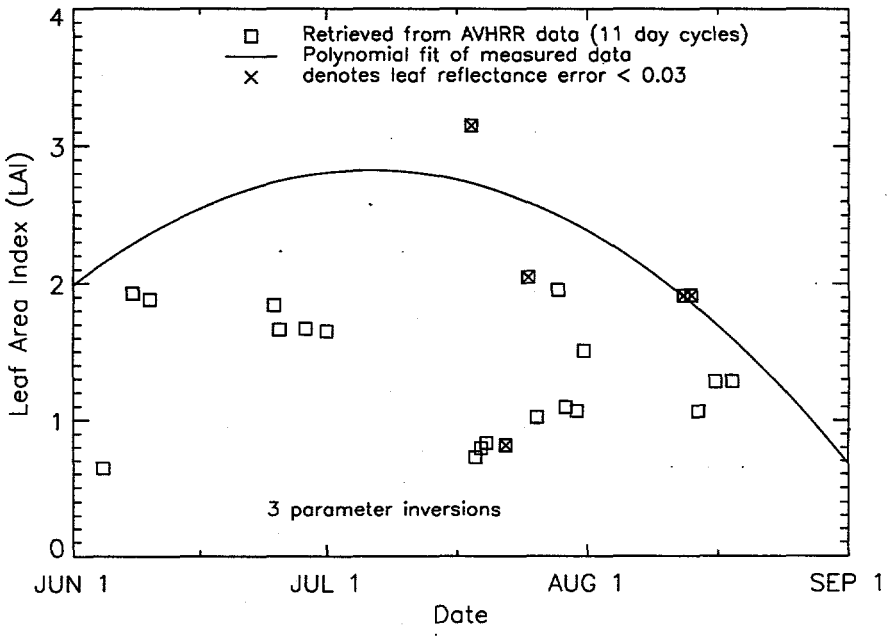

Figure 9.19a. Comparison of AVHRR-retrieved and measured LAI over FIFE during 1987. BRDF model was inverted for three parameters.

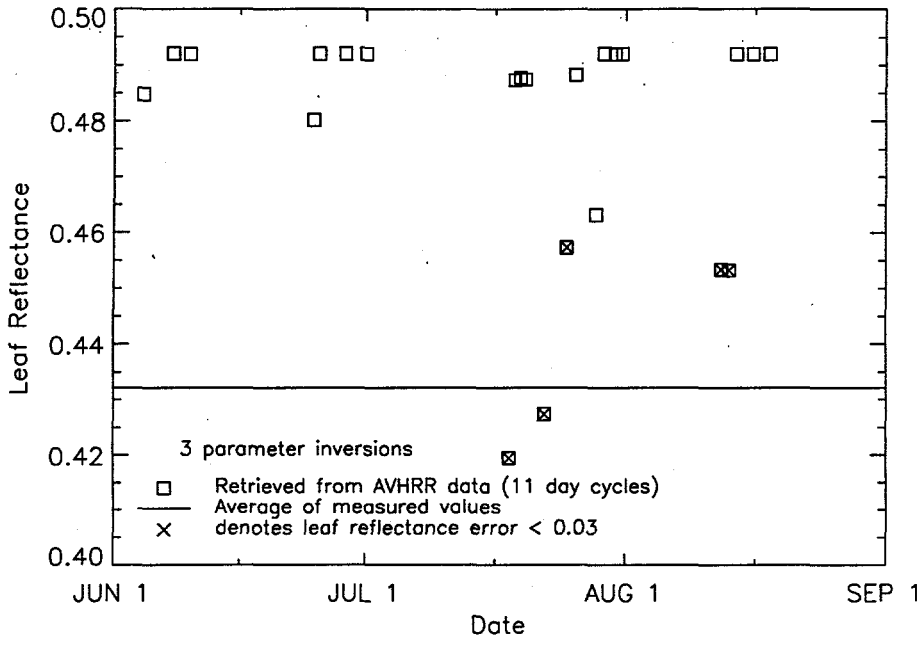

Figure 9.19b. Comparison of AVHRR-retrieved and measured leaf reflectance over FIFE during 1987. BRDF model was inverted for three parameters.

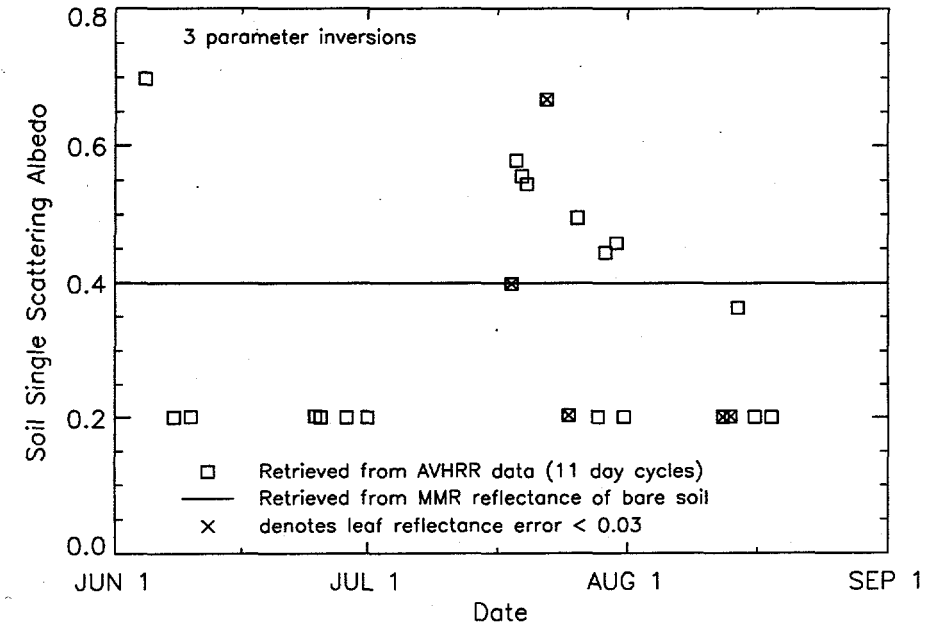

Figure 9.19c. Comparison of AVHRR-retrieved and measured soil single scattering albedo over FIFE during 1987. BRDF model was inverted for three parameters.

N. Other Uses of Directional Sensitivity

In this study, $S_{i,j}$ was only found for NIR wavelengths. However, multispectral data could be accommodated simply by adding another degree of freedom, e.g., $S_{i,j,k}$, where k denotes the spectral band. Additional degrees of freedom might accommodate other parameters, such as atmospheric variables, model accuracy (if directionally dependent) and soil moisture.

To more explicitly emphasize the retrieval accuracy of one parameter over another, the directional sensitivities of the two parameters may be ratioed, such as

$$w_j = \frac{S_{1,j}}{S_{2,j}}, \tag{9.8}$$

where the accuracy of parameter c_1 is deemed more important than the accuracy of parameter c_2. Moreover, one parameter inversions may be attempted sequentially. In this case, the directional sensitivities of c_1 may be used initially to determine its value. Upon optimization, the problem could be reconfigured by fixing c_1 with the retrieved value. A second inversion could be conducted using the directional sensitivities of c_2. The cycle might be repeated to improve estimation.

Optimization routines relying on line minimizations (e.g., quasi-Newton routines) might be most effective using variable weighting sets. In this case, the directional sensitivity could be uniquely formulated for each line minimization. For example, the weight for sample j might be formed by a simple vector product,

$$S_j = \hat{n} \bullet \vec{S_j} \tag{9.9}$$

where \o(n,^) defines the unit vector in the parameter space direction of the current line minimization, and $\vec{S_j} = S_{1,j}\,\hat{i} + S_{2,j}\,\hat{j} + \ldots + S_{p,j}\,\hat{p}$ represents the gradient of canopy reflectance (R_j) with respect to the model parameters. The hat (^) denotes a unit vector, and $\hat{i}$, $\hat{j}$, ..., $\hat{p}$ are the standard unit vectors. Equation (9.9) would weight merit function errors by the relative impact of each parameter on the merit

function along the given line. The impact for a parameter would be determined by the parameter's directional sensitivity and degree to which the line coincides with the parameter's axis. Note that upon minimizing each line for a given iteration, the merit function would have to be reevaluated at the final position using a standard weighting function. In this manner, minima determined over multiple iterations could be compared.

As shown in this study, optimal subsets of available satellite data might prove most reliable for inversion. Since the directional sensitivity method depends only on sample geometry, optimal subsets may be determined well before the data are collected. The time frame over which reflectance data can be collected is limited by the temporal variance of the surface. Surface variance may depend on date, climatology, root depth, soil water capacity, canopy age and health, anomalous events (insect infestation, disease, fire), etc. As stated in Chapter II, at least p samples must be available for inversion. The number p depends on the inversion configuration. The ability to collect the samples in a given time frame is a function of many variables, including the number and sampling strategy of the sensor(s) and the cloudiness of an area. If large areas of homogeneous cover exist, samples from different targets might be combined in the same inversion. Clearly, sampling strategies for most environmental satellites (SPOT, Landsat) were not designed to suit operational BRDF model inversions. Indeed, although AVHRR was not designed for this purpose, it is nevertheless most suitable.

The utility of the directional sensitivity method is significant. Still, the sets $S_{i,j}$ are unique for each canopy. Therefore, in a global operation, a different set should be generated for each class cover (e.g., coniferous forest, deciduous forest, grassland, tundra). Regardless of these issues, it appears that in multiple parameter inversions, contending with the inverse relationship between LAI and leaf albedo will be a significant challenge. Indeed, despite the directional sensitivity method, consistent results were only retrieved in one parameter inversions. By confining the parameter space and reducing errors in data, multiple parameter inversions should eventually be more successful.

O. Conclusions

Based on its wide range of sampling geometries, global coverage, and high temporal resolution, AVHRR data was chosen for use in model inversions. Because satellite data contains significant noise due to atmospheric and surface effects (topography, cover heterogeneity), a scheme was developed for differentially weighting the empirical data. The scheme is based on the sensitivity of TOC reflectance at a given sun-target-sample geometry to model parameters. Directions for which reflectance is more sensitive to a given parameter has a larger weight than directions for which reflectance is less sensitive. Simulations with synthetic data verified that merit function gradients increased when this weighting scheme was applied. Steeper gradients were found to improve optimization accuracy and efficiency.

Mean parameter values were determined over the entire FIFE site via various averaging schemes. Using atmospherically corrected AVHRR data from 1987, the coupled soil and canopy model was partially validated. Model estimates agreed reasonably well with empirical data from mid-June through mid-August. Errors in data gathered before mid-June and after mid-August were attributed to non-green surface conditions (burned and senescent canopies, respectively).

The model was configured for inversion by fixing LAD with the site-wide value. Moreover, leaf transmittance was coupled to leaf reflectance using a regression equation determined from empirical data. The remaining three parameters—LAI, leaf reflectance/transmittance, and soil single scattering albedo—remained variable. Estimates of γ were determined using a radiative transfer model and empirical-based equations for atmospheric properties. The weighting scheme was used to select promising 11-day subsets of AVHRR data for inversions. Using the LAI and leaf reflectance/transmittance weighting schemes, site-wide LAI and leaf optical properties were accurately retrieved in one parameter inversions. Solutions from inversions with two adjustable parameters were less accurate, but were acceptable in some cases. Finally, additional uses of the weighting scheme were outlined.

Due to the limited bandwidths of AVHRR, fAPAR and shortwave albedo were not computed. Myneni et al. [1992b] demonstrated that incomplete coverage of the solar spectrum by AVHRR could result in albedo errors of up to 30%.

CHAPTER X

CONCLUSIONS

The investigations in this study were conducted to determine the limitations of and an efficient strategy for bidirectional reflectance model inversions. Both of these objectives were achieved. General conclusions from this study are stated below.

Inversions can only retrieve parameters which substantially affect the top-of-canopy (TOC) reflectance. A sensitivity study suggested that at very low optical depths (LAI < 1), only soil parameters may be accurately retrieved. At moderate optical depths (1 < LAI < 3), soil single scattering albedo and canopy parameters may be retrieved, and at high optical depths (LAI > 3), only canopy parameters may be retrieved. The accurate determination of LAI generally requires that the soil affect TOC reflectance. Otherwise, the canopy is effectively semi-infinite and reflectance is not sensitive to LAI perturbations. Parameters to which TOC reflectance is not sensitive may be fixed at constant values (even if somewhat incorrect) with little negative effect on results.

Inversions with noise-free, synthetic data suggest accurate estimation of surface parameters is possible except for cases of high LAI (8), low SZA, and when the LAD was incorrectly specified. Accurate inversions are difficult for low SZA since the azimuthal asymmetry of the TOC reflectance decreases as SZA decreases. This reduces the information available to the inversion. In addition, unless LAD is adjustable during inversion, some prior knowledge of the LAD is required. Inversions using synthetic data collected under satellite sampling schemes (MISR and AVHRR) should permit the accurate estimation of parameters. The only exception found in this study was for MISR viewing geometries in the orthogonal plane. Indeed, results suggest samples in or near the principal plane are highly advantageous to the inversion.

Surface state parameters—spectral albedo, absorbed radiation, and canopy photosynthetic efficiency (under known conditions)—may be accurately determined despite relatively large errors in retrieved model parameters. Since surface state parameters essentially describe integrated radiation quantities, determination of their instantaneous values is tantamount to accurately estimating reflectance for non-data directions. Multiple solutions (some incorrect) may produce reasonable integrated quantities. However, if state parameters are to be predicted for times at which radiance data are unavailable, accurate determination of model parameters is important. Otherwise, TOC reflectance changes with SZA may be incorrect.

A model of anisotropic background (soil) reflectance appears necessary for canopy model inversions with relatively high LAI values (<8). This is particularly true when samples near the hot spot are used. Lambertian backgrounds may be suitable for higher LAI conditions or when samples are not near the hot spot. Visible bands are most susceptible to errors due to Lambertian approximations.

Inversions of the soil model of Jacquemoud et al. [1992], using field data from a ground-based radiometer, suggest the "invariant" soil parameters must be determined using a reflectance set representing widely varying conditions (solar and viewing angles, spectral bands, and soil moisture). However, the resulting solution for a prairie soil fit 580 data points with an average of 3.5% absolute values of errors. This implies that a general solution which depends only on soil single scattering albedo can be used regardless of surface and sampling conditions.

A sensitivity study with DISORD, using the anisotropic soil background, showed that leaf optical properties and LAI are the most influential parameters affecting TOC reflectance of typical midwestern grasslands. This result was confirmed for different spectral bands and SZA. Inversions of DISORD with principal plane samples from the ground-based MMR radiometer suggest LAI and LAD are most accurately retrieved at NIR wavelengths and at low SZA. Leaf optical properties are generally retrieved more accurately at high SZA—probably since soil effects are decreased. For NIR bands, leaf reflectance is more accurately determined at low SZA. Soil single scattering albedo appears to be retrievable at low SZA since the canopy optical depth is lower.

In practical terms, NIR wavelengths appear to be most useful for inversions. Due to the relatively low leaf absorption at NIR, the canopy remains optically finite over a greater LAI range than for visible radiation. Hence, LAI may be determined over a greater range of canopy conditions. If LAI < 3, red wavelengths may be equally suitable. However, atmospheric effects are greater at shorter wavelengths.

Estimates of shortwave albedo were obtained by spectrally integrating the spectral albedo values for each MMR band. Results were most accurate when canopy parameters retrieved at preferred wavelengths and SZA were used to estimate spectral albedo. The mean absolute value of errors was less than 4%. Estimates of fAPAR were less accurate, however this may be due to difficulties in measuring transmitted radiation under a canopy, spatial heterogeneities at FIFE, errors in the soil model solution or the assumption that TOC and soil albedo are equal. Estimates of the total (soil + canopy) APAR were highly accurate.

Finally, experiments suggested that the gradient of the merit function near the minimizer largely determines the efficiency and accuracy of the optimization. To insure steep gradients, only model parameters significantly affecting the TOC radiance should remain variable. This theory was developed into a weighting scheme for the merit function. In this scheme, each reflectance error is magnified by the directional reflectance sensitivity for the given sun-target-scanner geometry. Reflectance errors for highly sensitive geometries therefore impact the merit function more than errors for less sensitive geometries.

This weighting function was applied to model inversions with atmospherically-corrected AVHRR data from the First ISLSCP Field Experiment (FIFE). Results demonstrate that 2-3 parameters (LAI, leaf optical properties, soil single scattering albedo) can be estimated from AVHRR (during the Eos era, MODIS) over grasslands. However, the retrieval accuracies of different parameters are not independent. Thus, accurate retrieval of LAI depends on the accuracy of the leaf optical property estimates, and vice-versa. A consistent value of soil single scattering albedo was not retrieved.

Throughout this study, numerical vegetation BRDF models, rigorously based on physical principles, were used. Naturally, numerical models are relatively computationally expensive. Hence,

they may not be ideal for operational use. Nevertheless, CANTEQ and DISORD are based on turbid medium theory. Although other modeling schemes may be more useful sometimes, turbid medium models are probably the most generally applicable for operational inversions with satellite data. By regarding results in this study as turbid medium benchmarks, inaccuracies resulting from inversions with less rigorous models— e.g., those based on analytical solutions to a simplified transport equation—may be understood and quantified. Moreover, by using rigorous models, the true potential of the angular radiation signal can be assessed.

The success in estimating grassland LAI and leaf reflectance/transmittance directly from AVHRR data is encouraging. Although the remaining model parameters were specified with reasonable values in these cases, estimation of their values may be possible for many canopies. Indeed, although surface conditions varied over the 15 km x 15 km FIFE area—sometimes significantly (e.g., highways and buildings)—the use of mean leaf optical data from just two species was sufficient to allow accurate LAI estimation. The potential for accurately estimating LAI over larger grassland areas appears substantial.

The determination of surface data sets for process models is a difficult task at best. Many methods have been proposed, yet few have been operationally applied with satellite data. Those that were featured relatively poor thematic resolution (e.g., land cover classifications from NDVI) in part because of data behavior for which the simple statistical models could not account (e.g., reflectance anisotropy, effects of different background reflectance). The inversion scheme presented here is strongly based on physical principles. Hence, accurate estimation of some grassland parameters was possible with a scheme that is not site or sampling condition dependent. At the very least, this method should allow improved thematic resolution and the detection of more subtle canopy changes due to natural and anthropogenic forces.

Much work remains to be done, including using multiple AVHRR bands simultaneously during inversion, applying inversion methods to other canopy types, quantifying effects of surface heterogeneity, and improving atmospheric correction schemes. Some of this work is presently being addressed elsewhere.

Conclusions are presented in bullet format below.

- 2-3 parameters (LAI, leaf optical properties, soil single scattering albedo) could be estimated from AVHRR or MODIS data collected over grasslands. This requires reasonably accurate estimates of other model parameters, however.
- MISR sampling geometry should allow the accurate retrieval of the same parameters when the ground track is close to the principal plane.
- Retrieval accuracy for LAI depends on the accuracy in leaf optical property estimates, and vice-versa.
- LAI and soil properties can be accurately estimated only for thin canopy (LAI < 3) cases.
- Leaf optical properties can only be estimated accurately for canopies of LAI > 1.
- NIR bands are superior for the determination of spectrally independent parameters of grasslands. At very low LAI (<1), red bands may be superior.
- LAI, soil properties and LAD are most accurately estimated with low SZA and VZA. SZA should not be less than 10°, however, or azimuthal asymmetry is lost.
- Leaf optical properties are most accurately estimated at high SZA and VZA.
- Surface state parameters (fAPAR, albedo, etc.) may be accurately estimated for the time of sampling even if moderate errors occur in the retrieved soil and canopy parameters.
- Surface state parameters can only be accurately estimated at other times if errors are small in the retrieved soil and canopy parameters.
- An anisotropic soil model is required to accurately model relatively thick canopies (LAI < 8), especially if reflectance near the hot spot is estimated. Inversions of the model of Jacquemoud et al. [1992] requires data from multiple spectral bands, at multiple VZA and SZA, and in multiple azimuthal planes to produce generally applicable estimates of roughness and phase function parameters.
- Optimization routines work best when the merit function surface is steep and does not contain local minima. The slope of the merit function around the minimizer can be steepened via weighting the merit function terms by the partial derivative of directional reflectance with respect to model parameters. This increases the efficiency and accuracy of the inversion.

REFERENCES

Abrams, M. D. and Hulbert, L. C. (1987), Effect of topographic position and fire on species composition in tallgrass prairie in northeast Kansas, *Am. Midland Naturalist*, 117:442-445.

Antyufeev, V. S. and Marshak, A. L. (1990), Inversion of a Monte Carlo model for estimating vegetation canopy parameters, *Remote Sens. Environ.*, 33:201-209.

Asrar, G., Myneni, R. B., Li, Y. and Kanemasu, E. T. (1989), Measuring and modeling spectral characteristics of a tallgrass prairie, *Remote Sens. Environ.*, 27:143-155.

Badhwar, G. C., Carnes, J. G. and Austin, W. W. (1982), Use of Landsat-derived temporal profiles for corn-soybean feature extraction and classification, *Remote Sens. Environ.*, 12:57-79.

Baldwin, D., Emery, W. J., and Cheeseman, P. (1995), High resolution data from repeat images of moderate resolution AVHRR data, *IEEE Trans. Geosci. Remote Sens.* (submitted).

Borel, C. C., Gerstl, S. A. W. and Powers, B. (1991), The radiosity method in optical remote sensing of structured 3-D surfaces, *Remote Sens. Environ.*, 36:13-44.

Camillo, P. (1987), A canopy reflectance model based on an analytical solution to the multiple scattering equation, *Remote Sens. Environ.*, 23:453-477

Chance, J. E. and LeMaster, E. W. (1977), Suits reflectance models for wheat and cotton: Theoretical and experimental tests, *Appl. Optics*, 16:407-412.

Cierniewski, J. (1987), A model for soil surface roughness influence on the spectral response of bare soils in the visible and near infared range, *Remote Sens. Environ.*, 23:97-115.

Collatz, G. J., Ball, J. T., Grivet, C. and Berry, J. A. (1991), Physiological and environmental regulation of stomatal conductance, photosynthesis and transpiration: a model that includes a laminar boundary layer, *Agric. For. Meteorol.*, 54:107-136.

Collins, D. C. and Avissar, R. (1994), An evaluation with the Fourier amplitude sensitivity test (FAST) of which land-surface parameters are of greatest importance in atmospheric modeling, *J. Climate*, 7:681-703.

Coombs, J., Hall, D. O., Long, S. P. and Scurlock, J. M. O. (1985), Techniques in bioproductivity and photosynthesis (Editors), Pergamon Press, New York, 298 pp.

Cooper, K. D. and Smith, J. A. (1985), A Monte-Carlo reflectance model for soil surfaces with three-dimensional structure, *IEEE Trans. Geosci. Remote Sens.*, GE-23:668-673.

Davis, F. W., Schimel, D. S., Friedl, M. A., Michaelsen, J. C., Kittel, T. J. F., Dubayah, R. and Dozier, J. (1992), Covariance of biophysical data with digital topographic and land use maps over the FIFE site, *J. Geophys. Res.*, 97(D17):19009-19021.

Deering, D. W. and Eck, T. F. (1987), Atmospheric optical depth effects on angular anisotropy of plant canopy reflectance, *Int. J. Remote Sens.*, 8:893-916.

Deering, D. W., Eck, T. F. and Otterman, J. (1990), Bidirectional reflectances of selected desert surfaces and their three-parameter soil characterization, *Agric. For. Meteorol.*, 52:71-93.

Demetriades-Shah, T. H, Kanemasu, E. T., Flitcroft, I. D. and Su, H. (1992), Comparison of ground- and satellite-based measurements of the fraction of photosynthetically active radiation intercepted by tallgrass prairie, *J. Geophys. Res.*, 97:18947-18950.

Dickinson, R. E. (1983), Land surface processes and climate-surface albedos and energy balance, *Adv. Geophys.*, 25:305-353.

Dickinson, R. E., Pinty, B. and Verstraete, M. M. (1990), Relating surface albedos in GCMs to remotely-sensed data, *Agric. For. Meteorol.*, 32:109-131.

Diner, D. J., Bruegge, C. J., Martonchik, J. V., Ackerman, T. P., Davies, R., Gerstl, S. A. W., Gordon, H. R., Sellers, P. J., Clark, J., Daniels, J. A., Danielson, E. D., Duval, V. G., Klaasen, K. P., Lilienthal, G. W., Nakamoto, D. I., Pagano, R. J. and Reilly, T. H. (1989), A multi-angle imaging spectroradiometer for geophysical and climatological research from EOS, *IEEE Trans. Geosci. Remote Sens.*, GE-27:200-214.

Eck, T. F. and Holben, B. N. (1994), AVHRR split window temperature differences and total precipitable water over land surfaces, *Int. J. Remote Sens.*, 15: 567-582.

Fraser, R. S. and Kaufman, Y. J. (1985), The relative importance of aerosol scattering and absorption in remote sensing, *IEEE Trans. Geosci. Remote Sens.*, GE-23(5):625-633.

Gerstl, S. A. and Simmer, C. (1986), Radiation physics and modeling for off-nadir satellite-sensing of non-Lambertian surfaces, *Remote Sens. Environ.*, 20:1-29.

Goel, N. S. (1988), Models of vegetation canopy reflectance and their use in estimation of biophysical parameters from reflectance data, *Remote Sens. Rev.*, 4:1-213.

Goel, N. S. and Strebel, D. E. (1983), Inversion of vegetation canopy reflectance models for estimating agronomic variables. I. Problem definition and initial results using the Suits' model, *Remote Sens. Environ.*, 13:487-507.

Goel, N. S. and Strebel, D. E. (1984), Simple beta distribution representation of leaf orientation in vegetation canopies, *Agron. J.*, 76:800-803.

Goel, N. S. and Thompson, R. L. (1984a), Inversion of vegetation canopy reflectance models for estimating agronomic variables. III. Estimation using only canopy reflectance data as illustrated by Suits' model, *Remote Sens. Environ.*, 15:223-236.

Goel, N. S. and Thompson, R. L. (1984b), Inversion of vegetation canopy reflectance models for estimating agronomic variables. IV. Total inversion of the SAIL model, *Remote Sens. Environ.*, 15:237-253.

Goel, N. S. and Thompson, R. L. (1984c), Inversion of vegetation canopy reflectance models for estimating agronomic variables. V. Estimation of leaf area index and average leaf angle using measured canopy reflectances, *Remote Sens. Environ.*, 16:69-85.

Goel, N. S. and Thompson, R. L. (1985), Optimal solar/viewing geometry for an accurate estimation of leaf area index and leaf angle distribution from bidirectional canopy reflectance data, *Int. J. Remote Sens.*, 6:1493-1520.

Goel, N. S., Strebel, D. E. and Thompson, R. L. (1984), Inversion of vegetation canopy reflectance models for estimating agronomic variables II. Use of angle transforms and error analysis as illustrated by Suits' model, *Remote Sens. Environ.*, 14:77-111.

Goel, N. S., Rozehnal, I. and Thompson, R. L. (1991), A computer graphics based model for scattering from objects of arbitrary shapes in the optical region, *Remote Sens. Environ.*, 36:73-104.

Goetz, S. J. (1995), Multi-sensor analysis of NDVI and surface temperature dynamics at a mixed grassland site, *Int. J. Remote Sens.* (submitted).

Goward, S. N. and Huemmrich, K. F. (1992), Vegetation canopy PAR absorptance and the normalized difference vegetation index: an assessment using the SAIL model, *Remote Sens. Environ.*, 39:119-140.

Hall, F. G., Huemmrich, K. F. and Goward, S. N. (1990), Use of narrow band spectra to estimate the fraction of absorbed photosynthetically active radiation, *Remote Sens. Environ.*, 32:47-56.

Hall, F. G., Huemmrich, K. F., Goetz, S. J., Sellers, P. J. and Nickeson, J. E. (1992), Satellite remote sensing of surface energy balance: success, failures, and unresolved issues in FIFE, *J. Geophys. Res.*, 97:19061-19090.

Hall, F. G., Shimabukuro, Y. E. and Huemmrich, K. F. (1994), Remote sensing of biophysical structure in boreal stands of *Picea Mariana* using mixture decomposition and geometric reflectance models, *Ecol. Appl.* (submitted).

Hapke, B. (1981), Bidirectional reflectance spectroscopy, 1. Theory, *J. Geophys. Res.*, 86:3039-3054.

Hapke, B. W., Nelson, R. M. and Smythe, W. D. (1993), The opposition effect of the moon: the contribution of coherent backscatter, *Science*, 260:509-511.

Henderson-Sellers, A. and Wilson, M. F. (1983), Surface albedo data for climatic modeling, *Rev. Geophys. Space Physics*, 21:1743-1778.

Holben, B., Kimes, D. and Fraser, R. S. (1986), Directional reflectance response in AVHRR red and near-IR bands of three cover types and varying atmospheric conditions, *Remote Sens. Environ.*, 19:213-236.

Iaquinta, J. and Pinty, B. (1994), Adaptation of a bidirectional reflectance model including the hot spot to an optically thin canopy, in *Proc. 6th Int. Symp. Physical Measurements and Signatures in Remote Sens.*, Val D'Isère, France, January 17-21, 1994.

Irons, J. R., Campbell, G., Norman, J. M., Graham, D. W. and Kovalick, W. M. (1992), Prediction and measurement of soil bidirectional reflectance, *IEEE Trans. Geosci. Remote Sens.*, GE-30:249-260.

Jacquemoud, S. (1993), Inversion of the PROSPECT+SAIL canopy reflectance model from AVIRIS equivalent spectra: theoretical study, *Remote Sens. Environ.*, 44:281-292.

Jacquemoud, S., Baret, F. and Hanocq, J. F. (1992), Modeling spectral and bidirectional soil reflectance, *Remote Sens. Environ.*, 41:123-132.

Jacquemoud, S., Flasse, S., Verdebout, J. and Schmuck, G. (1994), Comparison of several optimization methods to extract canopy biophysical parameters -- application to CAESAR data, in *Proc. 6th Int. Symp. Physical Measurements and Signatures in Remote Sens.*, Val D'Isère, France, January 17-21, 1994.

Jasinski, M. F. (1990), Functional relation among subpixel canopy cover, ground shadow, and illuminated ground at large sampling scales, in *Soc. of Photo Optical Instrumentation Engineers*, Orlando, FL.

Kaufman, Y. J. and Holben, B. N. (1993), Calibration of the AVHRR visible and near-IR bands by atmospheric scattering, ocean glint and desert reflection, *Int. J. Remote Sens.*, 14:21-52.

Kauth, R. J. and Thomas, G. S. (1976), The tasseled-cap: a graphic description of the spectral-temporal development of agricultural crops as seen by Landsat, *Proc. Symp. Machine Processing of Remote Sens. Data,* pp. 41-51.

Kidwell, K. B. (1991), NOAA polar orbiter data users guide, National Oceanic and Atmospheric Administration, Washington, D. C., 20233.

Kimes, D. S. (1983), Dynamics of directional reflectance factor distributions for vegetation canopies, *Appl. Optics,* 22:1364-1372.

Kimes, D. S. and Kirchner, J. A. (1982), Radiative transfer model for heterogeneous three-dimensional scenes, *Appl. Optics*, 21:4119-4129.

Kimes, D. S. and Kirchner, J. A. (1983), Diurnal variations of vegetation canopy structure, *Int. J. Remote Sens.*, 4:257-271.

Kimes, D. S. and Sellers, P. J. (1985), Inferring hemispherical reflectance of the earth's surface for global energy budgets from remotely sensed nadir or directional radiance values, *Remote Sens. Environ.*, 18:205-223.

Kimes, D. S., Smith, J. A. and Ranson, K. J. (1980), Vegetation reflectance measurements as a function of solar zenith angle, *Photogramm. Eng. and Remote Sens.*, 46:1563-1573.

Kimes, D. S., Newcomb, W. W., Tucker, C. J., Zonneveld, I. S., Van Wijngaarden, W., de Leeuw, J. and Epema, G. F. (1985), Directional reflectance factor distributions for cover types of Northern Africa, *Remote Sens. Environ.*, 18:1-19.

Kimes, D. S., Norman, J. M. and Walthall, C. L. (1985), Modeling the radiant transfers of sparse vegetation canopies, *IEEE Trans. Geosci. Remote Sens.*, GE-23:695-704.

Kittel, T. G. F., Knapp, A. K., Seastedt, T. and Schimel, D. S. (1990), A landscape view of biomass, LAI, and photosynthetic capacity, in *Symp. on FIFE: First ISLSCP Field Exper.* (F. Hall and P.J. Sellers, Eds.), Am. Meteorol. Soc., Boston, Mass, pp. 66-69.

Kuusk, A. (1991a), The angular distribution of reflectance and vegetation indices in barley and clover canopies, *Remote Sens. Environ.*, 37:143-151.

Kuusk, A. (1991b), The determination of vegetation canopy parameters from optical measurements, *Remote Sens. Environ.*, 37:207-218.

Kuusk, A. (1994a), A fast invertible canopy reflectance model, *Remote Sens. Environ.* (forthcoming).

Kuusk, A. (1994b) A Markov model of canopy reflectance, *Agric. For. Meteor.* (submitted).

Lee, T. Y. and Kaufman, Y. J. (1986), Non-Lambertian effects on remote sensing of surface reflectance and vegetation index, *IEEE Trans. Geosci. Remote Sens.*, 24:699-707.

Lewis, P. and Muller, J.-P. (1992), The advanced radiometeric ray-tracer: ARARAT for plant canopy reflectance simulation, *Int. Arch. Photogramm. Remote Sens.*, 29 (Commission VII):26-34.

Li, X. and Strahler, A. H. (1985), Geometrical-optical modeling of a conifer forest canopy, *IEEE Trans. Geosci. Remote Sens.*, 23:705-721.

Li, X. and Strahler, A. H. (1994), A hybrid geometric optical-radiative transfer approach for modeling albedo and directional reflectance of discontinuous canopies, *IEEE Trans. Geosci. Remote Sens.* (submitted).

Liang, S. and Strahler, A. H. (1994a), Retrieval of surface BRDF from multiangle remotely sensed data, *Remote Sens. Environ.*, 50:18-30.

Liang, S. and Strahler, A. H. (1994b), An analytical BRDF model of canopy radiative transfer and its inversion, *IEEE Trans. Geoscience Remote Sens.*, 31:1081-1092.

Liang, S. and Strahler, A. H. (1994c), An analytical radiative transfer model for a coupled atmosphere and leaf canopy, *J. Geophys. Res.* (submitted).

Marshak, A. L. (1989), The effect of the hot spot on the transport equation in plant canopies, *J. Quant. Spectrosc. Radiat. Transfer*, 42:615-630.

Monsi, M. and Saeki, T. (1953), Uber den Lichtfaktor in den Pflanzengessellschafte und seine Bedeuting fur die Stoffproduktion, *Jap. J. Bot.*, 14:22-52.

Monteith, J. L. (1972), Solar radiation and productivity in tropical ecosystems, *J. Appl. Ecol.*, 9:747-766.

Myneni, R. B. and Ganapol, B. D. (1991), A simplified formulation of photon transport in leaf canopies with scatterers of finite dimensions, *J. Quant. Spectrosc. Radiat. Transfer*, 46:135-140.

Myneni, R. B. and Ross, J. (1991), *Photon-Vegetation Interactions* (Editors), Springer-Verlag, New York, 565 pp.

Myneni, R. B., Gutschick, V. P., Asrar, G. and Kanemasu, E. T. (1988), Photon transport in vegetation canopies with anisotropic scattering, Parts I through IV, *Agric. For. Meteorol.*, 42:1-40 and 87-120.

Myneni, R. B., Asrar, G. and Hall, F. G. (1992a), A three dimensional radiative transfer model for optical remote sensing of vegetated land surfaces, *Remote Sens. Environ.* 41:85-103.

Myneni, R. B., Asrar, G., Tanré, D. and Choudhury, B. J. (1992b), Remote sensing of solar radiation absorbed and reflected by vegetated land surfaces, *IEEE Trans. Geosci. Remote Sens.*, GE-30:302-314.

Myneni, R. B., Impens, I. and Asrar, G. (1993), Simulation of space measurements of vegetation canopy bidirectional reflectance factors, *Remote Sens. Rev.*, 7:19-41.

NASA (1993), *Earth Observing System 1993 Reference Handbook*, Goddard Space Flight Center, Greenbelt, MD, 20771.

Nelder, J. A. and Mead, R. (1965), A simplex method for function minimization, *Computer J.*, 7:308-313.

Nicodemus, F. E. (1970), Reflectance nomenclature and directional reflectance and emissivity, *Appl. Optics*, 9:1474-1475.

Nilson, T. and Kuusk, A. (1989), A reflectance model for homogeneous plant canopies and its inversion, *Remote Sens. Environ.*, 27:157-167.

Norman, J. M. and Welles, J. M. (1983), Radiative transfer in an array of canopies, *Agron. J.*, 75:481-488.

Norman, J. M., Welles, J. M. and Walter, E. A. (1985), Contrasts among bidirectional reflectance of leaves, canopies and soils, *IEEE Trans. Geosci. Remote Sens.*, GE-23:659-667.

Numerical Algorithms Group (1990), *The NAG Fortran Library, Mark 14, Volume 3*, NAG Inc., Downers Grove, IL.

Otterman, J. (1981), Reflection of soil with sparse vegetation, *Adv. Space Res.*, 1:115-119.

Otterman, J. (1984), Albedo of a forest modeled as a plane with dense protrusions, *J. Climate Appl. Meteorol.*, 23:297-307.

Otterman, J., Strebel, D. E. and Ranson, K. J. (1987), Infering spectral reflectances of plant elements by a simple inversion of bidirectional reflectance measurements, *Remote Sens. Environ.*, 21:215-228.

Pearcy, R. W. (1989), Radiation and light measurements, in *Plant physiological ecology, field methods and instrumentation* (R. W. Pearcy, J. Ehleringer, H. A. Mooney and P. W. Rundel, Eds.), Chapman and Hall, New York, pp. 97-116.

Pinty, B., Verstraete, M. M. and Dickinson, R. E. (1989), A physical model for predicting bidirectional reflectances over bare soil, *Remote Sens. Environ.*, 27:273-288.

Pinty, B., Verstraete, M. M. and Dickinson, R. E. (1990), A physical model of the directional reflectance of vegetation canopies II. Inversion and validation, *J. Geophys. Res.*, 95:11767-11775.

Press, W. H., Flannery, B. P., Teukolsky, S. A. and Vetterling, W. T. (1986), *Numerical Recipes*, Cambridge University Press, New York, pp. 274-312.

Privette, J. L., Myneni, R. B., Tucker, C. J. and Emery, W. J. (1994), Invertibility of a 1-D discrete ordinates canopy reflectance model, *Remote Sens. Environ.*, 48:89-105.

Privette, J. L., Myneni, R. B., Emery, W. J. and Pinty, B. (1995), Inversion of a soil reflectance model for use in vegetation BRDF models, *J. Geophys. Res.* (in press).

Privette, J. L., Myneni, R. B., Emery, W. J. and Hall, F. G. (1995), Optimal sampling conditions for estimating grassland parameters via reflectance model inversions, *IEEE Trans. Geosci. Remote Sens.* (in press).

Rahman, H., Pinty, B. and Verstraete, M. M. (1994), A coupled surface-atmosphere reflectance (CSAR) model Part 2: a semi-empirical surface model useable with NOAA/AVHRR data, *J. Geophys. Res.*, 98(D11):20791-20801.

Ranson, K. J., Biehl, L. L. and Daughtry, C. S. T. (1981), Soybean canopy reflectance modeling data sets, *Lab. for Appl. of Remote Sens. Tech. Report*, Purdue Univ. 071584, 46 pp.

Rosborough, G., Baldwin, D. and Emery, W. J. (1994), Precise AVHRR image navigation, *IEEE Trans. Geosci. Remote Sens.*, 32:644-657.

Ross, J. K. (1981), *The Radiation Regime and Architecture of Plant Stands*, W. Junk Publishers, The Netherlands, 391 pp.

Ross, J. K. and Nilson, T. A. (1966), A mathematical model of the radiation regime of vegetation, in *Actinometry and Atmospheric Optics* (V. K. Pyldmaaa, Ed.), Translated by *Israel Progr. Sci. Transl.*, Cat. No. 5835, pp. 253-274, Jerusalem, 1971.

Ross, J. K. and Marshak, A. L. (1988), Calculation of canopy bidirectional reflectance using the Monte Carlo method, *Rem. Sensing Environ.*, 24:213-225.

Roujean, J.-L., Leroy, M. and Deschamps, P.-Y. (1992), A bidirectional reflectance model of the earth's surface for the correction of remote sensing data, *J. Geophys. Res.*, D18:20455-20468.

Schimel, D. S., Kittel, T G. F., Knapp, A. K. and Seastedt, T. R. (1991), Physiological interactions along resource gradients in a tallgrass prairie, *Ecology*, 72(2):672-684.

Schlüessel, G., Dickinson, R. E., Privette, J. L., Emery, W. J. and Kokaly, R. (1994), Modeling the bidirectional reflectance distribution function of mixed finite plant canopies and soil, *J. Geophys. Res.*, 99:10577-10600.

Sellers, P. J. (1993), International satellite land surface climatology project workshop report (Editor), Columbia, MD, June 23-26, 1992.

Sellers, P. J., Mintz, Y., Sud, Y. C. and Dalcher, A. (1986), A simple biosphere model (SiB) for use within general circulation models, *J. Atmos. Sci.*, 43(6):505-531.

Sellers, P. J., Hall, F. G., Asrar, G., Strebel, D. E. and Murphy, R. E. (1988), The first ISLSCP field experiment (FIFE), *Bull. Amer. Met. Soc.*, 69(1):22-27.

Shifrin, K. S. (1953), Concerning the theory of albedo, *Trans. Main. Geophys. Obs.*, 101:244-257 (in Russian).

Shukla, J. and Y. Mintz (1982), Influence of land-surface evapotranspiration on the earth's climate, *Science*, 215:1498-1501.

Shultis, J. K. and Myneni, R. B. (1988), Radiative transfer in vegetation canopies with anisotropic scattering, *J. Quant. Spectrosc. Radiat. Transfer*, 39:115-129.

Simmer, C. and Gerstl, S. A. W. (1985), Remote sensing of angular characteristics of canopy reflectances, *IEEE Trans. Geosci. Remote Sens.*, GE-23:648-659.

Starks, P. J., Norman, J. M., Blad, B. L., Walter-Shea, E. A. and Walthall, C. L. (1991), Estimation of shortwave hemispherical reflectance (albedo) from bidirectionally reflected radiance data, *Remote Sens. Environ.*, 38:123-134.

Stewart, R. D. (1990), Modeling radiant energy transfer in vegetation canopies, Masters Thesis, Kansas State Univ., Manhattan, KS 66506.

Strahler, A. H. (1994), Vegetation canopy reflectance modeling -- recent developments and remote sensing perspectives, in *Proc. 6th Int. Symp. Physical Measurements and Signatures in Remote Sens.*, Val D'Isère, France, January 17-21, 1994.

Strahler, A. H. and Li, X. (1981), An invertible coniferous forest canopy reflectance model, *Proc. 15th Int. Symp. Remote Sens. Environ.*, Ann Arbor, MI.

Taconet, O., Bernard, R. and Vidal-Madjar, D. (1986), Evapotranspiration over an agricultural region using a surface flux/temperature model based on NOAA-AVHRR data, *J. Clim. Appl. Meteor.*, 25:284-307.

Tanré, D., Deroo, C., Duhaut, P., Herman, M., Morcrette, J. J., Perbos, J. and Deschamps, P. Y. (1990), Description of a computer code to simulate the satellite signal in the solar spectrum: the 5S code, *Int. J. Remote Sens.*, 11:659-668.

Tanré, D., Holben, B. N. and Kaufman, Y. J. (1992), Atmospheric correction algorithms for NOAA-AVHRR products: theory and application, *IEEE Trans. Geosci. Remote Sens.*, 30:231-248.

Tucker, C. J. and Miller, L. D. (1977), Soil spectra contributions to grass canopy spectral reflectance, *Photogramm. Engin. Remote Sens.*, 43:721-726.

Tucker, C. J., Townshend, J. R. G. and Goff, T. E. (1985), African land cover classification using satellite data, *Science*, 227:369-375.

Turner, C. L., Seastedt, T. R., Dyer, M. I., Kittel, T. G. F. and Schimel, D. S. (1992), Effects of management and topography on the radiometric response of tallgrass prairie, *J. Geophys. Res.*, 97:18855-18866.

Vanderbilt, V. C. and Grant, L. (1985), Plant canopy specular reflectance model, *IEEE Trans. Geosci. Remote Sens.*, GE-23:722-730.

Vanderbilt, V. C., Grant, L. and Ustin, S. L. (1991), Polarization of light by vegetation, in *Photon-Vegetation Interactions* (R. Myneni and J. Ross, Eds.), Springer-Verlag, New York, pp. 191-227.

Van Leeuwen, W. and Huete, A. (1993), Unpublished data from HAPEX-SAHEL.

Verhoef, W. (1984), Light scattering by leaf layers with application to canopy reflectance modeling, the SAIL model, *Remote Sens. Environ.*, 16:125-141.

Vermote, E., Tanré, D., Deuzé, J. L., Herman, M. and Morcrette, J. J. (1994), Second simulation of the satellite signal in the solar spectrum (6S), *6S User Guide Version 0*, NASA-Goddard Space Flight Center, Washington, D. C.

Verstraete, M. M., Pinty, B. and Dickinson, R. E. (1990), A physical model of the bidirectional reflectance of vegetation canopies 1. Theory, *J. Geophys. Res.*, 95:11755-11765.

Verstraete, M. M., Pinty, B. and Myneni, R. B. (1994), Satellite remote sensing of the terrestrial biosphere, *Remote Sens. Environ.* (submitted).

Walter-Shea, E. A., Blad, B. L., Hays, C. J., Mesarch, M. A., Deering, D. W. and Middleton, E. M. (1992), Biophysical properties affecting vegetative canopy reflectance and absorbed photosynthetically active radiation at the FIFE site, *J. Geophys. Res.*, 97:18925-18934.

Walthall, C. L., Norman, J. M., Welles, J. M., Campbell, G. and Blad, B. (1985), Simple equation to approximate the bidirectional reflectance from vegetative canopies and bare soil surfaces, *Appl. Optics*, 24:383-387.

Welles, J. M. and Norman, J. M. (1991), Instrument for indirect measurement of canopy architecture, *Agron. J.*, 83(5):818-825.

Wessman, C. A. (1994), Estimating canopy biochemistry through imaging spectrometry, in *Imaging spectrometry - a tool for environmental observations* (J. Hill and J. Megier, Eds.), Kluwer Academic Publishers, Boston, pp. 57-69.

Wu, Y. and Strahler, A. H. (1994), Remote estimation of crown size, stand density and biomass on the Oregon transect, *Ecol. Appl.*, 4:299-310.